ISBN 978-82-326-2992-3 (printed ver.)
ISBN 978-82-326-2993-0 (electronic ver.)
ISSN 1503-8181

Doctoral theses at NTNU, 2018:101

Hongliang Liu

Modeling and simulation of the soft palate for improved understanding of the obstructive sleep apnea syndrome

NTNU
Norwegian University of Science and Technology
Thesis for the Degree of
Philosophiae Doctor
Faculty of Engineering
Department of Structural Engineering

Hongliang Liu
Doctoral thesis
Doctoral theses at NTNU, 2018:101
NTNU

NTNU
Norwegian University of Science and Technology

NTNU
Norwegian University of Science and Technology

Hongliang Liu

Modeling and simulation of the soft palate for improved understanding of the obstructive sleep apnea syndrome

Thesis for the Degree of Philosophiae Doctor

Trondheim, April 2018

Norwegian University of Science and Technology
Faculty of Engineering
Department of Structural Engineering

NTNU
Norwegian University of
Science and Technology

NTNU
Norwegian University of Science and Technology

Thesis for the Degree of Philosophiae Doctor

Faculty of Engineering
Department of Structural Engineering

ISBN 978-82-326-2992-3 (printed ver.)
ISBN 978-82-326-2993-0 (electronic ver.)
ISSN 1503-8181

IMT-report 2018:101

Doctoral theses at NTNU, 2018:101

Printed by NTNU Grafisk senter

Preface

This thesis is submitted to the Norwegian University of Science and Technology (NTNU) for partial fulfilment of the requirements for the degree of philosophiae doctor. This doctoral work has been performed at the Department of Structural Engineering, NTNU, Trondheim, with Professor Bjørn Helge Skallerud as the main supervisor and with associate Professor Victorien Emile Prot as the co-supervisor.

The thesis was financially supported by the Research Council of Norway and NTNU from January 2015 to December 2017. This support is greatly appreciated.

Abstract

Obstructive sleep apnea (OSA) influences a large part of the population and is increasingly recognized as a major global health problem. For OSA patients, the collapse of the soft palate has been clarified to be a common feature for the obstructive breathing. A comprehensive study of the biomechanical mechanism underlying the soft palate collapse is needed to obtain a deep insight of the mechanical mechanism in the OSA process.

To address this challenge, beginning from the 3-dimensional (3D) patient-specific model, series work has been done to investigate the global response of the soft palate. First, based on the corresponding histology study and the acorresponding quantitative tissue composition analysis, a tissue composition based model was created, including three main tissue layers: posterior pharynx supersurface adipose tissue layer, medial muscle tissue and connective tissue layer and the anterior oral surface glandular tissue layer. Specific material properties were assigned to each specific tissue layer considering the nonlinear property and anisotropic behavior. Nonlinear behavior of the global response of the soft palate in response to the negative pressure loading on the upper airway was presented. Second, in order to investigate the palatal implant surgery efficacy for improving the patients' sleep condition, pillar placement numerical simulation with 3D patient-specific geometry was achieved. The Young's modulus of the pillar implants material was obtained through performing a uniaxial test with some implants samples. A new surgery scheme that implanting the pillars in the transverse direction was provided, and its strengthening efficacy was tested to be higher than the current longitudinal surgery scheme based on the numerical simulation results. Then, a phenomenological constitutive model was developed to represent the palatal muscle activation mechanism working to maintain the upper airway patency when the negative pressure is produced. OSA patients' muscle activation defectiveness was verified in the palatal muscle activation numerical simulation, in which the created constitutive model was considered. In addition, based on the experiment data published in the literature, the cohesive approach combined with the created 3D geometry was used to investigate the influence of the adhesion effect from the lining liquid between the soft palate and the tongue on the global response of the soft palate. The cohesive properties were obtained through fitting the numerical simulation results to the experimental test data. Finally, a new anisotropic finite strain viscoelastic model was presented, based on the Holzapfel type anisotropic hyperelastic strain-energy function. A new method to develop the evolution equations of the internal variables was presented. The cor-

responding analytical validation for positive dissipation energy, using the second law of thermodynamics, was also provided. Some numerical simulations were achieved, and the proposed constitutive model was tested to represent the anisotropic viscoelastic behavior efficiently. This might lie a guide for future investigations of the soft palate's viscoelastic behavior.

In the future study of the soft palate or solid mechanics research for the OSA, more anatomical and physiological numerical simulation is needed, in order to provide more useful information to the clinical research and to facilitate some operations in the clinical surgery. This current thesis provides a basic framework and presents comprehensive knowledge for further more physiological study of the OSA.

Acknowledgement

In China, there is a saying: one drop of water is needed, a corresponding spring is returned. In these three years for my PhD study, I obtained great support and help from my family, my supervisors and my friends, for both the academic suggestions and life encouragements. Without this, I couldn't achieve this PhD thesis so efficiently. Here, I want to express my gratitude to all of you.

Big thanks to my main supervisor, Bjørn Helge Skallerud. I always got powerful support from you for my academic challenges that I faced in my PhD study and in the process of finishing my thesis. You are always creative and patient, and provided constructive ideas for my research. You showed me the basic knowledge for the biomechanics theory, and you also taught me how to write and submit an academic paper. Thanks for all the discussions and talkings with you through these three years. I learnt a lot for how to generate an innovative idea and develop an accurate model. Thanks for your detailed comments for every manuscript I sent to you, including every language problem and every equation's expression. Thanks for your detailed suggestions when I revised my submitted manuscript. Thanks again, Bjørn.

Many thanks to my co-supervisor, Victorien Emile Prot. I learnt a lot from you, such as how to write the paper with the decent language, how to use ABAQUS user subroutines and how to verify my numerical simulations in my PhD thesis. I am also very grateful for all the discussions and meetings with you relating to my academic research.

Many thanks to Professor Gerhard A. Holzapfel. Thank you very much for providing me a strong theory support for the constitutive modeling relating to the hyperelastic theory. In addition, I am grateful for you giving me a lot of constructive comments on the anisotropic viscoelastic model.

Many thanks to all my colleagues working together in the research project "Modeling of Obstructive Sleep Apnea by Fluid-Structure Interaction in the Upper Airways". I learnt a lot from the project workshop's discussions. Special thanks to Mads Henrik Strand Moxness. Thanks for your great contribution for our joint paper relating to the palatal implants simulation. In addition, many thanks for Ståle Nordgård and Mads for providing the specific patients' CT images.

Many thanks to all my colleagues at our department-the Department of Structural Engineering. I am grateful for the nice and friendly working environment in our department. Many thanks to all the colleagues in the biomechanics division for nice group activities.

Many thanks to my Chinese friends. Thanks very much for your social

life that I really appreciate. Also, thanks very much for your nice and delicious Chinese cooking food.

Finally, I want to show the deep thanks to my family, especially for my fiancee's love and big support for my abroad study.

List of Papers

This thesis consists of an introductory part and five papers, which are appended as the following:

Paper 1:
Tissue composition based nonlinear FEM simulation of the soft palate using patient-specific 3D anatomy
Authors: Hongliang Liu, Victorien Emile Prot, Bjørn Helge Skallerud
Published in MekIT17, Ninth National Conference on Computational Mechanics, Trondheim 11-12 May 2017, ISBN 978-84-947311-1-2

Paper 2:
Palatal implant surgery effectiveness in treatment of obstructive sleep apnea: a numerical method with 3D patient-specific geometries
Authors: Hongliang Liu, Mads Henrik Strand Moxness, Victorien Emile Prot, Bjørn Helge Skallerud
Published in Journal of Biomechanics
https://doi.org/10.1016/j.jbiomech.2017.11.006

Paper 3:
Soft palate muscle activation: a modeling approach for improved understanding of obstructive sleep apnea
Authors: Hongliang Liu, Victorien Emile Prot, Bjørn Helge Skallerud
Submitted to Biomechanics and Modeling in Mechanobiology

Paper 4:
3D patient-specific numerical modeling of the soft palate considering adhesion from the tongue
Authors: Hongliang Liu, Victorien Emile Prot, Bjørn Helge Skallerud
Submitted to Journal of Biomechanics

Paper 5:
Anisotropic finite strain viscoelasticity - constitutive modeling and finite element implementation
Authors: Hongliang Liu et al.
To be submitted

Besides these article contributions, I also took part in some academic

conferences and had the oral presentations:

A single degree of freedom dynamic model of epiglottis in the upper airway
Authors: Hongliang Liu, Victorien Emile Prot, Bjørn Helge Skallerud
28th Nordic Seminar on Computational Mechanics; 22-23 10 2015, Tallinn

Modeling of the soft palate including polyethylene reinforcements
Authors: Hongliang Liu, Victorien Emile Prot, Bjørn Helge Skallerud
XIV International Conference on Computational Plasticity - COMPLAS 2017; 05-07 09 2017, Barcelona

Contents

Chapter 1

Introduction

1.1 Research background and motivation

This PhD thesis is related to the research project "Modeling of Obstructive Sleep Apnea by Fluid-Structure Interaction in the Upper Airways", and this work focuses on the soft tissue modeling within the solid mechanics realm.

Many people have experienced obstructive sleep problems, which are caused by different reasons including physiological and mental effects. Long term obstructive sleeping conditions bring widely adverse influences on daily life, such as hypertension [1], development of insulin resistance [2], and the risk for increased daytime sleepiness and motor vehicle accidents [3]. This severe syndrome is called obstructive sleep apnea (OSA), which is clinically characterized as repetitive episodes breathing stops during sleep, and usually is associated with a blood oxygen saturation reduction [4]. It has been estimated that at least 4% of men and 2% of women are suffering this annoying obstructive sleep syndrome [5]. The breathing stop during sleep is caused by the collapse of the soft tissue in the upper airway (Figure 1.1), including the soft palate, tongue and other pharyngeal soft tissues. Among them, collapse of the soft palate is commonly observed in the clinical diagnosis. For the obstructive site locating in the upper airway, it has been evaluated that 73% of the patients have the obstructive site in the soft palate region [6].

The direct reason for the collapse of the soft palate is attributed to the negative pressure that may be caused by the narrower upper airway compared with the normal case. In addition, pathological reasons to the soft palate collapse are attributed to enlarged volume of the soft palate and the defectiveness of the palatal muscle activation level [7]. Obesity increases the risk of suffering from OSA [8], since the enlarged volume percentage of

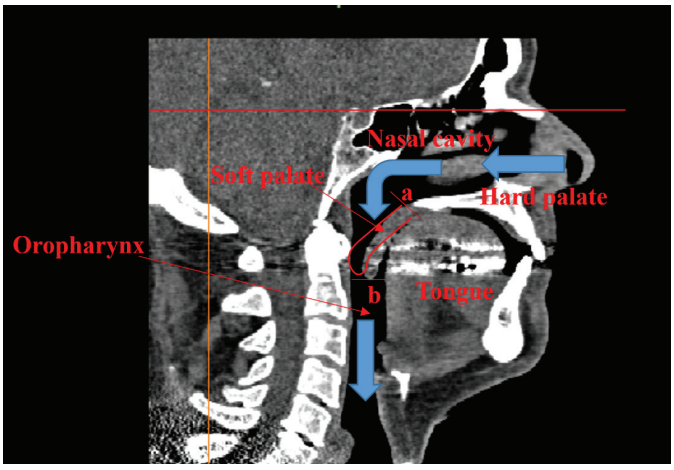

Figure 1.1: CT image of the upper airway. We use "a" "b" markers to have a clear description of the soft palate's position in the following description. "a" section means the side between the soft palate and the hard palate, "b" section means the bottom edge of the soft palate tip. A schematic of the soft palate collapse (red) is also presented as well as the airflow (blue).

adipose tissue in the soft palate not only brings a softer soft palate, but also produces a narrower airway for breathing. Upper airway narrowing, presented as a decreasing cross section area of the upper airway, makes the pressure distributed in the soft palate region more negative than the normal level, corresponding to an easier collapse of the soft palate (Figure 1.1). Additionally, in response to the negative pressure, a neurogenic reflex from the muscle tissue helps to prevent the soft tissue from collapse. For the soft palate, palatal muscle activation has been pointed out to play a key role in prohibiting the soft palate collapse [9]. The patients' pharyngeal dilator muscle activation level in awake condition has been investigated to be higher than that for the healthy people [10], corresponding to easier upper airway collapse. Moreover, during sleep, a hypothesis that the muscular activation is reduced for OSA patients was put forward. This was measured by McGinley et al. [11], and a defectiveness of the neuromuscular compensation for the OSA patients during sleep was observed.

With respect to the negative pressure, a critical value that makes the soft palate in contact with the pharynx wall, called the closing pressure, has been addressed to evaluate the OSA severity. For healthy subjects, the closing pressure has been found to be around -13 cm H_2O [14]. In addition, the closing pressure in clinical tests has been found to be in the range -10

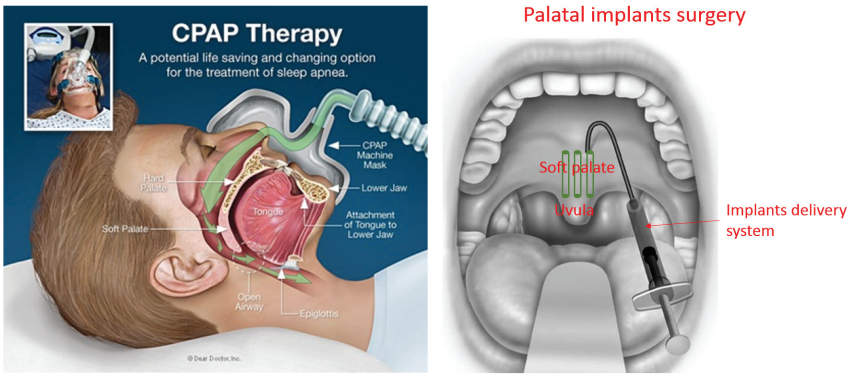

(a) Positive airway pressure (b) Palatal impants surgery

Figure 1.2: Schematic of the clinical treatments to the OSA patients according to [12] and [13].

to -15 cm H_2O [11]. For OSA patients, a softer palate was observed, as well as narrower airway, and the corresponding closing pressure was found to be less negative than the healthy subjects. Typical closing pressure for OSA patients was investigated to be in the range -4-(-8) cm H_2O [15].

Treatment of OSA varies among different subjects and is often based on patients' upper airway anatomical characteristics and the apnea hypopnoea index (AHI), which is used to evaluate the patients' severity degree of the obstructive breathing during sleep (higher AHI more serious). It reflects the fact that the underlying mechanisms causing the disease are poorly understood. The conservative line of treatment consists of: physical weight loss and sleep position altering. The interventional line of treatment consists of either some forms of positive airway pressure (CPAP/biPAP), or surgery. Weight loss and altering sleep position are often found to be the first step of OSA treatment. CPAP/biPAP treatment (Figure 1.2(a)) inhibits the negative pressure drop by applying a pneumatic splint and has been shown to have high success rates, but the long term compliance to the patients may be a problem [16]. The surgical therapy by removing redundant tissue is called uvulopalatopharyngoplasty (UPPP) [17], but the long term success rates have been shown to be moderate [18]. In addition to tissue removing surgery, the maxillomandibular advancement (MMA) surgery has been found to improve OSA in selected groups of patients [19]. Moreover, in recent years, another surgery typical for the soft palate called palatal implant surgery (Figure 1.2(b)) has been presented [20]. It has the advantage of being a minimal invasive procedure with little discomfort for the patients

and is easily performed under local anesthesia. The main characteristic of the palatal implant surgery is that some pillar shape implants will be inserted into the soft palate through a specific implant system. The typical one is called the Palatal Implant System (Pillar^{TM} System, Restore Medical,St Paul, MN), consisting of an implant device and a delivery part. Through the palatal implant surgery, the stiffness of the soft palate is thought to be increased [20–22].

In general, a complex fluid-solid mechanical interaction governs the mechanical mechanism of OSA, including the fluid mechanics characteristic from the airflow and the solid mechanics behavior for the soft tissue collapse. Recently, computational modeling of the upper airway has been used widely to investigate the corresponding fluid mechanics characteristics, especially using the computational fluid dynamics (CFD) method or the fluid-solid interaction (FSI) method to calculate the velocity and pressure distributions in the upper airway, based on the obtained 3D anatomical geometry [23–25]. 3D patient-specific models based on magnetic resonance (MR) or computed tomography (CT) images can be achieved, using medical image processing software like MIMICS (Figure 1.3(a)). Moreover, the CFD presents as an efficient way to provide useful information to the clinical research, such as providing a result profile to show how the negative pressure distributes in the upper airway (Figure 1.3(b)) and finding the easiest collapse site in the upper airway.

In contrast to the comprehensive and deep study on the airflow features like velocity profile and pressure distribution with CFD and FSI simulations, the solid mechanics study for the soft tissue part remains in the linear elastic realm. For the soft palate, numerical modeling has been addressed to investigate the soft palate's response to the airway negative pressure. Berry et al. [28] presented an approximate 2D cantilever model of the soft palate and the collapse shape of the soft palate was obtained. Malhotra et al. [29] employed a 2D planar model to investigate the closing pressure of the soft palate. In their finite element (FE) model, based on clinical results, a fitted Young's modulus value of soft palate was obtained. Sun et al. [30] presented the movement of soft palate during breathing with a simplified 3D model. These initial studies presented a basic method for modeling, and provided a guide for more comprehensive numerical simulation of the soft palate. However, only the linear elastic behavior was addressed, and more anatomical and physiological simulation should be achieved, in order to represent the obstructive conditions and obtain a more accurate knowledge about the mechanism of the soft palate collapse.

Therefore, in order to design a more general and basic treatment scheme

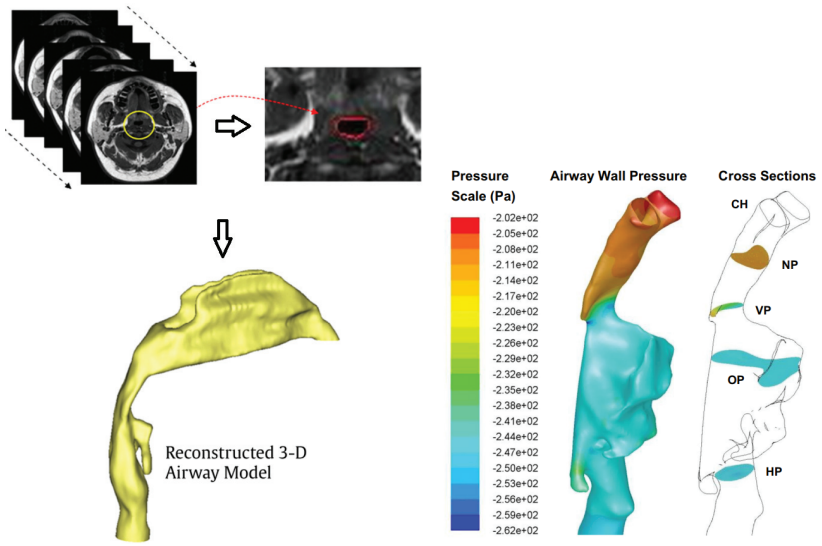

(a) 3D patient-specific modeling

(b) Pressure distribution in the upper airway

Figure 1.3: A 3D reconstruction example for upper airway based on the MR images [26] and an example for using CFD to calculate the upper airway pressure field [27].

in the clinical research, a comprehensive and deep study of biomechanics governing OSA still remains to be achieved, especially for the soft palate collapse. Until now, the mentioned studies for the soft palate's movement, corresponding to the upper airway negative pressure, mainly focus on the linear elastic realm with the 2D or simplified 3D geometry. According to the histology study, the soft palate presents as a complex tissue-layered structure, including the adipose tissue layer, muscle tissue layer and connective tissue layer. Nonlinear properties of the soft palate should be considered. In addition, palatal muscle activation has been pointed out to play a key role in preventing the soft palate from collapse. Moreover, influence of the tongue on the soft palate also remains to be investigated, especially the surface tension of the upper airway mucosal lining liquid has been clarified to produce an influence on the upper airway collapsibility [31].

Then, it motivates us to have a more comprehensive and physiological study of the soft palate with respect to a nonlinear constitutive model and 3D patient-specific geometry. The nonlinear hyperelastic theory and the anisotropic model considering the fiber tissue's strengthening effect can describe a more realistic and physiological mechanical behavior. In addi-

tion, the user subroutine UMAT for ABAQUS can be addressed to achieve efficient numerical implementations for the corresponding improved constitutive models. Existing 3D medical image modeling software like MIMICS also can be used to obtain a 3D anatomical geometry. This provides a foundation to achieve a more anatomically and physiologically representative simulation of the soft palate, which can provide deeper insight in the mechanisms underlying the OSA in the case of the soft palate collapse.

1.2 Aims of this study

The aim of this thesis is to establish a comprehensive numerical modeling framework for the soft palate collapse, associating with constitutive modeling and 3D patient-specific geometry. With this numerical modeling framework, a detailed study of mechanical mechanisms governing the soft palate collapse during OSA can be performed. Improved physiological simulations and mechanical characteristics may contribute to obtaining a deeper insight in the mechanism of the soft tissue collapse in the clinical research. Moreover, numerical simulation of palatal implant surgery illustrates how a biomechanics study result is applied in clinical treatment of OSA.

Chapter 2

Basic theory introduction, histology and 3D geometry

This chapter presents a simple introduction of the continuum mechanics framework, the hyperelastic theory and the corresponding numerical implementation with the user subroutine. Also, a simple introduction of the soft palate histology and the method for 3D patient-specific geometry modeling are also reported.

2.1 Hyperelastic theory and 3D numerical implementation

Hyperelastic material refers to materials where the work is independent of the load path and it is characterized by the existence of a stored strain-energy function, which is a potential function for the stress. Hyperelastic theory extends the calculation to the large strain scale, and nonlinear mechanical behavior is addressed. It is mainly applied to simulate rubber-like materials and soft tissues. It has been shown to be an efficient and accurate way to describe the soft tissue, including isotropic and anisotropic behaviors.

2.1.1 Kinematics

As shown in Figure 2.1, the domain of the body in the initial state is denoted by Ω_0 and called the reference configuration. The domain of the current configuration of the body is denoted as Ω. Assuming the material particle $\mathbf{X}$ with an initial position in Ω_0 moves to the position $\mathbf{x}$ at time t in the current

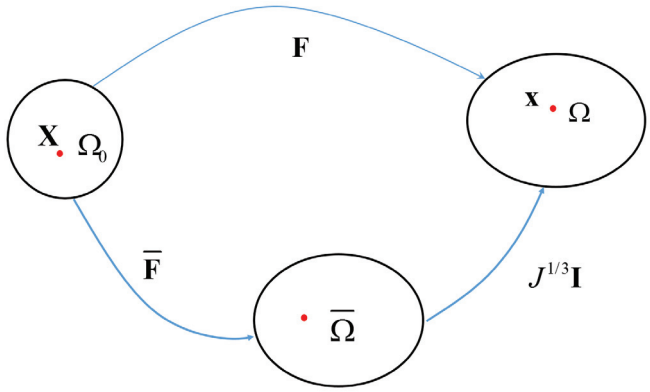

Figure 2.1: Initial and current configuration of a body.

configuration Ω, the deformation gradient can be defined as $\mathbf{F} = \partial\mathbf{x}/\partial\mathbf{X}$ and the modified deformation gradient is calculated as

$$\overline{\mathbf{F}} = J^{-1/3}\mathbf{F}. \tag{2.1}$$

The right and left Cauchy-Green tensors are

$$\mathbf{C} = \mathbf{F}^{\mathrm{T}}\mathbf{F}, \quad \mathbf{B} = \mathbf{F}\mathbf{F}^{\mathrm{T}}, \tag{2.2}$$

respectively. Correspondingly, the modified right and left Cauchy-Green tensors read

$$\overline{\mathbf{C}} = \overline{\mathbf{F}}^{\mathrm{T}}\overline{\mathbf{F}} = J^{-2/3}\mathbf{C}, \quad \overline{\mathbf{B}} = \overline{\mathbf{F}}\overline{\mathbf{F}}^{\mathrm{T}} = J^{-2/3}\mathbf{B}, \tag{2.3}$$

respectively. The principal invariants of the right Cauchy-Green tensor are defined as

$$I_1 = \mathrm{tr}\mathbf{C}, \quad I_2 = \frac{1}{2}\left[(\mathrm{tr}\mathbf{C})^2 - \mathrm{tr}\mathbf{C}^2\right], \quad I_3 = \det\mathbf{C} = J^2. \tag{2.4}$$

The modified forms are calculated as

$$\bar{I}_1 = \mathrm{tr}\overline{\mathbf{C}} = J^{-2/3}I_1, \quad \bar{I}_2 = \frac{1}{2}\left[\left(\mathrm{tr}\bar{\mathbf{C}}\right)^2 - \mathrm{tr}\bar{\mathbf{C}}^2\right] = J^{-4/3}I_2, \quad \bar{I}_3 = \det\overline{\mathbf{C}} = 1. \tag{2.5}$$

On the other hand, the anisotropy arising from fiber families can also be addressed. Assuming a fiber family embedded in the matrix, the direction of the fiber at particle $\mathbf{X}$ in the reference configuration Ω_0 can be defined by a unit vector $\mathbf{a}_0$. Hence, the new fiber direction at the associated particle $\mathbf{x}$

in Ω can be defined by a vector $\mathbf{a} = \mathbf{F}\mathbf{a}_0$. The corresponding modified form is expressed as

$$\bar{\mathbf{a}} = \overline{\mathbf{F}}\mathbf{a}_0. \tag{2.6}$$

The invariant of the fiber term and its modified form are calculated as

$$I_4 = \mathbf{C} : \mathbf{a}_0 \otimes \mathbf{a}_0, \quad \bar{I}_4 = \overline{\mathbf{C}} : \mathbf{a}_0 \otimes \mathbf{a}_0. \tag{2.7}$$

2.1.2 Strain-energy function

The strain-energy function for hyperelastic material can be defined as a function of the invariants (2.4) or (2.5), such as

$$\Psi = \Psi(\mathbf{C}, \mathbf{a}_0 \otimes \mathbf{a}_0) = \Psi(\bar{I}_1, \bar{I}_2, \bar{I}_3, \bar{I}_4) \tag{2.8}$$

For isotropic modeling, there are many choices like the neo-Hookean model, Rivlin model [32], and Ogden model [33]. The anisotropic model considering fiber families also has been achieved, and a commonly used one is the Holzapfel model [34]. In order to show the numerical implementation of the created constitutive model, a transversely isotropic example considering only one direction's fiber family is presented, combining the neo-Hookean model and the Holzapfel model. For a transversely isotropic material, the isotropic part refers to the matrix part and the fibers embedded represent the anisotropic part. The detailed strain-energy function is displayed as,

$$\begin{aligned}\Psi = & \underbrace{c(\bar{I}_1 - 3)}_{\text{isochoric-isotropic}} + \underbrace{\begin{cases} \frac{k_1}{2k_2}[e^{k_2(\bar{I}_4-1)^2} - 1] & \text{if} \quad I_4 \geq 1 \\ 0 & \text{if} \quad I_4 < 1 \end{cases}}_{\text{isochoric-anisotropic}} \\ & + \underbrace{\frac{1}{2}\kappa(J-1)^2}_{\text{volumetric}}.\end{aligned} \tag{2.9}$$

Here, c, k_1 and k_2 are the material parameters, κ is a positive penalty parameter that can fit the model to be nearly incompressible [35]. Note that the muscle fibers only have the strengthening effect when the fibers are stretched, and no additional stiffness produces in the compress condition.

2.1.3 Stress tensor and elasticity tensor

According to the defined strain-energy function, the second Piola-Kirchhoff stress tensor is calculated as the derivation $\mathbf{S} = 2\partial\Psi/\partial\mathbf{C}$. Based on (2.9), the detailed calculation result is:

$$\mathbf{S} = \mathbf{S}_{\text{iso}} + \mathbf{S}_{\text{ani}} + \mathbf{S}_{\text{vol}}, \tag{2.10}$$

with

$$\mathbf{S}_{\text{iso}} = 2c\mathbf{I} : \frac{\partial \overline{\mathbf{C}}}{\partial \mathbf{C}}, \tag{2.11}$$

$$\mathbf{S}_{\text{ani}} = 2k_1(\bar{I}_4 - 1)e^{k_2(\bar{I}_4-1)^2} \frac{\partial \bar{I}_4}{\partial \overline{\mathbf{C}}} : \frac{\partial \overline{\mathbf{C}}}{\partial \mathbf{C}}, \tag{2.12}$$

$$\mathbf{S}_{\text{vol}} = 2\kappa(J-1)\frac{\partial J}{\partial \mathbf{C}}. \tag{2.13}$$

Based on the description in [36], we have

$$\frac{\partial J}{\partial \mathbf{C}} = \frac{1}{2}J\mathbf{C}^{-1}, \quad \frac{\partial \overline{\mathbf{C}}}{\partial \mathbf{C}} = J^{-2/3}(\mathbb{I} - \frac{1}{3}\mathbf{C} \otimes \mathbf{C}^{-1}). \tag{2.14}$$

Here, $\mathbb{I}$ is the symmetric fourth order identity tensor with the index form $(\mathbb{I})_{ijkl} = \frac{1}{2}(\delta_{ik}\delta_{jl} + \delta_{il}\delta_{jk})$. Then, the second Piola-Kirchhoff stress tensor can be calculated as

$$\begin{aligned} \mathbf{S} = \; & 2cJ^{-2/3}(\mathbf{I} - \frac{1}{3}I_1\mathbf{C}^{-1}) \\ & + 2k_1(\bar{I}_4 - 1)e^{k_2(\bar{I}_4-1)^2}J^{-2/3}(\mathbf{a}_0 \otimes \mathbf{a}_0 - \frac{1}{3}\bar{I}_4\overline{\mathbf{C}}^{-1}) \\ & + \kappa(J^2 - J)\mathbf{C}^{-1}, \end{aligned} \tag{2.15}$$

where $\mathbf{I}$ is the second order identity tensor. The Cauchy stress tensor $\boldsymbol{\sigma}$ is obtained by a push-forward operation of the second Piola-Kirchhoff stress $\mathbf{S}$ to the current configuration as

$$\begin{aligned} \boldsymbol{\sigma} = \; & \frac{1}{J}\mathbf{F}\mathbf{S}\mathbf{F}^{\mathrm{T}} \\ = \; & \frac{2c}{J}\text{dev}\overline{\mathbf{B}} \\ & + \frac{2k_1}{J}(\bar{I}_4 - 1)e^{k_2(\bar{I}_4-1)^2}\text{dev}(\bar{\mathbf{a}} \otimes \bar{\mathbf{a}}) \\ & + \kappa(J-1)\mathbf{I}, \end{aligned} \tag{2.16}$$

where dev$(\bullet)$ means the deviatoric part of the second-order tensor $(\bullet)$.

The implementation of the constitutive model in the numerical simulation with finite element method is achieved with the definition of the elasticity tensor (or tangent modulus). The material form elasticity tensor based on the strain-energy function reads

$$\mathbb{C} = 2\frac{\partial \mathbf{S}}{\partial \mathbf{C}} = 4\frac{\partial^2 \Psi}{\partial \mathbf{C}\partial \mathbf{C}}. \tag{2.17}$$

In order to simplify the calculation, the following notations are adopted in the calculation,

$$\overline{\Psi}_i = \frac{\partial \Psi}{\partial \bar{I}_i}, \quad \overline{\Psi}_{ij} = \frac{\partial^2 \Psi}{\partial \bar{I}_i \partial \bar{I}_j}, \quad ij = 1, 4. \tag{2.18}$$

The detailed calculation is displayed as

$$\overline{\Psi}_1 = c, \quad \overline{\Psi}_{11} = 0, \tag{2.19}$$

$$\overline{\Psi}_4 = k_1(\bar{I}_4 - 1)e^{k_2(\bar{I}_4-1)^2}, \tag{2.20}$$

$$\overline{\Psi}_{44} = (1 + 2k_2(\bar{I}_4 - 1)^2)k_1 e^{k_2(\bar{I}_4-1)^2}. \tag{2.21}$$

The calculation can be split into isochoric part and volumetric part, according to the definition of the strain-energy function. For the isochoric part,

$$\begin{aligned} \mathbb{C}_{\text{isochoric}} = \; & 4\overline{\Psi}_{11} \frac{\partial \bar{I}_1}{\partial \mathbf{C}} \otimes \frac{\partial \bar{I}_1}{\partial \mathbf{C}} + 4\overline{\Psi}_1 \frac{\partial^2 \bar{I}_1}{\partial \mathbf{C} \partial \mathbf{C}} \\ & + 4\overline{\Psi}_{44} \frac{\partial \bar{I}_4}{\partial \mathbf{C}} \otimes \frac{\partial \bar{I}_4}{\partial \mathbf{C}} + 4\overline{\Psi}_4 \frac{\partial^4 \bar{I}_4}{\partial \mathbf{C} \partial \mathbf{C}}, \end{aligned} \tag{2.22}$$

where the detailed formulas read

$$\frac{\partial \bar{I}_1}{\partial \mathbf{C}} = J^{-2/3}(\mathbf{I} - \frac{1}{3}\bar{I}_1 \overline{\mathbf{C}}^{-1}), \tag{2.23}$$

$$\begin{aligned} \frac{\partial^2 \bar{I}_1}{\partial \mathbf{C} \partial \mathbf{C}} = & -\frac{1}{3} J^{-2/3}(\mathbf{C}^{-1} \otimes \mathbf{I} + \mathbf{I} \otimes \mathbf{C}^{-1}) \\ & + \frac{1}{9}\bar{I}_1 \mathbf{C}^{-1} \otimes \mathbf{C}^{-1} - \frac{1}{3}\bar{I}_1 \frac{\partial \mathbf{C}^{-1}}{\partial \mathbf{C}}, \end{aligned} \tag{2.24}$$

$$\frac{\partial \bar{I}_4}{\partial \mathbf{C}} = J^{-2/3}(\mathbf{a}_0 \otimes \mathbf{a}_0 - \frac{1}{3}\bar{I}_4 \overline{\mathbf{C}}^{-1}), \tag{2.25}$$

$$\begin{aligned} \frac{\partial^2 \bar{I}_4}{\partial \mathbf{C} \partial \mathbf{C}} = & -\frac{1}{3} J^{-2/3}(\mathbf{C}^{-1} \otimes \mathbf{a}_0 \otimes \mathbf{a}_0 + \mathbf{a}_0 \otimes \mathbf{a}_0 \otimes \mathbf{C}^{-1}) \\ & + \frac{1}{9}\bar{I}_4 \mathbf{C}^{-1} \otimes \mathbf{C}^{-1} - \frac{1}{3}\bar{I}_4 \frac{\partial \mathbf{C}^{-1}}{\partial \mathbf{C}}. \end{aligned} \tag{2.26}$$

For the volumetric part,

$$\mathbb{C}_{\text{vol}} = 2\kappa(J^2 - J)\frac{\partial \mathbf{C}^{-1}}{\partial \mathbf{C}} + 2\kappa(J^2 - J/2)\mathbf{C}^{-1} \otimes \mathbf{C}^{-1}. \tag{2.27}$$

The spatial description of the elasticity tensor $\mathbb{c}$ is defined as the push-forward operation of the material form $\mathbb{C}$, and in the index form it can be presented as [35]

$$c_{ijkl} = J^{-1} F_{iI} F_{jJ} F_{kK} F_{lL} C_{IJKL}. \tag{2.28}$$

The spatial isochoric part based on the above calculation reads

$$\begin{aligned} J\mathbb{c}_{\text{iso}} = \; & 4\overline{\Psi}_{11}\text{dev}\overline{\mathbf{B}} \otimes \text{dev}\overline{\mathbf{B}} \\ & + 4\overline{\Psi}_{1}[-\frac{1}{3}(\mathbf{I}\otimes\overline{\mathbf{B}} + \overline{\mathbf{B}}\otimes\mathbf{I}) + \frac{1}{9}\bar{I}_1\mathbf{I}\otimes\mathbf{I} + \frac{1}{3}\bar{I}_1\mathbb{I}] \\ & + 4\overline{\Psi}_{44}\text{dev}(\overline{\mathbf{a}}\otimes\overline{\mathbf{a}})\otimes\text{dev}(\overline{\mathbf{a}}\otimes\overline{\mathbf{a}}) \\ & + 4\overline{\Psi}_{4}[-\frac{1}{3}(\mathbf{I}\otimes\overline{\mathbf{a}}\otimes\overline{\mathbf{a}} + \overline{\mathbf{a}}\otimes\overline{\mathbf{a}}\otimes\mathbf{I}) \\ & + \frac{1}{9}\bar{I}_4\mathbf{I}\otimes\mathbf{I} + \frac{1}{3}\bar{I}_4\mathbb{I}]. \end{aligned} \tag{2.29}$$

Also, for the volumetric part,

$$J\mathbb{c}_{\text{vol}} = -2\kappa(J^2 - J)\mathbb{I} + 2\kappa(J^2 - J/2)\mathbf{I}\otimes\mathbf{I}. \tag{2.30}$$

2.2 Incompressible plane stress case and the analytical solution

The above formulation is the 3D formulation for the numerical implementation, considering the volumetric part. In addition, the specific incompressible plane stress can be used to obtain the analytical solution of the constitutive model, and the analytical solution can be used to verify the 3D numerical simulation.

2.2.1 Strain-energy function and stress tensor

In the incompressible plane stress case, the strain-energy function (2.9) can be rewritten as:

$$\begin{aligned} \Psi = \; & \underbrace{c(I_1 - 3)}_{\text{isotropic}} + \underbrace{\begin{cases} \frac{k_1}{2k_2}[e^{k_2(I_4-1)^2} - 1] & \text{if} \quad I_4 \geq 1 \\ 0 & \text{if} \quad I_4 < 1 \end{cases}}_{\text{anisotropic}} \\ & + \underbrace{p(J-1)}_{\text{penalty}}. \end{aligned} \tag{2.31}$$

Here, the penalty part can fit the calculation to be the plane stress state and p is the Lagrange parameter. Correspondingly, the second Piola-Kirchhoff

stress is calculated as,

$$\begin{aligned}\mathbf{S} &= \mathbf{S}_{\text{isotropic}} + \mathbf{S}_{\text{anisotropic}} \\ &= 2c\mathbf{I} + 2k_1(I_4 - 1)e^{k_2(I_4-1)^2}\mathbf{a}_0 \otimes \mathbf{a}_0 + p\mathbf{C}^{-1},\end{aligned} \tag{2.32}$$

and the Cauchy stress tensor is

$$\boldsymbol{\sigma} = 2c\mathbf{B} + 2k_1(I_4 - 1)e^{k_2(I_4-1)^2}\mathbf{a} \otimes \mathbf{a} + p\mathbf{I}. \tag{2.33}$$

2.2.2 Equibiaxial test

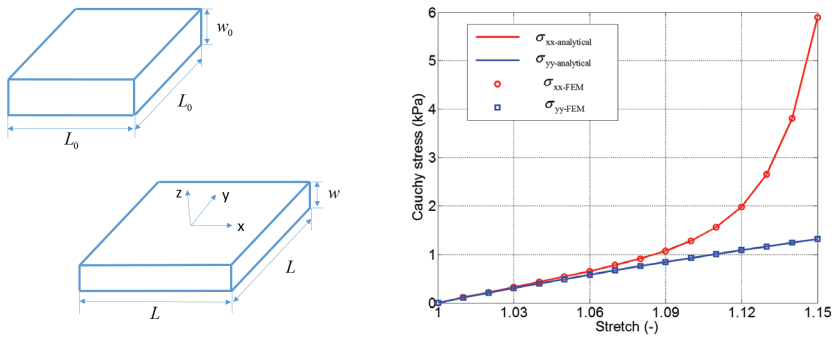

(a) Equibiaxial test

(b) Comparison between the analytical solution and numerical simulation

Figure 2.2: Numerical equi-biaxial test with one single element and its verification with the analytical solution. The numerical simulation implemented with the created stress tensor and elasticity tensor agrees well with the analytical solution.

The equibiaxial test can be used to show the comparison study between the numerical simulation with the 3D formulation and the analytical solution. The fiber strengthening effect can also be presented with the equibiaxial test. Corresponding to the plane stress state, the fiber is distributed in the x direction shown as Figure 2.2(a). According to Figure 2.2(a), the deformation gradient matrix $\mathbf{F}$ in the $x - y - z$ coordinate system reads

$$F = \begin{bmatrix} \lambda & 0 & 0 \\ 0 & \lambda & 0 \\ 0 & 0 & 1/\lambda^2 \end{bmatrix}, \tag{2.34}$$

with $\lambda = L/L_0$ (see Figure 2.2(a)). In order to fit the calculation to the plane stress state, the Lagrange parameter is calculated as

$$p = -2c/\lambda^4. \tag{2.35}$$

Then, the stress component in z direction is equal to 0, corresponding to the plane stress state. The numerical equibiaxial test was run in ABAQUS with a single element. The stretches in the x and y directions were imposed and the element was free to contract in the z direction. The constitutive model described as (2.9) was implemented with a UMAT user subroutine, and an eight noded hybrid element (C3D8H ABAQUS type) was used. The constitutive parameters were set as [37]: $c = 0.877$ kPa, $k_1 = 0.154$ kPa, $k_2 = 34.157$. The simulation results are shown as Figure 2.2(b), the fitted results between the numerical simulation and analytical solution are obtained.

In addition, as shown in Figure 2.2(b), the fiber strengthening effect is presented for the proposed transversely isotropic constitutive model. The nonlinear stress-stretch curve is also presented. This anisotropic nonlinear characteristic is typical for soft tissues with embedded muscle fibers. Soft palate consists of a complex tissue-layered structure. For the material property of the palatal muscle layer, anisotropy should be considered. Then, the above hyperelastic constitutive modeling and its numerical implementation with the user subroutine UMAT can provide an efficient way to characterize the nonlinear behaviors of the soft palate.

2.3 Histology and 3D patient-specific geometry

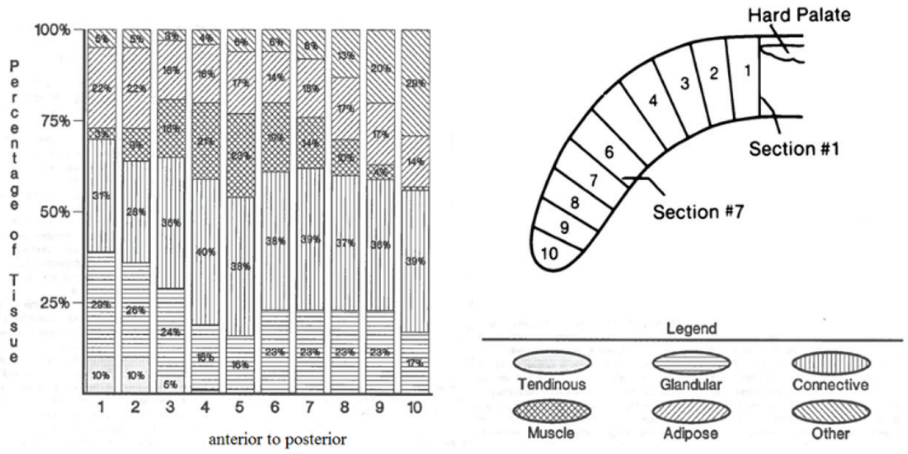

Figure 2.3: Histology study of the soft palate and the tissue composition analysis by Ettema and Kuehn [38].

The histology study of the soft palate shows that a typical adult soft palate consists of several major tissue layers, including the adipose tissue, two middle muscle layers, a superanterior veli palatini tendon layer and an inferior glandular tissue layer [39]. A further quantitative histology study of the human adult soft palate presented the tissue composition [38]. According to their study, the main composition of the soft palate includes the adipose tissue, the glandular tissue, the muscle tissue and the connective tissue (Figure 2.3). Among them, the muscle tissue layer plays a key role in controlling the soft palate's movement, such as the anisotropic characteristic in passive condition and the neurogenic activation in response to the airway negative pressure. In addition, the composition percentage of adipose tissue related with the obesity degree also has a significant influence on developing OSA.

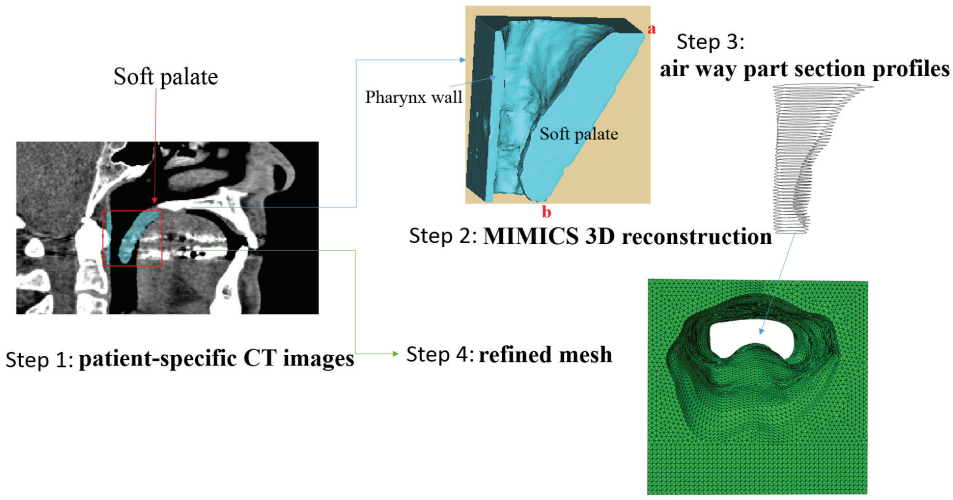

Figure 2.4: 3D geometry reconstruction of the soft palate with respect to the specific patient's CT images and commercial medical image using software MIMICS. The markers "a" and "b" denote the side between the soft palate and the hard palate and the bottom edge of the soft palate tip, respectively. The boundary between the soft palate and tongue is divided manually according to the CT images.

Recently, computational 3D modeling based on CT or MR images has been applied successfully for the upper airway [40, 41]. In this thesis for the soft palate numerical simulation, based on the specific patients' CT images from our research project, we present a way to model the 3D geometry

of the soft palate. Usage of the images was approved by the Norwegian Regional Committee for Medical Research Ethics (REK) and was registered in Clinicaltrials.gov. (NCT01282125).

In detail, first, the DICOM file was imported into the commercial software MIMICS for visualization including the horizontal, vertical and mid-sagittal views. Through some basic operations like segmentation and mask editing, the soft palate was then isolated with some parts of the pharynx wall, in which, the airway in the soft palate region is presented. The meshing capabilities of MIMICS can be used to generate a finite element mesh. However, in this thesis, complex geometry body division is needed, such as different tissue ingredient layers' partition and implants pillars' modeling. The MIMICS generated mesh will lead to an irregular mesh and further modeling difficulties. In order to obtain a smoother mesh, we exported the planar polylines representing the airway and applied a smoothing edit on these polylines. Then, by importing them into ABAQUS, the final geometry were generated and meshed (Figure 2.4). In addition, part of pharynx wall was modeled to determine the collapsing site of soft palate. It is also convenient to carry on some complex partition operations based on this geometry body generated in ABAQUS.

Chapter 3

Methodology

This chapter describes the basic research methodology for this thesis, including five main topics: a tissue composition based nonlinear simulation of the soft palate, the numerical simulation of the palatal implant surgery, a palatal muscle activation model for representing OSA patients' neurogenic impairment effect in response to the upper airway negative pressure, a cohesive model for investigating the adhesion effect from the tongue and a constitutive modeling framework for anisotropic viscoelasticity.

3.1 Tissue composition model

Until now, the soft palate's numerical simulation remains in the linear elastic realm with a defined Young's modulus. However, as the histology study introduced in Chapter 2.3, a complex tissue-layers structure of the soft palate is presented, including the adipose tissue layer, muscle tissue layer, connective tissue layer and glandular tissue layer. Among them, anisotropic mechanical behavior of the muscle fiber should be considered in order to achieve a more accurate simulation result.

In order to investigate the nonlinear behavior for the tissue-layered structure, using the quantitative histology study of the human adult soft palate [38], we divided the soft palate into three main tissue layers (Figure 3.1) each with the specific material property, including the adipose tissue layer, muscle and connective tissue layer and the glandular tissue layer. The hyperelastic models including the isotropic neo-Hookean model and anisotropic Holzapfel model were assigned, according to the mechanical characteristic of each tissue layer. The nonlinear behavior for the global response of the soft plate was presented and the detailed description is reported in appendix-paper 1.

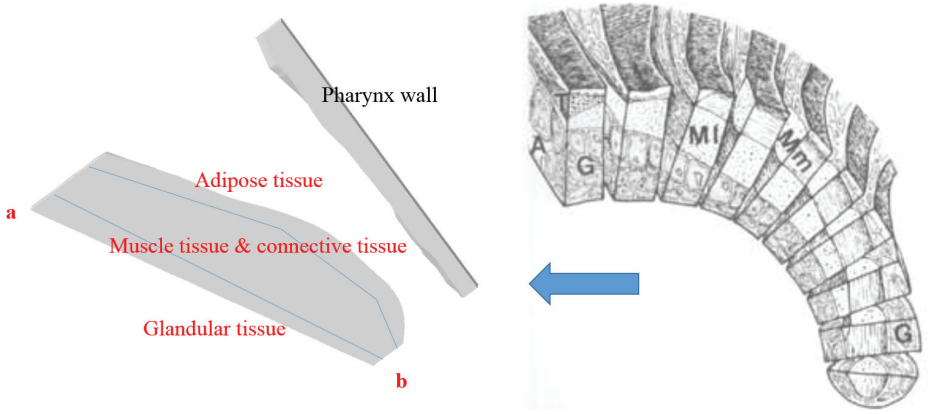

Figure 3.1: Three tissue layer division with respect to the 3D patient-specific model adapted from [39].

3.2 Palatal implants model

How biomechanics can help the medical doctors to improve the treatment of diseases is a topic that has widely been discussed. As mentioned in the background introduction, for OSA (Figure. 1.2(b)), palatal implant surgery, has been applied on some patients. However, for the OSA treatment, the success rate of the current palatal implant surgery varies from different patients, and the efficacy remains to be discussed. It has been pointed out that the overall effectiveness is not confirmed [42]. This conclusion is also supported by some other research works, such as [43] and [44]. Based on the created 3D soft palate model, in this thesis, we present a numerical simulation method to investigate the efficacy of the palatal implant surgery on improving the patients' sleep condition. It also shows a connection between the biomechanics study and the clinical research.

Based on the patient-specific 3D geometry, the pillar shape implants can be inserted numerically. In addition to the used longitudinal direction placement in current clinical surgery, another insertion direction in the transverse direction can be investigated with the 3D numerical simulation (Figure 3.2). The pillar arrangement, described with the array parameters shown as Figure 3.2, varies for different cases according to the published literature on the palatal implant surgery. With respect to the placement direction of pillars and its array parameters, different surgery schemes can be designed and simulated with the created numerical model. The most

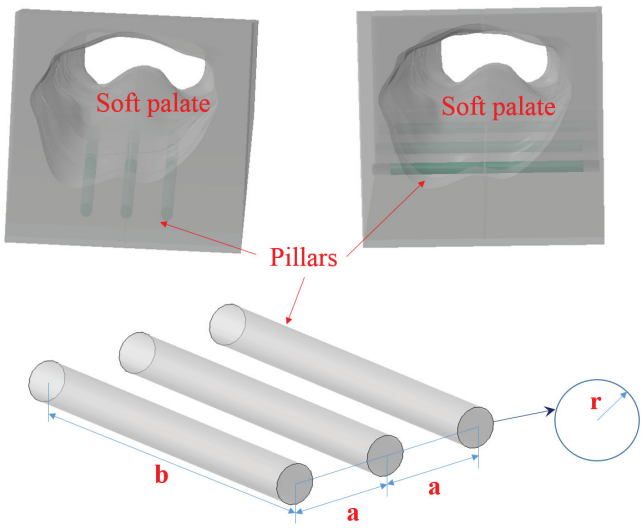

Figure 3.2: 3D numerical model for palatal implant numerical simulation including the longitudinal and transverse directions. The array parameters for the pillars are also presented.

efficient one can be chosen to provide a guide for the clinical doctors to improve the current implant schemes. The detailed description is reported in appendix-paper 2.

3.3 Muscle activation model

As mentioned in the background introduction, the defectiveness of palatal muscle activation in response to the upper airway negative pressure is one of the reasons to cause the soft palate collapse and OSA. Then, a numerical representing model for this defectiveness of the palatal muscle activation contributes to improving the understanding of the neurogenic impairment for OSA.

Numerical modeling of skeletal muscle has been received increased interest in recent years. For phenomenological models, most are based on the Hill model [46] that consists of three elements, including a contractile element with one elastic element in series and one parallel elastic element (Figure 3.3(a)). Odegard et al. [47] presented a constitutive model for skeletal muscle activation using an explicit strain-energy function. Similarly, some other skeletal muscle activation models with respect to the

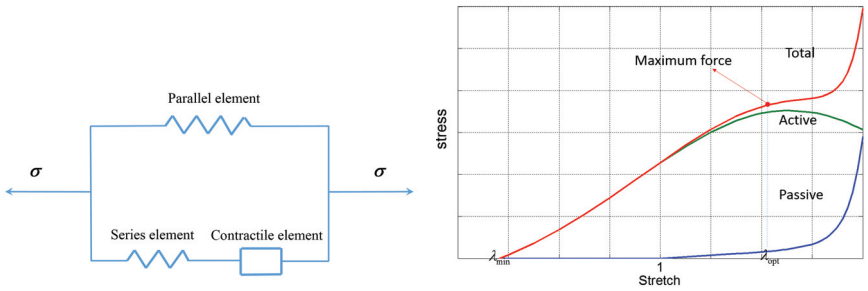

(a) Hill model

(b) A typical muscle activation stretch-stress curve plot adapted from [45]

Figure 3.3: Schematics for the Hill model and a phenomenological stretch-stress curve for muscle activation.

hyperelastic framework can be found, such as [45, 48–50]. A typical activation considered stretch-stress curve is shown as in Figure 3.3(b). Hence, based on the muscle activation phenomenological modeling method, using the hyperelastic theory, a 3D palatal muscle activation model can be created to investigate how the palatal muscle activation works to prevent the soft palate from collapse during sleep. The activation defectiveness for OSA patients also can be investigated. The detailed description is reported in appendix-paper 3.

3.4 Cohesive model

As shown in Figure 1.1, the anterior part of the soft palate contacts the posterior surface of the tongue. The surface tension of the upper airway mucosal lining liquid has an influence on the upper airway collapsibility [31]. The surface tension generated by the mucosal lining liquid between the soft palate and the tongue produces an adhesion force to prohibit the soft palate debonding from the tongue. In order to address the more physiological modeling of the soft palate, how this adhesion force works in the soft palate collapse process remains to be investigated.

Recently, a cohesive approach adhering to the finite element method has been presented to solve some fracture mechanics problems, such as the needle insertion [51] and failure of the brittle rocks [52]. The cohesive approach is based on an elastic traction-separation model where corresponding elastic moduli E are set in the normal and shear directions in the specific cohesive zone (Figure 3.4). The damage process is considered with a critical condi-

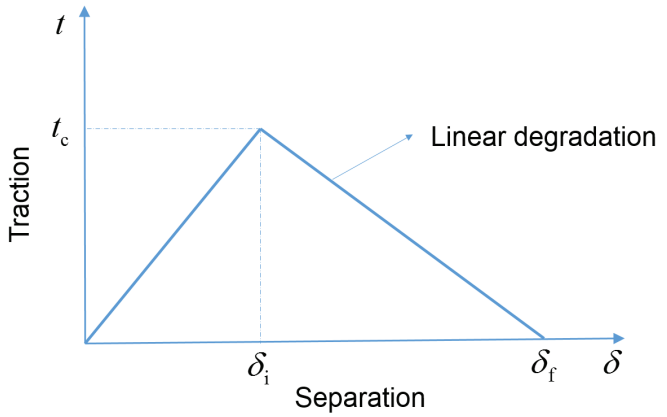

Figure 3.4: Traction-separation model for the cohesive approach, the damage initial separation and failure separation are presented.

tion evaluated with the stress or displacement. When the calculated value fits the critical condition, the damage begins and the debonding process starts. As shown in Figure 3.4, in the damage process, the initial separation corresponds to the critical stress t_c, and failure happens when the separation increases to δ_f. There are some applications of the cohesive approach on biomechanics problems, such as a phenomenological cell-matrix cohesive model recommended by Cóndor and García-Aznar [53], the cohesive model for the arterial dissection presented by Gasser and Holzapfel [54] and Noble et al. [55], a soft material tearing model using the cohesive zone provided by Bhattacharjee et al. [56]. Moreover, the pull-off experimental test for the upper airway lining liquid has been provided by Kirkness et al. [57]. Based on experimental test data and the cohesive approach, the soft palate numerical modeling considering the adhesion effect from the tongue can be achieved. The detailed description is reported in appendix-paper 4.

3.5 Finite strain anisotropic viscoelastic model

Another common biomechanics characteristic for the soft tissue is the viscoelastic property that is characterised by a loading creep behavior in the constant stress condition and a stress relaxation process with a constant strain. Viscoelastic behavior of the soft palate has been observed and a relaxation test has been presented in [58]. However, the anisotropic characteristic was not addressed. In addition, finite strain viscoelastic modeling has been applied in the tissue engineering and polymer simulations. The

finite strain viscoelastic modeling is an extension of the linear viscous theory that can be described by combination of elastic springs and viscous dashpots. The typical characteristic of the finite strain viscoelastic modeling is the multiplicative decomposition of the deformation gradient. This was first provided by Lubliner [59], based on the pioneering work of Green and Tobolsky [60]. According to their method, the deformation gradient can be decomposed into two parts: the elastic part and viscous part. In addition to the decomposition of the deformation gradient, another characteristic of the finite strain viscoelastic models is decomposing the strain-energy function into an equilibrium elastic part and a non-equilibrium viscous part.

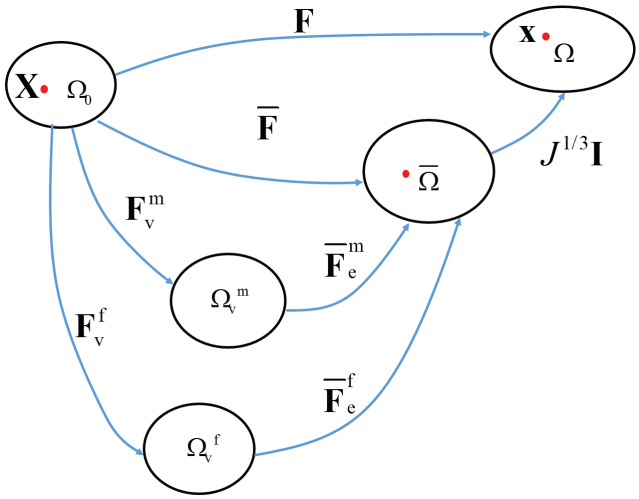

Figure 3.5: Initial and current configuration of a body and the multiplicative decomposition of the deformation gradient $\mathbf{F}$*. Independent matrix and fiber parts are considered.*

Moreover, for the anisotropic material, the anisotropic behavior should be considered. The extension of anisotropy in viscoelasticity has also been proposed in some research works, such as [61] and [62]. In this thesis, considering anisotropy, we put forward a new constitutive model for viscoelstic modeling with a multiplicative decomposition of the deformation gradient as shown in Figure 3.5. A corresponding strain-energy function is defined, as well as the numerical implementation framework including the stress tensor and elasticity tensor. The detailed description is reported in appendix-paper 5.

Chapter 4

Conclusions and future work

4.1 Conclusions

In this thesis, 3D numerical simulations of the soft palate are presented in study of the soft palate collapse, which has been pointed out to cause an obstructive sleeping condition for OSA patients. A patient-specific 3D model provides anatomically representative simulations accounting for more accurate boundary conditions. Nonlinear characteristics of the global response of the soft palate are addressed to investigate the large deformations of the soft palate. Based on the improved constitutive model, the typical mechanical behavior for the soft palate can be represented. According to the work that has been done, the main conclusions can be listed as:

For tissue composition based simulation, comparison of linear and nonlinear simulation of the global response of the soft palate is presented. In the large deformation simulations, the nonlinear properties of soft palate should be considered. In addition, with this anatomical and physiological model, the gravity's influence on the soft palate collapse was investigated. The results show that a side sleep body position alleviates the OSA patients' obstructive sleep condition, and the supine position contributes to the soft palate collapse.

For pillar implants, according to the simulation results, the current longitudinal palatal implant surgery can improve the stiffness of the soft palate, but the efficacy is moderate. This is coherent with the clinical trials that show moderate efficacy on OSA in adults. The influences of the pillars' array parameters are small, but increasing the length of the pillars will increase the strengthening efficacy. In addition, increasing the number of pillars may not be an efficient way. One new discovery is that placement of the implants in the transverse direction strengthens the soft palate much

more than placement in the longitudinal direction. This provides a guide for the clinical doctors to improve the surgery schemes.

For palatal muscle activation, an improved phenomenological constitutive model is provided. The simulation results show that palatal muscular activation inhibits the collapse of the soft palate, when a negative pressure is applied on the upper airway. In addition, the comment from the clinical research that the defectiveness of the palatal muscle stimulus makes the patient's soft palate collapse easier is verified based on the calculation results. This simulation provides a numerical presentation for the OSA patients' palatal muscle defectiveness during sleep, and may provide a guide for the clinical diagnosis and further improved palatal muscle activation modeling study.

For the adhesion effect from the tongue, its influence depends on the length ratio between the cohesive zone and the soft palate. When the contact length is smaller than half of the soft palate length, the adhesion's influence on the global response of the soft palate is very slight, while for a contact length larger than 70% of the length of the soft palate, the adhesion effect makes the closing pressure of the soft palate more negative. However, the improvement rate for the patients is moderate. Hence, in some cases, this adhesion effect from the tongue can be neglected.

Finally, for the viscoelastic constitutive modeling, the presented numerical examples show the proposed constitutive model can describe the anisotropic viscoelastic behavior efficiently. This provides a theoretical basis for further investigation of viscoelastic behavior of the soft palate. When corresponding experimental test data is provided, the constitutive model can be used for model fitting, and subsequent numerical simulation can be achieved.

In summary, this thesis presents a comprehensive numerical simulation framework for the soft palate with patient-specific 3D geometry. An investigation of the soft palate modeling in the solid mechanics realm is provided, including a tissue composition based model showing the nonlinear behavior, the palatal implant surgery simulation providing a method to connect the biomechanics study with the practical clinical research, the numerical model of palatal muscle activation impairment during sleep for OSA patients, the analysis of adhesion effect form tongue and a new constitutive model for anisotropic viscoelastic simulation contributing to the future research.

4.2 Future work direction

Until now, the experimental test data for the soft palate are analyzed assuming linear homogeneous elasticity, including the in vitro test provided in [58] and the in vivo test using MR elastography presented in [63]. This is useful for some simulations when the soft palate's deformation is limited to the small strain level. However, for the large deformation problems, nonlinear and heterogeneous test data contributes to obtaining more accurate and physiological simulation results. Therefore, a more detailed experimental test of the soft palate, focusing on the nonlinear properties, should be a main direction of the future work for improving simulations of the soft palate. In addition, for the tissue composition based simulation, the experimental data for each tissue composition was taken from other locations of the human body. If the specific tissue composition test data for the soft palate, such as the adipose tissue and palatal muscle tissue, can be obtained, the simulation results will be more useful for the clinical research.

In all the simulations presented in this thesis, the loading of the negative pressure has been set to be a uniformly distributed surface pressure. This can be used to simplify the simulation. However, in the real case, the negative pressure on the upper airway distributes not strictly uniformly. A more realistic negative pressure on the pharyngeal surface of the soft palate makes the simulation closer to the real case. This can be achieved with the FSI simulation. Since the collapse of the soft palate belongs to the large deformation problem, and the simulations for FSI now remains in the small strain range, the successful FSI simulation for the large deformation can develop the simulation of the soft palate to a more physiological level. However, it is challenging to solve the problem due to long computational times and numerical convergence problems. In addition, for the boundary conditions applied on the 3D soft palate model, the lateral sides were constrained in all three directions. In the real case, the constraint from the lateral sides' soft tissues may be softer. A more comprehensive investigation for the boundary conditions remains to be addressed in the further study.

Palatal implant surgery has been widely performed in many clinical operations and the efficacy varies among different patients. The transverse scheme tried in the numerical simulation presents to be a more efficient scheme than the current longitudinal placement type. A future work for palatal implants is to find out the most optimal placement scheme using a topology optimization method. With the topology optimization, the placement directions and the array parameters of the pillars can be confirmed for the most efficient scheme. The 3D patient-specific geometry and correspond-

ing biomechanical study provide a basis for this topology optimization.

In the thesis, palatal muscle activation modeling considered only the transverse direction distributed muscle, and the longitudinal muscle uvulae working mainly in the awake condition for speech was neglected. The transverse palatal muscles, including anterior tensor veli palatini, levator veli palatini and palatopharynx muscle, were lumped together in the activation simulation. Therefore, if a more anatomical distribution of these three fiber families can be achieved and modeled, the simulation will be more convincing.

Bibliography

[1] Brooks, D., Horner, R.L., Kozar, L.F., Render-Teixeira, C.L., and Phillipson, E.A. Obstructive sleep apnea as a cause of systemic hypertension. evidence from a canine model. *Journal of Clinical Investigation*, 99(1):106–109, 1997.

[2] Ip, M.S.M., Lam, B., Ng, M.M.T., Lam, W.K., Tsang, K.W.T., and Lam, K.S.L. Obstructive sleep apnea is independently associated with insulin resistance. *American Journal of Respiratory and Critical Care Medicine*, 165(5):670–676, 2002.

[3] Tregear, S., Reston, J., Schoelles, K., and Phillips, B. Obstructive sleep apnea and risk of motor vehicle crash: systematic review and meta-analysis. *J Clin Sleep Med*, 5(6):573–581, 2009.

[4] Strollo Jr, P.J. and Rogers, R.M. Obstructive sleep apnea. *New England Journal of Medicine*, 334(2):99–104, 1996.

[5] Wiegand, L. and Zwillich, C.W. Obstructive sleep apnea. *Disease-a-Month*, 40(4):202–252, 1994.

[6] Miyazaki, S., Itasaka, Y., Ishikawa, K., and Togawa, K. Acoustic analysis of snoring and the site of airway obstruction in sleep related respiratory disorders. *Acta Oto-Laryngologica*, 118(537):47–51, 1998.

[7] Eckert, D.J. and Malhotra, A. Pathophysiology of adult obstructive sleep apnea. *Proceedings of the American Thoracic Society*, 5(2):144–153, 2008.

[8] Schwartz, A.R., Patil, S.P., Laffan, A.M., Polotsky, V., Schneider, H., and Smith, P.L. Obesity and obstructive sleep apnea: pathogenic mechanisms and therapeutic approaches. *Proceedings of the American Thoracic Society*, 5(2):185–192, 2008.

[9] Tangel, D.J., Mezzanotte, W.S., and White, D.P. Influences of nrem sleep on activity of palatoglossus and levator palatini muscles in normal men. *Journal of Applied Physiology*, 78(2):689–695, 1995.

[10] Fogel, R.B., Malhotra, A., Pillar, G., Edwards, J.K., Beauregard, J., Shea, S.A., and White, D.P. Genioglossal activation in patients with obstructive sleep apnea versus control subjects: mechanisms of muscle control. *American Journal of Respiratory and Critical Care Medicine*, 164(11):2025–2030, 2001.

[11] McGinley, B.M., Schwartz, A.R., Schneider, H., Kirkness, J.P., Smith, P.L., and Patil, S.P. Upper airway neuromuscular compensation during sleep is defective in obstructive sleep apnea. *Journal of Applied Physiology*, 105(1):197–205, 2008.

[12] Cheng, E. The effect of continuous positive airway pressure on blood pressure. `https://sites.google.com/site/wcubiol537neglectedstate/change-the-banner/eric-cheng-cpap-sleep-apnea`. Accessed September 20, 2017.

[13] Friedman, M., Vidyasagar, R., Bliznikas, D., and Joseph, N.J. Patient selection and efficacy of pillar implant technique for treatment of snoring and obstructive sleep apnea/hypopnea syndrome. *Otolaryngol-ogyHead and Neck Surgery*, 134(2):187–196, 2006.

[14] Schwartz, A.R., Smith, P.L., Wise, R.A., Gold, A.R., and Permutt, S. Induction of upper airway occlusion in sleeping individuals with subatmospheric nasal pressure. *Journal of Applied Physiology*, 64(2):535–542, 1988.

[15] Han, D., Ye, J., Wang, Q., Yang, J., Lin, Y., and Wang, J. Determining the site of airway obstruction in obstructive sleep apnea with airway pressure measurements during sleep. *The Laryngoscope*, 112(11):2081–2085, 2002.

[16] Kribbs, N.B., Pack, A.I., Kline, L.R., Smith, P.L., Schwartz, A.R., Schubert, N.M., Redline, S., Henry, J.N., Getsy, J.E., and Dinges, D.F. Objective measurement of patterns of nasal cpap use by patients with obstructive sleep apnea. *American Review of Respiratory Disease*, 147(4):887–895, 1993.

[17] Fujita, S., Conway, W., Zorick, F., and Roth, T. Surgical correction of anatomic abnormalities in obstructive sleep apnea syndrome:

Uvulopalatopharyngoplasty. *Otolaryngology-Head and Neck Surgery*, 89(6):923–934, 1981.

[18] Sher, A.E., Schechtman, K.B., and Piccirillo, J.F. The efficacy of surgical modifications of the upper airway in adults with obstructive sleep apnea syndrome. *Sleep*, 19(2):156177, February 1996.

[19] Holty, J.E.C. and Guilleminault, C. Maxillomandibular advancement for the treatment of obstructive sleep apnea: A systematic review and meta-analysis. *Sleep Medicine Reviews*, 14(5):287 – 297, 2010.

[20] Nordgård, S., Wormdal, K., Bugten, V., Stene, B.K., and Skjøstad, K.W. Palatal implants: a new method for the treatment of snoring. *Acta Oto-Laryngologica*, 124(8):970–975, 2004.

[21] Friedman, M., Schalch, P., and Joseph, N.J. Palatal stiffening after failed uvulopalatopharyngoplasty with the pillar implant system. *The Laryngoscope*, 116(11):1956–1961, 2006.

[22] Friedman, M., Vidyasagar, R., Bliznikas, D., and Joseph, N.J. Patient selection and efficacy of pillar implant technique for treatment of snoring and obstructive sleep apnea/hypopnea syndrome. *Otolaryngology-Head and Neck Surgery*, 134(2):187–196, 2006.

[23] Wang, Y. and Elghobashi, S. On locating the obstruction in the upper airway via numerical simulation. *Respiratory Physiology & Neurobiology*, 193:1–10, 2014.

[24] Zhao, M., Barber, T., Cistulli, P., Sutherland, K., and Rosengarten, G. Computational fluid dynamics for the assessment of upper airway response to oral appliance treatment in obstructive sleep apnea. *Journal of Biomechanics*, 46(1):142–150, 2013.

[25] Zhao, M., Barber, T., Cistulli, P.A., Sutherland, K., and Rosengarten, G. Simulation of upper airway occlusion without and with mandibular advancement in obstructive sleep apnea using fluid-structure interaction. *Journal of Biomechanics*, 46(15):2586–2592, 2013.

[26] Mylavarapu, G., Murugappan, S., Mihaescu, M., Kalra, M., Khosla, S., and Gutmark, E. Validation of computational fluid dynamics methodology used for human upper airway flow simulations. *Journal of Biomechanics*, 42(10):1553–1559, 2009.

[27] Wootton, D.M., Sin, S., Luo, H., Yazdani, A., McDonough, J.M., Wagshul, M.E., Isasi, C.R., and Arens, R. Computational fluid dynamics upper airway effective compliance, critical closing pressure, and obstructive sleep apnea severity in obese adolescent girls. *Journal of Applied Physiology*, 121(4):925–931, 2016.

[28] Berry, D.A., Jerald B.M., and Kuehn, D.P. A finite element model of the soft palate. *The Cleft Palate-Craniofacial Journal*, 36(3):217–223, 1999.

[29] Malhotra, A., Huang, Y., Fogel, R.B., Pillar, G., Edwards, J.K., Kikinis, R., Loring, S.H., and White, D.P. The male predisposition to pharyngeal collapse. *American Journal of Respiratory and Critical Care Medicine*, 166(10):1388–1395, 2002.

[30] Sun, X., Yu, C., Wang, Y., and Liu, Y. Numerical simulation of soft palate movement and airflow in human upper airway by fluid-structure interaction method. *Acta Mechanica Sinica*, 23(4):359–367, 2007.

[31] Kirkness, J.P., Madronio, M., Stavrinou, R., Wheatley, J.R., and Amis, T.C. Relationship between surface tension of upper airway lining liquid and upper airway collapsibility during sleep in obstructive sleep apnea hypopnea syndrome. *Journal of Applied Physiology*, 95(5):1761–1766, 2003.

[32] Rivlin, R.S. Large elastic deformations of isotropic materials. iv. further developments of the general theory. *Philosophical Transactions of the Royal Society of London A: Mathematical, Physical and Engineering Sciences*, 241(835):379–397, 1948.

[33] Ogden, R.W. *Non-linear elastic deformations*. Courier Corporation, 1997.

[34] Holzapfel, G.A., Gasser, T.C., and Ogden, R.W. A new constitutive framework for arterial wall mechanics and a comparative study of material models. *Journal of Elasticity and the Physical Science of Solids*, 61(1-3):1–48, 2000.

[35] Prot, V. and Skallerud, B. Nonlinear solid finite element analysis of mitral valves with heterogeneous leaflet layers. *Computational Mechanics*, 43(3):353–368, 2009.

[36] Holzapfel, G.A. *Nonlinear Solid Mechanics. A Continuum Approach for Engineering*. Wiley Chichester, 2000.

[37] Trabelsi, O., Del Palomar, A.P., López-Villalobos, J.L., Ginel, A., and Doblaré, M. Experimental characterization and constitutive modeling of the mechanical behavior of the human trachea. *Medical Engineering & Physics*, 32(1):76–82, 2010.

[38] Ettema, S.L. and Kuehn, D.P. A quantitative histologic study of the normal human adult soft palate. *Journal of Speech, Language, and Hearing Research*, 37(2):303–313, 1994.

[39] Kuehn, D.P. and Kahane, J.C. Histologic study of the normal human adult soft palate. *The Cleft Palate-Craniofacial Journal*, 27(1):26–35, 1990.

[40] Sera, T., Uesugi, K., Yagi, N., and Yokota, H. Numerical simulation of airflow and microparticle deposition in a synchrotron micro-ct-based pulmonary acinus model. *Computer Methods in Biomechanics and Biomedical Engineering*, 18(13):1427–1435, 2015.

[41] Sung, S.J., Jeong, S.J., Yu, Y.S., Hwang, C.J., and Pae, E.K. Customized three-dimensional computational fluid dynamics simulation of the upper airway of obstructive sleep apnea. *The Angle Orthodontist*, 76(5):791–799, 2006.

[42] Steward, D.L., Huntley, T.C., Woodson, B.T., and Surdulescu, V. Palate implants for obstructive sleep apnea: Multi-institution, randomized, placebo-controlled study. *Otolaryngology-Head and Neck Surgery*, 139(4):506–510, 2008.

[43] Maurer, J.T., Sommer, J.U., Hein, G., Hörmann, K., Heiser, C., and Stuck, B.A. Palatal implants in the treatment of obstructive sleep apnea: a randomised, placebo-controlled single-centre trial. *European Archives of Oto-Rhino-Laryngology*, 269(7):1851–1856, 2012.

[44] Choi, J.H., Kim, S.N., and Cho, J.H. Efficacy of the pillar implant in the treatment of snoring and mild-to-moderate obstructive sleep apnea: A meta-analysis. *The Laryngoscope*, 123(1):269–276, 2013.

[45] Ehret, A.E., Böl, M., and Itskov, M. A continuum constitutive model for the active behaviour of skeletal muscle. *Journal of the Mechanics and Physics of Solids*, 59(3):625–636, 2011.

[46] Hill, A.V. The heat of shortening and the dynamic constants of muscle. *Proceedings of the Royal Society of London B: Biological Sciences*, 126(843):136–195, 1938.

[47] Odegard, G.M., Donahue, T.L.H., Morrow, D.A., and Kaufman, K.R. Constitutive modeling of skeletal muscle tissue with an explicit strain-energy function. *Journal of Biomechanical Engineering*, 130(6):061017, 2008.

[48] Johansson, T., Meier, P., and Blickhan, R. A finite-element model for the mechanical analysis of skeletal muscles. *Journal of Theoretical Biology*, 206(1):131–149, 2000.

[49] Tang, C.Y., Zhang, G., and Tsui, C.P. A 3d skeletal muscle model coupled with active contraction of muscle fibres and hyperelastic behaviour. *Journal of Biomechanics*, 42(7):865–872, 2009.

[50] Marcucci, L., Reggiani, C., Natali, A.N., and Pavan, P.G. From single muscle fiber to whole muscle mechanics: a finite element model of a muscle bundle with fast and slow fibers. *Biomechanics and Modeling in Mechanobiology*, pages 1–11, 2017.

[51] Oldfield, M., Dini, D., Giordano, G., and Baena, F.R.y. Detailed finite element modelling of deep needle insertions into a soft tissue phantom using a cohesive approach. *Computer Methods in Biomechanics and Biomedical Engineering*, 16(5):530–543, 2013.

[52] Gui, Y., Bui, H.H., Kodikara, J., Zhang, Q., Zhao, J., and Rabczuk, T. Modelling the dynamic failure of brittle rocks using a hybrid continuum-discrete element method with a mixed-mode cohesive fracture model. *International Journal of Impact Engineering*, 87:146 – 155, 2016.

[53] Cóndor, M. and García-Aznar, J.M. A phenomenological cohesive model for the macroscopic simulation of cell–matrix adhesions. *Biomechanics and Modeling in Mechanobiology*, pages 1–18, 2017.

[54] Gasser, T.C. and Holzapfel, G.A. Modeling the propagation of arterial dissection. *European Journal of Mechanics-A/Solids*, 25(4):617–633, 2006.

[55] Noble, C., Sluis, O., Voncken, R.M.J., Burke, O., Franklin, S.E., Lewis, R., and Taylor, Z.A. Simulation of arterial dissection by a penetrating external body using cohesive zone modelling. *Journal of the Mechanical Behavior of Biomedical Materials*, 71:95 – 105, 2017.

[56] Bhattacharjee, T., Barlingay, M., Tasneem. H., Roan, E., and Vemaganti, K. Cohesive zone modeling of mode i tearing in thin soft materials. *Journal of the Mechanical Behavior of Biomedical Materials*, 28:37 – 46, 2013.

[57] Kirkness, J.P., Christenson, H.K., Wheatley, J.R., and Amis, T.C. Application of the 'pull-off' force method for measurement of surface tension of upper airway mucosal lining liquid. *Physiological Measurement*, 26(5):677, 2005.

[58] Birch, M.J. and Srodon, P.D. Biomechanical properties of the human soft palate. *The Cleft Palate-Craniofacial Journal*, 46(3):268–274, 2009.

[59] Lubliner, J. A model of rubber viscoelasticity. *Mechanics Research Communications*, 12(2):93–99, 1985.

[60] Green, M.S. and Tobolsky, A.V. A new approach to the theory of relaxing polymeric media. *The Journal of Chemical Physics*, 14(2):80–92, 1946.

[61] Nguyen, T.D., Jones, R.E., and Boyce, B.L. Modeling the anisotropic finite-deformation viscoelastic behavior of soft fiber-reinforced composites. *International Journal of Solids and Structures*, 44(25):8366–8389, 2007.

[62] Latorre, M. and Montáns, F.J. Anisotropic finite strain viscoelasticity based on the sidoroff multiplicative decomposition and logarithmic strains. *Computational Mechanics*, 56(3):503–531, 2015.

[63] Cheng, S., Gandevia, S.C., Green, M., Sinkus, R., and Bilston, L.E. Viscoelastic properties of the tongue and soft palate using mr elastography. *Journal of Biomechanics*, 44(3):450–454, 2011.

Paper I

Appendix A

Appended papers

A.1 Paper 1

Tissue composition based nonlinear FEM simulation of the soft palate using patient-specific 3D anatomy

Authors: Hongliang Liu, Victorien Emile Prot, Bjørn Helge Skallerud
Published in MekIT17, Ninth National Conference on Computational Mechanics, Trondheim 11-12 May 2017

Tissue composition based nonlinear FEM simulation of the soft palate using patient-specific 3D anatomy

Hongliang Liu, Victorien Emile Prot, Bjørn Helge Skallerud

Biomechanics Division, Department of Structural Engineering, The Norwegian University of Science and Technology, NTNU, NO-7491 Trondheim, Norway

Abstract

Obstructive sleep apnea syndrome affects a large part of the population. In the current study, modeling and simulation of the response of the soft palate in the upper airway is addressed. A 3 dimensional (3D) patient-specific finite element model is developed based on computed tomography (CT) images. The quantitative histology study of (Ettema and Kuehn, Journal of Speech, Language, and Hearing Research: 37, 303-313, 1994) is used as a basis for soft tissue organization and modeling. The tissue is simplified to consist of three types, each with their specific constitutive models and corresponding parameters: muscle and connective tissue (three cases including the Holzapfel type anisotropic model and neo-Hookean model), adipose tissue (accounting for fiber dispersion according to Holzapfel model), and glandular tissue (neo-Hookean model). The influence of different boundary conditions is also investigated, comparing response obtained with a cantilever plate model and a plate constrained on three sides (corresponding to the actual anatomy). Comparison of homogenous and layered tissue response predictions is provided. Finally, using the patient-specific 3D model, the influence of gravity is examined. The results show that anatomically representative boundary conditions should be accounted for, and that a detailed layered material model may make the simulation more physiological.

Keywords: Soft palate; biomechanics; anisotropy; nonhomogeneous; 3D modeling; tissue composition

1. Introduction

The soft palate is a complex soft tissue structure located at the back of the mouth that prevents food and fluids from entering the nasal cavity during swallowing and guides the airflow through either the mouth or the nose during breathing. In addition, the anatomy and the biomechanical behavior of the soft palate play a key role in understanding Obstructive Sleeping Apnea (OSA) (Cho et al., 2013; Balsevičius et al., 2015). During the upper airway obstruction process with mouth closed, the soft palate comes into contact with the posterior pharynx wall due to the pressure drop and this will close the upper airway and bring corresponding sleeping problems to the patients. Therefore, detailed mechanical modeling of the soft palate in the upper airway (see Fig. 1) may improve our understanding of OSA.

Upper airway models have been used to investigate the air flow features including the pressure distribution and velocity variation using computational fluid dynamics (CFD) simulations (Zhao et al., 2013a; Wang and

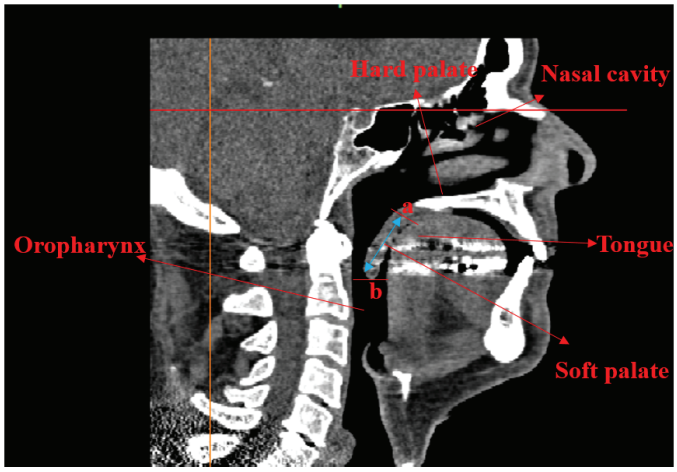

Fig. 1. CT image of the upper airway. The markers "a" and "b" denote the side between the soft palate and the hard palate and the bottom edge of the soft palate tip, respectively.

Elghobashi, 2014) or fluid-solid interaction (FSI) simulations (Zhao et al., 2013b; Pirnar et al., 2015). Additionally, the soft palate's response to the airway's pressure field has been investigated. Berry et al. (1999) presented an approximate 2D cantilever model of the soft palate and the collapse shape of the soft palate was obtained. Malhotra et al. (2002) employed a 2D planar model to investigate the closing pressure of the soft palate. In their finite element (FE) model, based on clinical results, a fitted Young's modulus value of soft palate was obtained. Huang et al. (2007) further developed a partial three dimensional upper airway model including the soft palate in which the midsagittal profile of the soft palate was used. Sun et al. (2007) presented the movement of soft palate during breathing with a simplified 3D soft palate geometry model. All the above research works for the soft palate are based on 2D and simplified 3D models. Therefore, it motivates to create a more accurate anatomic and physiologic model of the soft palate to study pharyngeal collapse, which is one of the key physiological factors for OSA.

Material and geometrical nonlinearities, non-uniform and time varying pressure distribution have to be taken into account in numerical analysis of the global response of the soft palate. FSI procedures using detailed 3D geometries of the upper airway may be successful to obtain a physiological air pressure field. However, this is computationally expensive. Wang et al. (2012) developed anatomically accurate FSI models of the upper airway and soft palate. The deformations of the soft palate obtained in their study were somewhat small and the soft palate was modeled as a homogeneous linear elastic material.

Previous numerical studies of the soft palate have focused on 2D and 3D models with linear elastic homogeneous materials. Linear elasticity may be sufficient under particular conditions (Wang et al., 2012; Pirnar et al., 2015). However, in order to investigate pharyngeal collapse due to the soft palate, analyses of large deformations need to be addressed and thus material nonlinearities accounted for. Additionally, Ettema and Kuehn

(1994) showed that the structure of soft palate resembles a composite material. Hence, the material properties of its different constituents need to be considered.

Muscle activation has an influence on the biomechanical behavior of the soft palate and the neuromuscular response of the soft palate to the airway narrowing was observed by Mortimore et al. (1995). However, during sleep, the OSA patients' neuromuscular response is much smaller than that of normal people (Patil et al., 2007). This neuromuscular compensation defectiveness during sleep for the obstructive sleep apnea patients is further validated by the study of McGinley et al. (2008). A comparison study between the OSA patients group and control normal group showed that the neuromuscular response is smaller in the patient group than for the normal group. Therefore, it may be sufficient to consider only the passive condition for numerical modeling of OSA.

Medical imaging technologies, such as computed tomography (CT) or magnetic resonance (MR) are valuable tools in order to reconstruct the soft palate geometries. These techniques have been used to create upper airway models (Sung et al., 2006; Mihaescu et al., 2008; Mylavarapu et al., 2009; Sera et al., 2015), but soft palate models reconstructed from medical images are scarce (see (Wang et al., 2012)). Therefore, in this study, we present a nonlinear FE model of the soft palate reconstructed from CT images and taking into account material nonlinearities (i.e. hyperelasticity and anisotropy) and heterogeneities. This model is used to investigate the global response of the soft plate of a specific patient suffering from OSA. Our goals are: to provide a guide on how to assign different material properties to the different constituents of the soft palate, to investigate the importance of boundary conditions and anisotropy in such models and to quantify the influence of gravity on the global response of the soft palate. The predicted OSA closing pressures are compared to measured clinical patient data from the literature.

The paper is organized as follows. First, the histology of the soft palate is described, providing a guide to assign material models to different tissues and also pointing out the simplification when one assumes a homogeneous material. Then, simplified 3D and anatomical 3D shape models are presented with corresponding finite element meshes and alternative constitutive models to be employed in the simulations. In addition, the influence of different boundary conditions are provided here. Results from simplified 3D simulations and patient-specific 3D simulations (with different boundary conditions and material models) are then provided, followed by a discussion and concluding remarks.

2. Materials and methods

2.1. Histology

The histology study of the soft palate shows that a typical adult soft palate consists of several major tissue layers including: the oral aspect adipose tissue, two middle muscle layers, a super anterior veli palatini tendon layer and an inferior glandular tissue layer (Kuehn and Kahane, 1990). A further quantitative histology study of the human adult soft palate presented the tissue composition (Ettema and Kuehn, 1994). According to their study, the main composition of the soft palate includes the adipose tissue, the glandular tissue, the muscle tissue and the connective tissue. Therefore, we can divide the soft palate into three layers (Fig. 2): the adipose tissue

top layer, the muscle and connective tissue middle layer and the glandular tissue dominant bottom layer. Other material constituents, contributing with much lower percentages to the soft palate tissue, were lumped into the glandular tissue layer and given the same material properties as for the glandular tissue.

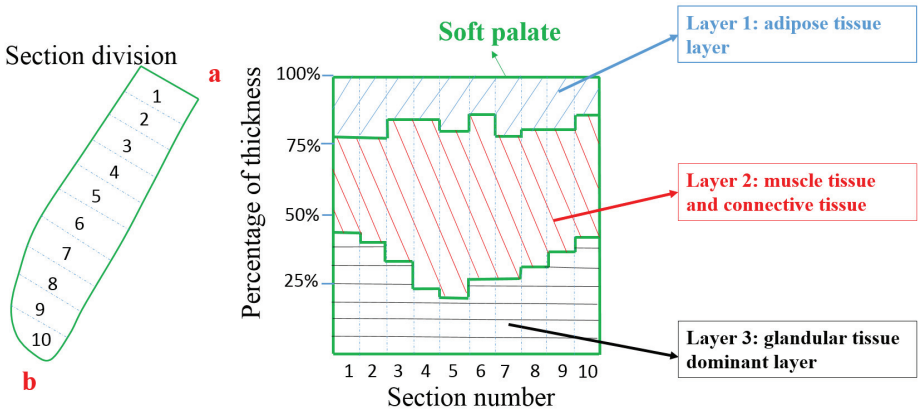

Fig. 2. Tissue composition layers division based on the quantitative histology study of the human adult soft palate (adapted from Figure 10 in the reference paper (Ettema and Kuehn, 1994)). In this reference figure, the percentage composition of each tissue ingredient of soft palate is displayed clearly by dividing the soft palate into 10 sections from the anterior side to the posterior side.

To the authors' knowledge, a detailed tissue composition based 3D nonlinear finite element method (FEM) simulation of the soft palate has not been presented yet. In this study, according to the quantitative histology study for tissue composition, the soft palate is divided into three tissue layers and we will assign a specific material model to each layer. The detailed description will be presented in Section 2.5.

2.2. Simplified 3D geometry

A simplified geometry of the soft palate was obtained based on the CT images of a 68-year-old male patient and his apnea-hypopnea index (AHI) was found to be 22.8. This academic use of the CT images was approved by the Norwegian Regional Committee for Medical Research Ethics (REK) and was registered in Clinicaltrials.gov. (NCT01282125). During CT scan, the patient's body position was calibrated by a medical doctor trying to keep the airway axis normal to the CT scan plane. As shown in Fig. 3, the length, width and the inclination angle were measured manually using the commercial software MIMICS. From these measurements, a simplified geometry was generated by extruding the sagittal midsection profile of the soft palate, see Fig. 4.

2.3. 3D patient-specific geometry

In this section, we present the 3D patient-specific finite element model (Fig. 5) obtained from corresponding computed tomography (CT) images of the patient. First the DICOM file (CT images file) was imported into the

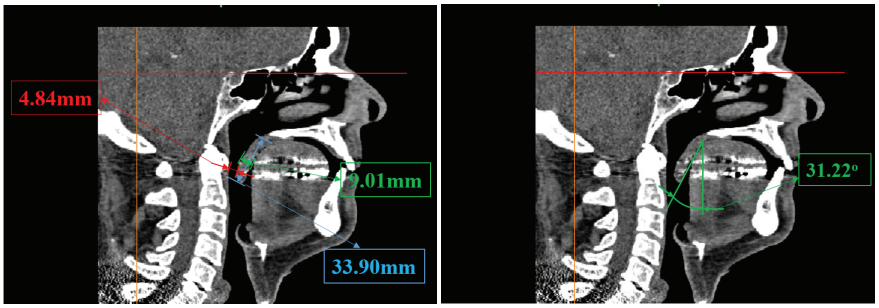

(a) Dimensions of the soft palate

(b) Inclination angle of the soft palate

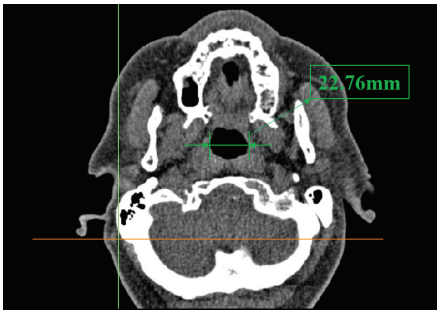

(c) Width of the air way

Fig. 3. Soft palate's CT images from a male patient. The length and the thickness of the soft palate were measured on the medical images using the commercial software MIMICS. In addition, the inclination angle and the width were measured to be 31.22 degree and 22.76 mm, respectively.

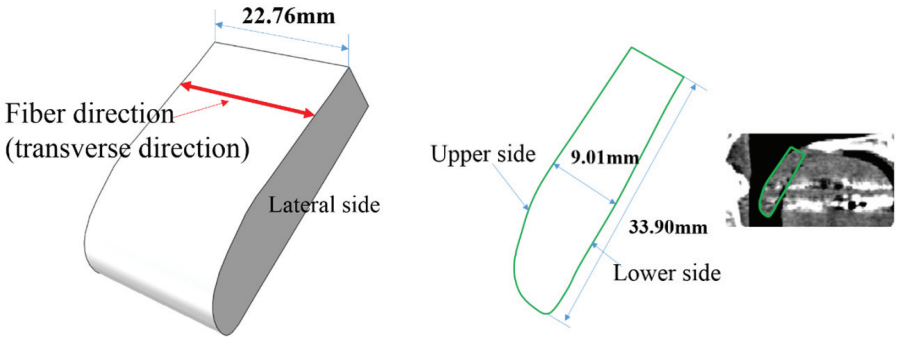

(a) Simplified 3D geometry of soft palate

(b) Sagittal midsection profile

Fig. 4. Simplified geometry modeling through sweeping the midsagittal profile in the transverse direction.

commercial software MIMICS for visualization. Through some basic operations like segmentation and mask editing, the soft palate was then isolated with some parts of the pharynx wall. The meshing capabilities of MIMICS can be used to generate a finite element mesh. In our case, this leads to an irregular mesh and some numerical difficulties in the finite element analyses. In order to obtain a smoother geometry, we exported planar polylines representing the airway for 44 parallel slices every 0.7 mm in the commercial software MIMICS. The polylines were imported into ABAQUS/CAE and the final geometry was generated and meshed through some smooth editing operations.

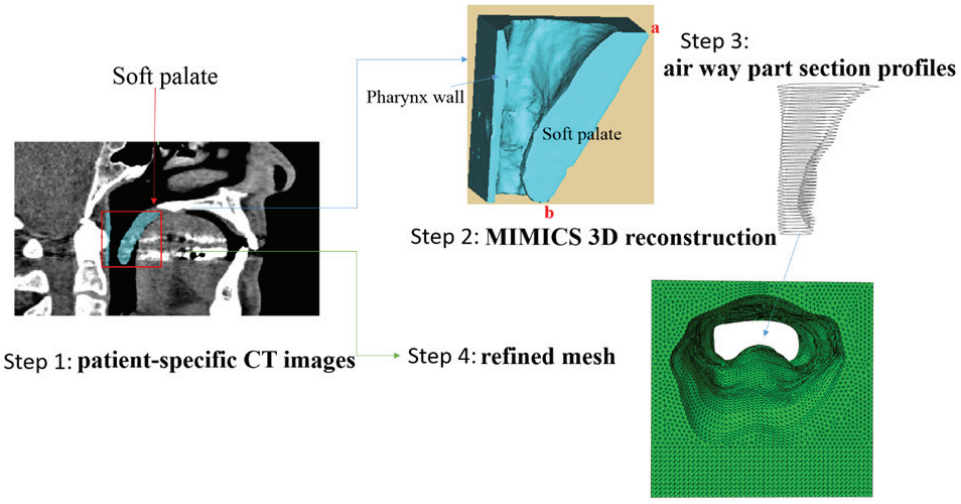

Fig. 5. 3D geometry reconstruction of the soft palate with respect to the specific patient's CT images. The markers "a" and "b" denote the side between the soft palate and the hard palate and the bottom edge of the soft palate tip, respectively.

The 3D model includes the airway in the soft palate region and a part of the pharynx wall to account for the airway's obstruction when the soft palate inclines backward toward the pharynx wall. On the other hand, the geometric boundary between the soft palate and tongue was detected manually according to the CT images. Note that the tongue's influence on the soft palate's biomechanical behavior is neglected in this study.

2.4. Homogeneous tissue assumption material models

We assigned homogenous material properties to our simplified model. In addition, we tested two material constitutive models: an isotropic hyperelastic material model for comparison with different boundary conditions and a transversely isotropic material model to investigate the influence of anisotropy on the global response.

For the isotropic case, we used a neo-Hookean material model defined by the following strain-energy function:

$$\Psi(\bar{I}_1, J) = \underbrace{c(\bar{I}_1 - 3)}_{\text{isochoric}} + \underbrace{\frac{1}{D_1}(J-1)^2}_{\text{volumetric}}. \tag{1}$$

Here, $\bar{I}_1$ is the modified form of the first invariant of the right Cauchy-Green tensor $\mathbf{C}$, and c, D_1 are material parameters derived from the Young's modulus E and Poisson's ratio ν with the following relations (Berry et al., 1999):

$$c = \frac{E}{4(1+\nu)}, \quad D_1 = \frac{6(1-2\nu)}{E}. \tag{2}$$

For the transversely isotropic case, we used the following Holzapfel type strain-energy function:

$$\Psi(\bar{I}_1, \bar{I}_4, J) = \underbrace{c(\bar{I}_1 - 3)}_{\text{isochoric-isotropic}} + \underbrace{\frac{k_1}{2k_2}[e^{k_2(\bar{I}_4-1)^2} - 1]}_{\text{isochoric-anisotropic}} + \underbrace{\frac{1}{D_1}(J-1)^2}_{\text{volumetric}}. \tag{3}$$

Here, $\bar{I}_4 = \mathbf{a}_0 \cdot \overline{\mathbf{C}}\mathbf{a}_0 = \overline{\mathbf{C}} : \mathbf{a}_0 \otimes \mathbf{a}_0$ with $\mathbf{a}_0$ a unit vector defining the fiber orientation in the undeformed configuration, and k_1, k_2 are material parameters.

2.5. Histology based nonhomogeneous material models

In order to treat the soft palate as a nonhomogeneous composite material, based on the quantitative histology study of the human adult soft palate in section 2.1, we divided the patient-specific 3D geometry model (Fig. 5) into three layers. The different components (i.e. adipose, muscle+connective and glandular tissues) material properties were assigned to specific layers of the soft palate model. In order to simplify the calculation, the soft palate model was divided into two parts: the anterior and the posterior parts, each with three tissue layers (Fig. 6). The discrete stepwise tissue distribution in Fig. 2 was smoothed. The connective tissue was lumped with the muscle tissue and the anisotropy was taken into consideration.

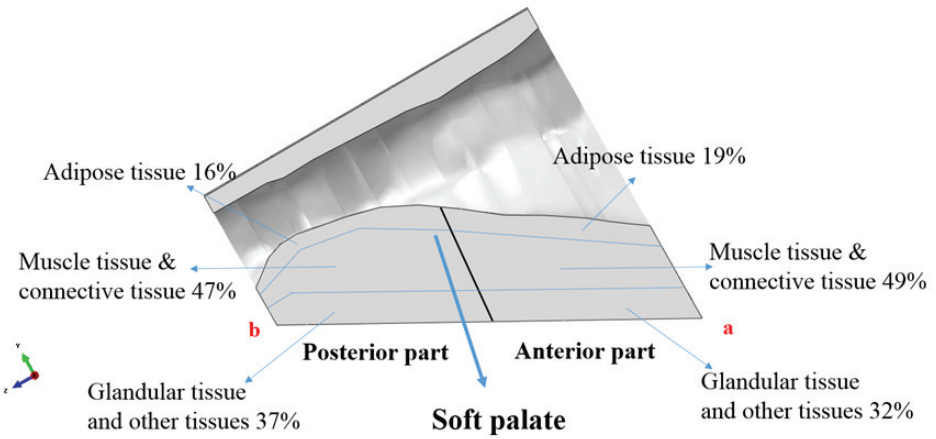

Fig. 6. Schematic of tissue layers based on the quantitative histology study of the human soft palate in the midsection view. The percentage composition of each tissue ingredient was calculated according to Fig. 2 based on the corresponding quantitative histology study (Ettema and Kuehn, 1994).

Muscle and connective tissue

In this study, the passive condition of the muscle tissue is considered to investigate the global response of the soft palate for the OSA patient. The same material property was set to the muscle tissue and the connective tissue. According to the histology study of the soft palate (Kuehn and Kahane, 1990), there are two middle layers mainly consisting of transverse muscle tissue of the levator veli palatini and one longitudinal musculus uvulae fiber layer. Since the longitudinal musculus uvulae mainly controls the motion of uvula in active condition and its percentage composition is smaller than that of the middle transverse levator veli palatini, in this study, we consider only the fiber families in the transverse direction.

Unfortunately, the experimental data for soft palate muscle tissue is still not presented in the literature. However, data of muscle tissue in other parts of the human body is available. The test data of the passive human thigh muscle and brachialis muscle are presented in (Gennisson et al., 2010) and (Affagard et al., 2015). Trabelsi et al. (2010) presented a test of the upper airway trachea muscle. In their experiments, two fiber families were presented, and the one in the longitudinal direction contributes to movements of the trachea during swallowing. This is similar to the levator veli palatini that contracts and elevates the soft palate during swallowing (Matsuo and Palmer, 2008). In detail, the muscle types and the fitted constitutive models for the above three kinds of human muscle tissues are summarized in Table 1. The original data of brachialis muscle provided in the reference paper is the shear modulus. Here, we fitted it to the neo-Hookean model with an assumed Poisson's ratio of 0.49.

Table 1: Human muscle tissue locations and the corresponding constitutive material models previously reported in the literature.

Positions	Constitutive models	Reference papers	Model parameters
Thigh muscle tissue	neo-Hookean model (Eq.(1))	Affagard et al. (2015)	$c = 11.6$ kPa
			$D_1 = 0.0119$ kPa^{-1}
Brachialis muscle tissue	neo-Hookean model (Eq.(1))	Gennisson et al. (2010)	$c = 7.4$ kPa
			$D_1 = 0.00272$ kPa^{-1}
Trachea muscle tissue	Holzapfel type model(Eq.(3))	Trabelsi et al. (2010)	$c = 0.877$ kPa
			$k_1 = 0.154$ kPa
			$k_2 = 34.157$

Based on the obtained parameters of the above fitted constitutive models, uniaxial stretch and stress relationships can be calculated as shown in Fig. 7. The results show different mechanical behaviors for the three human muscle tissues, and the trachea smooth muscle is softer than the skeletal muscles. Therefore, we employ three cases of the muscle tissue to investigate the global response of the soft palate: case 1, case 2 and case 3 correspond to the thigh muscle tissue material property, brachialis muscle tissue material property and trachea muscle tissue material property, respectively. Note that the incompressibility and the anisotropy were considered in case 3 with the Holzapfel type model (Eq. (3)) and the fiber orientation was set to be in the transverse direction.

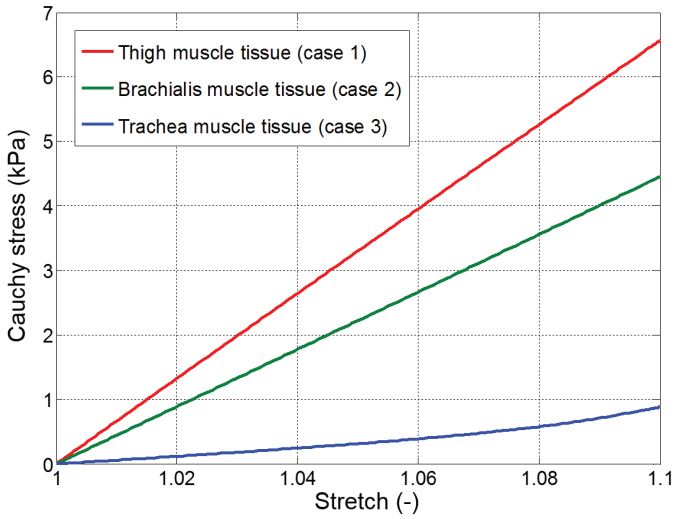

Fig. 7. Uniaxial stretch-stress relationships of the human muscle tissues reported in Table 1.

Adipose tissue

The adipose tissue's main constituent is lipid filled cells called adipocytes. Mechanical data on adipose tissue of the human soft palate are not available. However, data on the mechanical behavior of adipose tissue in other parts of the human body have been reported (Samani and Plewes, 2004; Sommer et al., 2013; Affagard et al., 2015). The types and corresponding constitutive models are summarized in Table 2.

Table 2: Human adipose tissue locations and the corresponding constitutive material models previously reported in the literature.

Positions	Constitutive models	Reference papers	Model parameters
Abdominal adipose tissue	Holzapfel model(Eq.(4))	Sommer et al. (2013)	$c = 0.3$ kPa
			$k_1 = 0.8$ kPa
			$k_2 = 47.3$
			$\kappa = 0.09$
Thigh adipose tissue	neo-Hookean model (Eq.(1))	Affagard et al. (2015)	$c = 0.64$ kPa
			$D_1 = 0.0294$ kPa^{-1}
Female breast adipose tissue	Polynomial model	Samani and Plewes (2004)	$c_{10} = 0.31$ kPa
	$\Psi(\bar{I}_1, \bar{I}_2) =$		$c_{01} = 0.31$ kPa
	$\sum_{i+j=1}^{2} c_{ij}(\bar{I}_1 - 3)^i(\bar{I}_2 - 3)^j$		$c_{11} = 2.25$ kPa
			$c_{20} = 3.8$ kPa
			$c_{02} = 4.72$ kPa

Based on the obtained parameters of the above fitted constitutive models, uniaxial stretch and stress rela-

tionships can be calculated as shown in Fig. 8. The stretch level in the 3D patient-specific soft palate model was estimated to be close to 1.05. As can be seen in Fig. 8, when the stretch is smaller than 1.05, the difference between these three kinds of adipose tissues is small. Moreover, we performed a comparison of global response using the above constitutive material models. The results indicated that the difference in closing pressure between the simulations using the stiffest material property (the abdominal adipose tissue) and the softest material property (the thigh adipose tissue) is smaller than 10%. Therefore, we choose one adipose tissue data

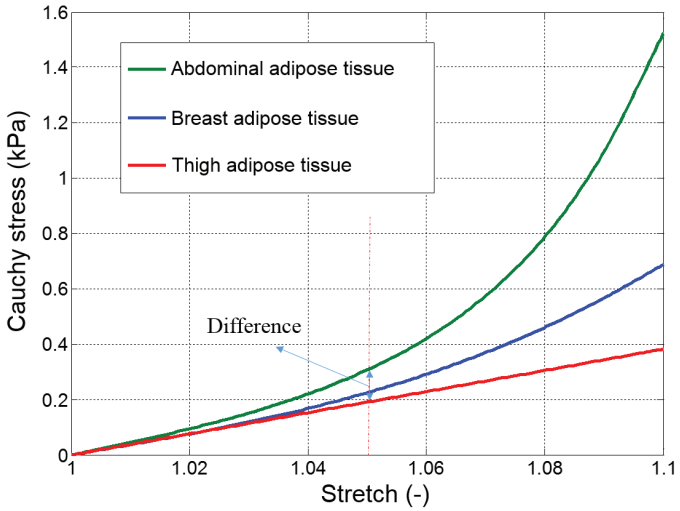

Fig. 8. Uniaxial stretch-stress relationships of the human adipose tissues reported in Table 2.

set to simulate the soft palate. The study of Sommer et al. (2013) is comprehensive and based on a thorough analysis of abdominal adipose tissue. We used the following strain-energy function proposed in their study in the analyses of our soft palate model.

$$\Psi(\bar{I}_1, \bar{I}_4) = \frac{c}{2}(\bar{I}_1 - 3) + \frac{k_1}{k_2}\left(e^{k_2[\kappa \bar{I}_1 + (1-3\kappa)\bar{I}_4 - 1]^2} - 1\right). \tag{4}$$

Here, κ is an anisotropy degree parameter and is used to account for fiber dispersion (Gasser et al., 2006). The corresponding material parameters are shown in Table 2. The mean fiber dispersion direction for the adipose tissue was set to be parallel to the transverse direction. In addition, as the test assumed incompressible material, the adipose tissue was modeled as an incompressible material in our study.

Glandular tissue

We assumed the glandular tissue to be isotropic and the neo-Hookean model described in Eq. (1) was chosen to define its material property. Material properties for in vivo human breast glandular tissue can be found in Li et al. (2015) and Jiang et al. (2015). In addition, Cheng et al. (2011) presented in vivo magnetic resonance elastography measurements of the human soft palate and the shear modulus of the human soft palate was found to be 2.53 kPa. The corresponding Young's modulus and material parameters c and D_1 can be

obtained assuming a Poisson's ratio of 0.49 (Zhu et al., 2012). As Table 3 shows, the difference of the Young's modulus between the human breast glandular tissue and the soft palate is small. This motivates us to use the data of the whole soft palate to define the material properties of the glandular tissue dominant layer.

Table 3: The in vivo material properties of the human breast glandular tissue and soft palate previously reported in the literature.

	Young's modulus (kPa)	Poisson's ratio	c (kPa)	D_1 (kPa^{-1})
Human soft palate Cheng et al. (2011)	7.539	0.49	1.265	0.0159
Breast glandular tissue Li et al. (2015)	6.593	0.49	1.106	0.0182
Breast glandular tissue Jiang et al. (2015)	6.0	0.5	1.0	–

In addition, in the 3D patient-specific geometry model, part of the pharynx wall is included. Because of its influence on the global response of the soft palate is very slight, we assumed its material property to be same as that of the soft palate presented in Table 3.

2.6. Boundary conditions

The simplified 3D model of the soft palate was created to test the different boundary conditions. Two types of boundary conditions were tested. First, according to the previous 2D model of the soft palate proposed by Berry et al. (1999), only the nodes connected to the hard palate were constrained in all directions. This corresponds to a cantilever model. However, according to the anatomy of the soft palate, the lateral sides are connected to the surrounding soft tissue. This means that a cantilever model may not be physiological. Therefore, we tested a second set of boundary conditions where the lateral sides (see Fig. 4) were also constrained. We call it full boundary conditions.

Finally, we applied a uniform pressure field corresponding to the pressure difference between the lower and upper sides of the soft palate (Fig. 4). This pressure drop is called the negative pressure in this study:

$$P_{\text{negative}} = P_{\text{upper}} - P_{\text{lower}}. \tag{5}$$

When the negative pressure develops, the soft palate will have a posterior oblique deformation. If the negative pressure is large enough, the soft palate will stick to the pharynx wall and OSA occurs. We call this critical negative pressure the closing pressure. The specific value for the closing pressure will vary from different patients. According to Han et al. (2002), the closing pressures of OSA patients were estimated to be -4--8 cm H_2O. In addition, the average closing pressure in normal adults was found to be -13 cm H_2O (Schwartz et al., 1988). The negative pressure was applied on the upper surface for the simplified model and on the internal surface of the soft tissue in contact with the airflow for the 3D patient-specific geometry model.

2.7. Finite element mesh

The simplified FE model was meshed with eight noded hybrid solid elements (C3D8H ABAQUS type) and the 3D patient-specific FE model with four noded hybrid tetrahedral elements (C3D4H ABAQUS type). Mesh convergence studies were performed on both models. A -5 cm H_2O negative pressure was applied in both the simplified model and the 3D patient-specific model. The neo-Hookean model with the data of the soft palate (Table 3) was assigned to the simplified model and the layered material model with the thigh muscle tissue's data was used for the 3D patient-specific model.

The displacement magnitude of a point in the mid-section of the soft palate was chosen as a critical parameter and compared for different mesh densities (Fig. 9). For the simplified model, four mesh densities were tested with 10 660, 30 818, 54 280 and 77 688 elements, corresponding to Mesh 1, Mesh 2, Mesh 3, and Mesh 4, respectively. The difference for the critical parameter between Mesh 3 and Mesh 4 was 0.17%. For the patient-specific model, four mesh densities were also tested with 131 403, 313 258, 463 856 and 560 221 elements, corresponding to Mesh 1, Mesh 2, Mesh 3, and Mesh 4, respectively. The difference for the critical parameter between Mesh 3 and Mesh 4 was 0.4%.

Therefore, considering the simulation accuracy and computational time efficiency, we used a mesh composed of 54 280 elements and a mesh composed of 463 856 elements for the simplified model and the patient-specific model, respectively, in the remaining of this paper.

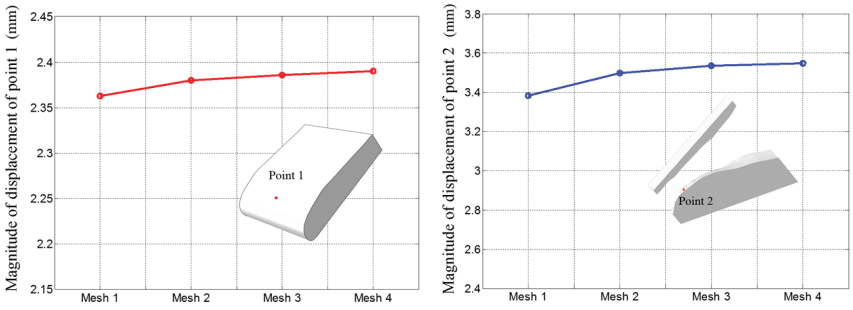

(a) Simplified model (b) 3D patient-specific model

Fig. 9. Mesh size convergence analyses for the simplified model (a) and 3D patient-specific geometry model (b).

3. Results

3.1. Simplified 3D models, homogeneous material, and effect of boundary conditions

First, we compare the global response of the simplified 3D model subjected to the negative pressure using the two types of boundary conditions presented in Section 2.6. In this comparison, the soft palate is modeled as a homogeneous material using the neo-Hookean strain energy function (Eq. (1)) and the material parameters

presented in Table 3. The loading negative pressure was set to be -0.5 cm H_2O (much less negative than the physiological closing pressure). Using the cantilever boundary conditions, the displacement of the tip's posterior surface was found to be 20.55 mm (Fig. 10), which is much larger than the CT measured value 4.84 mm (Fig. 3(a)). On the other hand, when the lateral sides of the soft palate are also constrained, the displacement was found to be 0.26 mm. Therefore, the cantilever model overestimates the displacement of the soft palate.

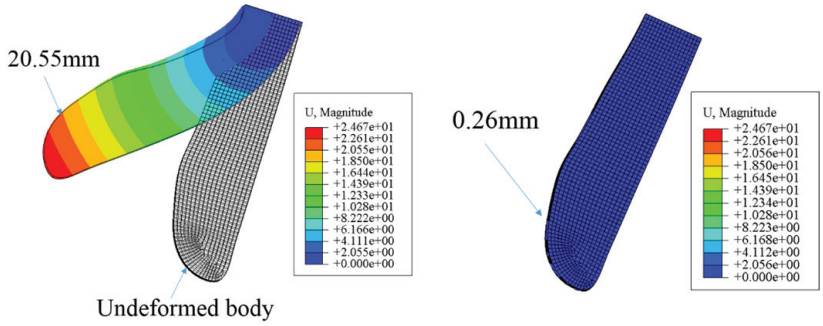

(a) Cantilever boundary conditions (b) Full boundary conditions

Fig. 10. Displacement magnitudes for different boundary conditions with the simplified soft palate model.

Second, we compare the global response of the simplified model when the soft palate is modeled as a homogeneous material using a neo-Hookean material model (Eq. (1)) and a hyperelastic transversely isotropic material model (Eq. (3)). As the fiber stiffness contributes mainly when the deformations are large, in this comparison, we set the negative pressure value to be -5 cm H_2O. Moreover, the fiber direction was defined parallel to the transverse direction (Fig. 4) according to the histology study of soft palate (Kuehn and Kahane, 1990). The mentioned parameters of the transversely isotropic model for case 3 of the muscle tissue in Section 2.5 was used: $c = 0.877$ kPa, $k_1 = 0.154$ kPa, $k_2 = 34.157$. For the neo-Hookean isotropic model, the parameter c was set with the same value ($c = 0.877$ kPa) and the Poisson ratio was set to be 0.49. In this comparison, the full boundary conditions were used.

According to our calculation results (Fig. 11), the displacement of the soft palate is smaller when anisotropy is taken into account, i.e. 3.18 mm versus 3.57 mm. Therefore, it is reasonable to consider the anisotropic property in the large deformation calculation of soft palate.

3.2. Finite element analyses of the patient-specific model with layered tissue properties of the soft palate

Based on the simulation results obtained from the simplified model, we chose to constrain the lateral sides of the soft palate. In addition, the pharynx wall was also constrained considering it is attached to the cervical vertebra. Therefore, the boundary conditions of our patient-specific 3D model were confirmed as Fig. 12. The material models were assigned based on different tissue layers. Note that we tested three cases for the muscle

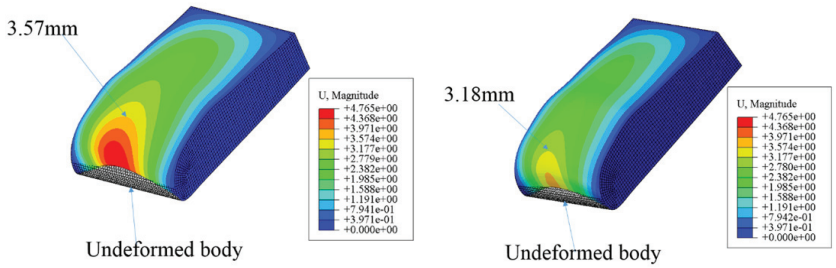

(a) Isotropic constitutive model (b) Anisotropic constitutive model

Fig. 11. Displacement magnitudes for the simplified soft palate model using isotropic and anisotropic constitutive models.

tissue layer's material property. The collapse of the soft palate in the upper airway can be observed directly

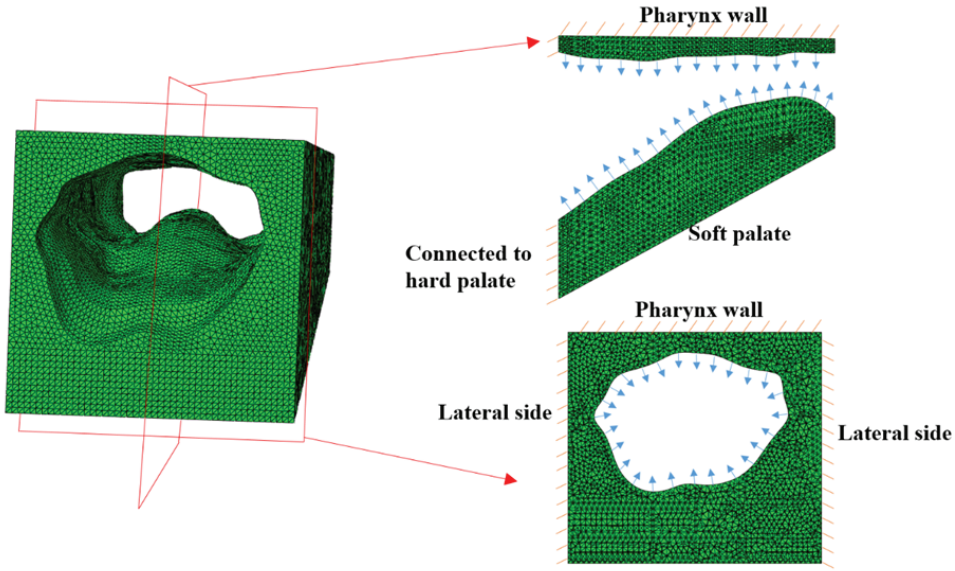

Fig. 12. Boundary conditions for the 3D patient-specific model: the external side of the pharynx wall, the lateral sides and the side connected to the hard palate are constrained in all directions. The negative pressure is set on the tissue-airway contact surface.

in the 3D patient-specific geometry as shown in Fig. 13. Additionally, we used the norm of the displacement of point A to present the inclination displacement of the posterior surface of the soft palate tip, see Fig. 14 (note that the point A is different from the point 2 in Fig. 9(b)). As can be seen from Fig. 15, the norm of the displacement of Point A exhibits a nonlinear behavior. Fig. 15 also shows that the soft palate closing pressure in case 1 is -7.9 cm H_2O, -6.7 cm H_2O in case 2 and -4.4 cm H_2O in case 3. This means that case 1 with

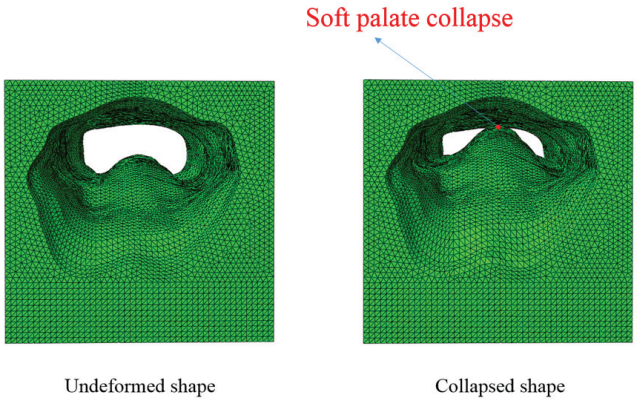

Fig. 13. Collapsed deformation of the 3D patient-specific geometry tissue composition based soft palate model (view from the nasopharynx cavity).

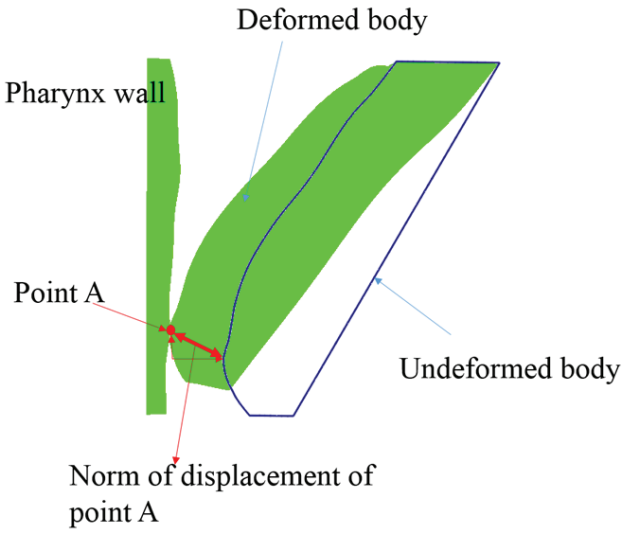

Fig. 14. Definition of point A and of the norm of its displacement in the 3D patient-specific geometry model in the sagittal midsection plane. Point A is defined to be the first point of the soft palate posterior surface to be in contact with the pharynx wall in the sagittal midsection plane. The displacement of point A is used to represent the inclination displacement of soft palate tip's posterior surface.

the stiffest thigh muscle material property has a -3.52 cm H_2O (79.8%) lower closing pressure than the softest case 3 with the trachea muscle tissue's property. Therefore, the closing pressures obtained in the above cases are less negative than the normal adults' closing pressure -13 cm H_2O (Schwartz et al., 1988) and correspond to the clinical research for the OSA patients (Han et al., 2002). Here, the closing pressure is the pressure at which the soft palate posterior surface and the pharynx wall are in contact.

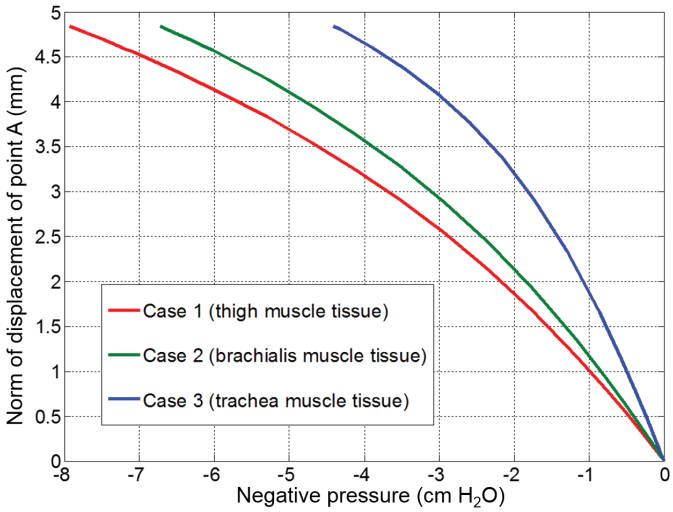

Fig. 15. Negative pressure versus the norm of the displacement of Point A for the 3D patient-specific tissue composition based model including three cases for the muscle tissue properties.

3.3. Comparison between the reference 2D model from Malhotra et al. (2002) and our 3D patient-specific model using an isotropic homogeneous constitutive model

In this section, we compare our 3D patient-specific model with the 2D model presented by Malhotra et al. (2002). In their study, a 2D model of the soft palate for normal adult was created using a linear constitutive model with a Young's modulus of 6 kPa to estimate the soft palate's deformations for different negative pressures in the passive condition. Moreover, the Young's modulus was obtained by fitting the FEM calculation results to clinical data. In this comparison, the material of our 3D patient-specific model is first modeled with a Hookean model using a Young's modulus of 6 kPa and a Poisson's ratio 0.49. Second, using the same Young's modulus and Poisson' ratio, we also model the material with the neo-Hookean model from Eq. (1) and the corresponding material parameters c and D_1 derived from Eq. (2).

According to Malhotra et al. (2002), the closing pressure of their 2D model with the Hookean linear elastic material for a male adult is -5 cm H_2O. On the other hand, in our study, for the 3D model, the closing pressure value is -4.39 mm H_2O (Fig. 16), which is 12.2% less negative than that of their 2D model. This is reasonable, as the patient suffers OSA. Meanwhile, as can be seen from Fig. 16, we observe very similar results concerning the norm of displacement of Point A (see Fig. 14) when using a Hookean elastic material or a neo-Hookean hyperelastic material with our 3D patient-specific model. In addition, the relation between the norm of the displacement of Point A and pressure (Fig. 16) seems to be almost linear in these cases.

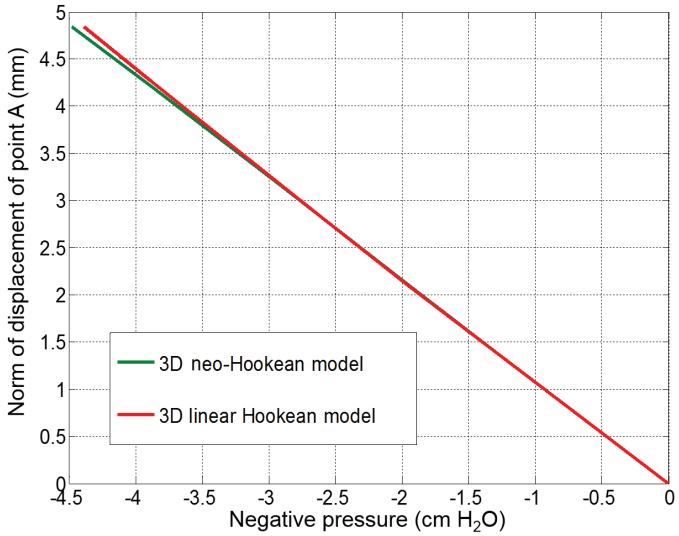

Fig. 16. Negative pressure versus the norm of the displacement of Point A for the 3D patient-specific shape model with the isotropic elastic Hookean model and neo-Hookean hyperelastic model.

3.4. Influence of gravity

To the best of our knowledge, the gravity's influence on soft palate's biomechanical behavior has not been addressed yet. Based on the 3D patient-specific geometry tissue composition model, we investigated the gravity's influence on the global response of the soft palate. Two common body positions were investigated: the lying down and the seated positions (Fig. 17). The tissue's density was set to be 1110 kg/m3 (van der Velden et al., 2016). Since the CT images were recorded with a supine position for the patient, we have considered the lying down position gravity in the above simulation process. Then, we tested the other case that corresponds to the seated position. An inverse lying down direction gravity coupling with the seated direction gravity were applied to the model in an initial load step followed by a second load step where the negative pressure was ramped. This leads to an initial negative displacement of point A compared to the lying down case for zero pressure in Fig. 18. As our simulation results show, the gravity brings different global responses of the soft palate for the tested two body positions. Additionally, for the seated position, a more negative closing pressure is obtained compared with the lying down position. Here, in order to investigate the influence of the gravity on the OSA patient, we used the softest muscle tissue property with the data of the trachea muscle tissue.

4. Discussion

In the present work, we employ a 3D refined mesh FE model of the human soft palate with a patient-specific geometry and inhomogeneous material properties. The geometry is obtained from CT images, taken from one male patient, processed with the commercial software MIMICS. The material properties are assigned according

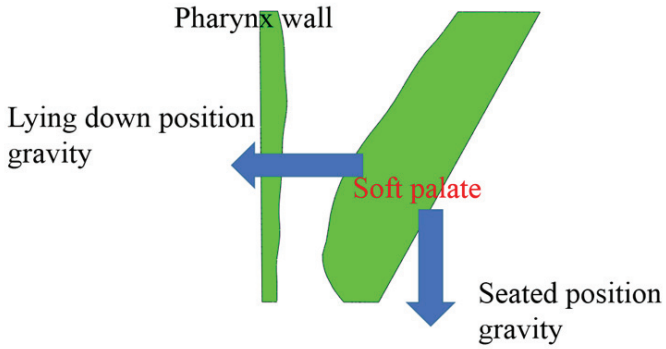

Fig. 17. Gravity's directions applied to the soft palate in the sagittal midsection view corresponding to two positions.

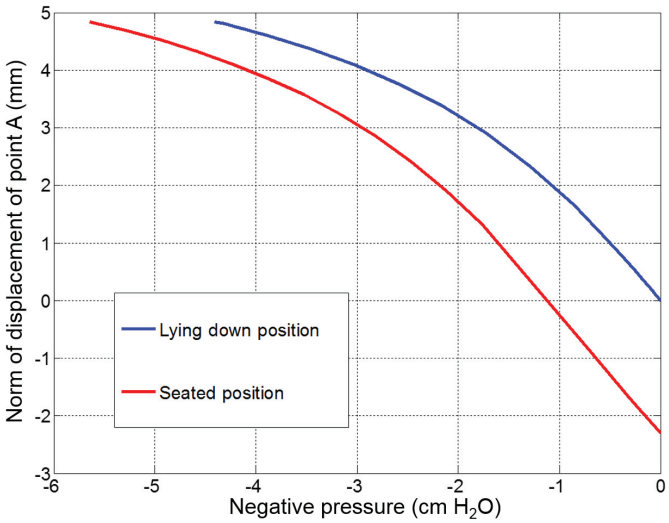

Fig. 18. Negative pressure versus the displacement of Point A for the gravity's influence including two human body positions. The negative displacement means the soft palate has an anterior oblique deformation.

to histology provided by Ettema and Kuehn (1994). Herein, three material layers are considered: the muscle and connective tissue layer, the adipose tissue layer and the glandular tissue dominant layer. The anisotropy of the muscle and connective tissue layer is taken into account (case 3). Comparing the tissue composition based inhomogeneous calculation results (Fig. 15) with the isotropic homogeneous calculation results (Fig. 16), nonlinear behavior occurs in the tissue composition based model.

In addition, we use a simplified 3D model to investigate the influence of the boundary conditions on the global response of the soft palate. Our results show that when the soft palate is modeled as a cantilever plate,

the displacement of the soft palate tip is overestimated (Fig. 10). Therefore, we conclude the influence of the soft tissues surrounding the lateral sides of the soft palate must be accounted for in the FE analysis. Moreover, our simplified model shows that the anisotropy arising from the muscle and connective tissue may have an influence on the global response of the soft palate. In this study, as the corresponding experimental data of the soft palate is not available, we used data retrieved from other parts of the human body to define the material properties of the muscle tissue and adipose tissue. Considering the stretch levels obtained in the soft palate at closing pressure, the difference between the three adipose models is small. For the three muscle models, the difference is larger. However, the closing pressures obtained for this specific OSA patient agree with the clinical research for all muscle model cases employed. In future studies local material experimental tests of the soft palate's muscle tissue and adipose tissue will contribute to acquiring more accurate calculation results. Additionally, we only considered the passive properties of the materials, i.e. muscle activation is not accounted for. We make this assumption based on the following: the presence of neuromuscular compensation defectiveness during sleep for the patient (McGinley et al., 2008). Nevertheless, the influence arising from the muscle activation should be investigated in future work.

The histology study of the soft palate (Kuehn and Kahane, 1990) shows that two muscle fiber layers are imbedded in the soft palate tissue and are mainly distributed in the transverse direction. In our simulation process, the fiber orientation was set in the transverse direction to investigate the influence of the fiber stiffness on the soft palate's biomechanical behavior. In the real case, the fiber may not be strictly distributed in the transverse direction. This needs to be further investigated. In addition, for simplicity, we assumed the muscle tissue and connective tissue have the same material property. More experimental mechanical tests on the different ingredients of the soft palate are needed in order to refine our model.

We defined the pressure drop between the lower surface and upper surface of the soft palate (Fig. 4) as the negative pressure (Eq. (5)). In order to simplify the calculation, we applied the negative pressure as a uniformly distributed load. However, this is not the case in reality. Therefore, fluid-structure interaction analysis may be employed in order to predict a more realistic pressure distribution for the large deformation problems. This will be a task in further studies of the soft palate's biomechanical response. Moreover, in our study, we neglected the influence of the tongue on the deformation of the soft palate. According to the results in Kirkness et al. (2005), a surface tension should be considered for the upper airway tissues. Hence, how this surface tension from the tongue influences the deformation of the soft palate remains to be investigated in further work.

The gravity's influence on two human body positions is estimated. The lying down position seems to increase the motion of the soft palate towards the pharynx wall and the seated position may prevent the soft palate from collapsing. Therefore, considering the gravity influence on the soft palate's global response, we can conclude that the lying down position will make the obstructive situation in the patient's upper airway worse.

Finally, note that the specific patient CT images were obtained from the patient with his mouth closed. With mouth open, the midsection profile and the position of soft palate with respect to the pharynx wall may be different. Hence, the mouth open case needs to be investigated in the future research of the soft palate.

References

Affagard, J., Feissel, P., Bensamoun, S., 2015. Identification of hyperelastic properties of passive thigh muscle under compression with an inverse method from a displacement field measurement. Journal of Biomechanics 48, 4081–4086.

Balsevičius, T., Uloza, V., Sakalauskas, R., Miliauskas, S., Jarutienė, I., 2015. Efficacy of radiofrequency treatment of the soft palate for patients with mild to moderate obstructive sleep apnea hypopnea syndrome: treatment protocol with nine lesions to the soft palate. Sleep and Breathing 19, 1003–1009.

Berry, D., Moon, J., Kuehn, D., 1999. A finite element model of the soft palate. The Cleft Palate-Praniofacial Journal 36, 217–223.

Cheng, S., Gandevia, S., Green, M., Sinkus, R., Bilston, L., 2011. Viscoelastic properties of the tongue and soft palate using mr elastography. Journal of Biomechanics 44, 450–454.

Cho, J., Kim, J., Lee, H., Yoon, J., 2013. Surgical anatomy of human soft palate. The Laryngoscope 123, 2900–2904.

Ettema, S., Kuehn, D., 1994. A quantitative histologic study of the normal human adult soft palate. Journal of Speech, Language, and Hearing Research 37, 303–313.

Gasser, T., Ogden, R., Holzapfel, G., 2006. Hyperelastic modelling of arterial layers with distributed collagen fibre orientations. Journal of the Royal Society Interface 3, 15–35.

Gennisson, J., Deffieux, T., Macé, E., Montaldo, G., Fink, M., Tanter, M., 2010. Viscoelastic and anisotropic mechanical properties of in vivo muscle tissue assessed by supersonic shear imaging. Ultrasound in Medicine & Biology 36, 789–801.

Han, D., Ye, J., Wang, Q., Yang, J., Lin, Y., Wang, J., 2002. Determining the site of airway obstruction in obstructive sleep apnea with airway pressure measurements during sleep. The Laryngoscope 112, 2081–2085.

Huang, Y., White, D., Malhotra, A., 2007. Use of computational modeling to predict responses to upper airway surgery in obstructive sleep apnea. The Laryngoscope 117, 648–653.

Jiang, Y., Li, G., Qian, L., Hu, X., Liu, D., Liang, S., Cao, Y., 2015. Characterization of the nonlinear elastic properties of soft tissues using the supersonic shear imaging (ssi) technique: inverse method, ex vivo and in vivo experiments. Medical Image Analysis 20, 97–111.

Kirkness, J., Christenson, H., Wheatley, J., Amis, T., 2005. Application of the âĂŸpull-offâĂŹforce method for measurement of surface tension of upper airway mucosal lining liquid. Physiological Measurement 26, 677.

Kuehn, D., Kahane, J., 1990. Histologic study of the normal human adult soft palate. Cleft Palate Journal 27, 26–35.

Li, X., Wang, J., Fan, Z., Kang, S., Liu, Y., Zhang, Y., Wang, X., 2015. Determination of the elasticity of breast tissue during the menstrual cycle using real-time shear wave elastography. Ultrasound in Medicine & Biology 41, 3140–3147.

Malhotra, A., Huang, Y., Fogel, R., Pillar, G., Edwards, J., Kikinis, R., Loring, S., White, D., 2002. The male predisposition to pharyngeal collapse: importance of airway length. American Journal of Respiratory and Critical Care Medicine 166, 1388–1395.

Matsuo, K., Palmer, J., 2008. Anatomy and physiology of feeding and swallowing: normal and abnormal. Physical Medicine and Rehabilitation Clinics of North America 19, 691–707.

McGinley, B., Schwartz, A., Schneider, H., Kirkness, J., Smith, P., Patil, S., 2008. Upper airway neuromuscular compensation during sleep is defective in obstructive sleep apnea. Journal of Applied Physiology 105, 197–205.

Mihaescu, M., Murugappan, S., Kalra, M., Khosla, S., Gutmark, E., 2008. Large eddy simulation and reynolds-averaged navier–stokes modeling of flow in a realistic pharyngeal airway model: An investigation of obstructive sleep apnea. Journal of Biomechanics 41, 2279–2288.

Mortimore, I., Mathur, R., Douglas, N., 1995. Effect of posture, route of respiration, and negative pressure on palatal muscle activity in humans. Journal of Applied Physiology 79, 448–454.

Mylavarapu, G., Murugappan, S., Mihaescu, M., Kalra, M., Khosla, S., Gutmark, E., 2009. Validation of computational fluid dynamics methodology used for human upper airway flow simulations. Journal of Biomechanics 42, 1553–1559.

Patil, S., Schneider, H., Marx, J., Gladmon, E., Schwartz, A., Smith, P., 2007. Neuromechanical control of upper airway patency during sleep. Journal of Applied Physiology 102, 547–556.

Pirnar, J., Dolenc-Grošelj, L., Fajdiga, I., Žun, I., 2015. Computational fluid-structure interaction simulation of airflow in the human upper airway. Journal of Biomechanics 48, 3685–3691.

Samani, A., Plewes, D., 2004. A method to measure the hyperelastic parameters of ex vivo breast tissue samples. Physics in Medicine and Biology 49, 4395.

Schwartz, A., Smith, P., Wise, R., Gold, A., Permutt, S., 1988. Induction of upper airway occlusion in sleeping individuals with subatmospheric nasal pressure. Journal of Applied Physiology 64, 535–542.

Sera, T., Uesugi, K., Yagi, N., Yokota, H., 2015. Numerical simulation of airflow and microparticle deposition in a synchrotron micro-ct-based pulmonary acinus model. Computer Methods in Biomechanics and Biomedical Engineering 18, 1427–1435.

Sommer, G., Eder, M., Kovacs, L., Pathak, H., Bonitz, L., Mueller, C., Regitnig, P., Holzapfel, G., 2013. Multiaxial mechanical properties and constitutive modeling of human adipose tissue: a basis for preoperative simulations in plastic and reconstructive surgery. Acta Biomaterialia 9, 9036–9048.

Sun, X., Yu, C., Wang, Y., Liu, Y., 2007. Numerical simulation of soft palate movement and airflow in human upper airway by fluid-structure interaction method. Acta Mechanica Sinica 23, 359–367.

Sung, S., Jeong, S., Yu, Y., Hwang, C., Pae, E., 2006. Customized three-dimensional computational fluid dynamics simulation of the upper airway of obstructive sleep apnea. The Angle Orthodontist 76, 791–799.

Trabelsi, O., Del Palomar, A., López-Villalobos, J., Ginel, A., Doblaré, M., 2010. Experimental characterization and constitutive modeling of the mechanical behavior of the human trachea. Medical Engineering & Physics 32, 76–82.

van der Velden, W., van Zuijlen, A., de Jong, A., Lynch, C., Hoeve, L., Bijl, H., 2016. Acoustic simulation of a patient's obstructed airway. Computer Methods in Biomechanics and Biomedical Engineering 19, 144–158.

Wang, Y., Elghobashi, S., 2014. On locating the obstruction in the upper airway via numerical simulation. Respiratory Physiology & Neurobiology 193, 1–10.

Wang, Y., Wang, J., Liu, Y., Yu, S., Sun, X., Li, S., Shen, S., Zhao, W., 2012. Fluid–structure interaction modeling of upper airways before and after nasal surgery for obstructive sleep apnea. International journal for Numerical Methods in Biomedical Engineering 28, 528–546.

Zhao, M., Barber, T., Cistulli, P., Sutherland, K., Rosengarten, G., 2013a. Computational fluid dynamics for the assessment of upper airway response to oral appliance treatment in obstructive sleep apnea. Journal of Biomechanics 46, 142–150.

Zhao, M., Barber, T., Cistulli, P., Sutherland, K., Rosengarten, G., 2013b. Simulation of upper airway occlusion without and with mandibular advancement in obstructive sleep apnea using fluid-structure interaction. Journal of Biomechanics 46, 2586–2592.

Zhu, J., Lee, H., Lim, K., Lee, S., Teo, L., Wang, D., 2012. Passive movement of human soft palate during respiration: A simulation of 3d fluid/structure interaction. Journal of Biomechanics 45, 1992–2000.

A.2 Paper 2

Paper II

Palatal implant surgery effectiveness in treatment of obstructive sleep apnea: a numerical method with 3D patient-specific geometries

Authors: Hongliang Liu, Mads Henrik Strand Moxness, Victorien Emile Prot, Bjørn Helge Skallerud
Published in Journal of Biomechanics
https://doi.org/10.1016/j.jbiomech.2017.11.006

Palatal implant surgery effectiveness in treatment of obstructive sleep apnea: a numerical method with 3D patient-specific geometries

Hongliang Liu[a], Mads Henrik Strand Moxness[b], Victorien Emile Prot[a], Bjørn Helge Skallerud[a,*]

[a] *Biomechanics Division, Department of Structural Engineering, The Norwegian University of Science and Technology, NTNU, NO-7491 Trondheim, Norway*

[b] *Department of Otolaryngology, Aleris Hospital and the Norwegian University of Science and Technology, department of Neuroscience, Trondheim, Norway*

Abstract

Obstructive sleep apnea (OSA) affects a large percentage of the population and is increasingly recognized as a major global health problem. One surgical procedure for OSA is to implant polyethylene (PET) material into the soft palate, but its efficacy remains to be discussed. In this study, we provide input to this topic based on numerical simulations. Three 3 dimensional (3D) soft palate finite element models including mouth-close and mouth-open cases were created based on three patient-specific computed tomography (CT) images. A simplified material modeling approach with the neo-Hookean material model was applied, and nonlinear geometry was accounted for. Young's modulus for the implant material was obtained from uniaxial tests, and the PET implant pillars were inserted to the 3D soft palate model. With the finite element model, we designed different surgical schemes and investigated their efficacy with respect to avoiding the soft palate collapse. Several pillar schemes were tested, including different placement directions, different placement positions, different settings for the radius and the array parameters of the implant pillars, and different Young's moduli for the pillars. Based on our simulation results, the longitudinal-direction implant surgery improved the stiffness of the soft palate to a small degree, and implanting in the transverse direction was evaluated to be a good choice for improving the existing surgical scheme. In addition, the Young's modulus of the polyethylene material implants has an influence on the reinforcement efficacy of the soft palate.

Keywords: Palatal implants, soft palate, 3D modeling, numerical simulation, obstructive sleep apnea

1. Introduction

Recently, obstructive sleeping apnea (OSA) has become an active research topic due to the increasing prevalence of the disease, with up to 34% of men and 17% of women suffering from this respiratory syndrome (Redline, 2017). Several medical conditions are linked to the development of OSA, with the most significant being hypertension (Brooks et al., 1997), the development of insulin resistance (IP et al., 2002), and the risk for increased daytime sleepiness and motor vehicle accidents (Tregear et al., 2009). In the upper airway, the soft palate's biomechanical behavior plays a key role in the investigation of OSA (Young et al., 2005; Cho et al.,

*Corresponding author
Email address: bjorn.skallerud@ntnu.no (Bjørn Helge Skallerud)

2013). During the upper airway obstruction process, the drop in pressure will result in complete or partial obstructions (Ryan and Bradley, 2005), which, in turn, are responsible for periods of oxygen desaturations and arousals during sleep.

The treatment of OSA is varied and is often based on differences in the individual upper airway anatomy and in the severity of the disease. The conservative line of treatment consists of: physical weight loss and sleep position altering. The interventional line of treatment consists of either some forms of positive airway pressure (CPAP/biPAP), or surgery. CPAP/biPAP treatment inhibits the negative pressure drop by applying a pneumatic splint and has been shown to have high success rates, but the long-term compliance of the patient may be a problem (Kribbs et al., 1993). Surgical therapy by removing redundant tissue is called uvulopalatopharyngoplasty (UPPP) (Fujita et al., 1981), but the long-term success rates have been shown to be moderate (Sher et al., 1996). In addition to tissue-removing surgery, the maxillomandibular advancement surgery (MMA) has been found to improve OSA in selected groups of patients (Holty and Guilleminault, 2010).

In recent years, another surgical treatment called palatal implant surgery has been presented (Nordgård et al., 2004). It has the advantage of being a minimally invasive procedure causing little discomfort for patients and is easily performed under local anesthesia. The main characteristic of palatal implant surgery is that some pillar-shaped implants are inserted into the soft palate through a specific implant system. The typical one is called the Palatal Implant System (Pillar^{TM} System, Restore Medical,St Paul, MN), consisting of an implant device and a delivery part. Through palatal implant surgery, the stiffness of the soft palate is thought to be increased (Nordgård et al., 2004; Friedman et al., 2006a,b). The palatal implant surgery's efficacy as a snoring treatment has been clarified to be ideal (Friedman et al., 2008). However, as an OSA treatment, the success rate of palatal implant surgery varies among patients and the efficacy remains to be discussed. It has been pointed out that the overall effectiveness has not been confirmed (Steward et al., 2008). This conclusion is also supported by some other research works, such as Maurer et al. (2012) and Choi et al. (2013).

Therefore, a study of the efficacy of palatal implants in OSA treatment is of interest. A clinical study requires patient participation, and the study management and outcome validation are complex. However, in recent years, computational biomechanics has been used to simulate the biomechanical behavior of human soft tissue. Huang et al. presented a computational model of the upper airway to estimate the implant surgery success rate and suggested that the computational modeling can be used to predict the efficacy of the clinical implants surgery (Huang et al., 2007). However, only 2D and partial 3D models were presented in their study. Recently, medical imaging technologies, such as computed tomography (CT) or magnetic resonance (MR), have been used to create the upper airway's 3D geometry (Mihaescu et al., 2008; Mylavarapu et al., 2009; Sera et al., 2015).

To achieve more representative anatomical simulations, we present three patient-specific 3D models of the soft palate based on the corresponding CT images including the mouth-close and mouth-open conditions to estimate the efficacy of palatal implant surgery. Additionally, different surgical schemes can be designed and tested including different placement directions of the pillar implants, different radiuses of the pillars, and

different interval spaces between the pillars. In comparing the efficacy of different schemes, we can determine the most efficient surgical scheme. The objective of this study was to employ 3D patient-specific geometries of the soft palate and numerical simulations to determine how different pillar insertions affect the soft palate stiffness. Procedures providing increased stiffness may improve the OSA state for the patients. The comparison of different surgical schemes may provide a guide for medical doctors to improve current treatments.

2. Materials and methods

2.1. Pillar implants surgery schemes

Table 1. Summary of palatal implants surgeries for OSA with different array parameters of the pillars previously presented in the literature

Reference	Orientation	a (mm)	b (mm)	r (mm)
Nordgard et al. (2006)	Longitudinal	5	18	0.75
Goessler et al. (2007)	Longitudinal	No data	18	1
O'Connor-Reina et al. (2008)	Longitudinal	3	18	0.75
Walker et al. (2006)	Longitudinal	2	18	0.9
Friedman et al. (2006b)	Longitudinal	3	Entire length (25)	No data

Table 2. Summary of designed surgical schemes in this study. Implant positions are described in Fig. 2 (A) for the longitudinal orientation and in Fig. 2 (B) for the transverse orientation.

No.	Position	a (mm)	b (mm)	r (mm)	orientation	Number of pillars	E (MPa)
Scheme 1	Anterior	5	18	0.75	Longitudinal	3	244
Scheme 2	Anterior	2	18	0.75	Longitudinal	3	244
Scheme 3	Anterior	5	25	0.75	Longitudinal	3	244
Scheme 4	Anterior	5	18	1	Longitudinal	3	244
Scheme 5	Anterior	5	25	1	Longitudinal	3	244
Scheme 6	Anterior – proximal	5	25	0.75	Transverse	3	244
Scheme 7	Anterior – distal	5	25	0.75	Transverse	3	244
Scheme 8	Anterior – proximal	5	25	1	Transverse	3	244
Scheme 9	Anterior – distal	5	25	1	Transverse	3	244
Scheme 10	Anterior	5	25	0.75	Longitudinal	3	2
Scheme 11	Anterior – distal	5	25	0.75	Transverse	3	2
Scheme 12	Posterior	5	18	0.75	Longitudinal	3	244
Scheme 13	Anterior	5	18	0.75	Longitudinal	5	244

In general, the common palatal implant surgical scheme presented in the literature involves three pillar-shaped implants (a segment of braided polyethylene terephthalate [PET]) implanted into the soft palate from

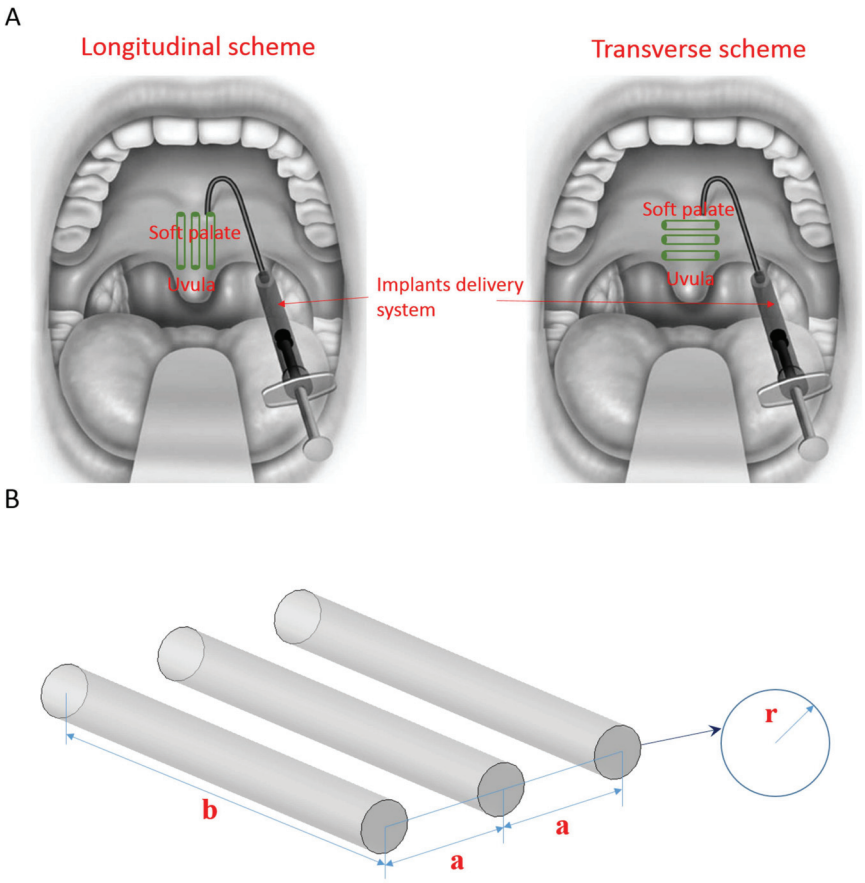

Fig. 1. Schematic of the palatal implant surgery: (A) the longitudinal and transverse implant surgeries adapted from the reference paper (Friedman et al., 2006b), (B) the array parameters for the pillar shape implants, the parameters a, b, and r denote the interval space, the length and the radius, respectively

the anterior side to the posterior side (see Fig. 1 (A)) with an implants delivery device. Up to now, the presented surgical schemes have all chosen the longitudinal implant type. In this study, we also investigated the alternative transverse-direction implant surgery (Fig. 1 (A)) with the finite element (FE) model.

In addition to the different implant directions, the array parameters (Fig. 1 (B)) of these three implants pillars also remained to be tested to investigate the efficacy of palatal implant surgery. Some of the surgical schemes from the literature for these three parameters are listed in Table 1. To surgically place the pillars into soft tissue with moderate trauma, the diameter cannot be too large. An implant diameter of 1.5-2 mm is optimal

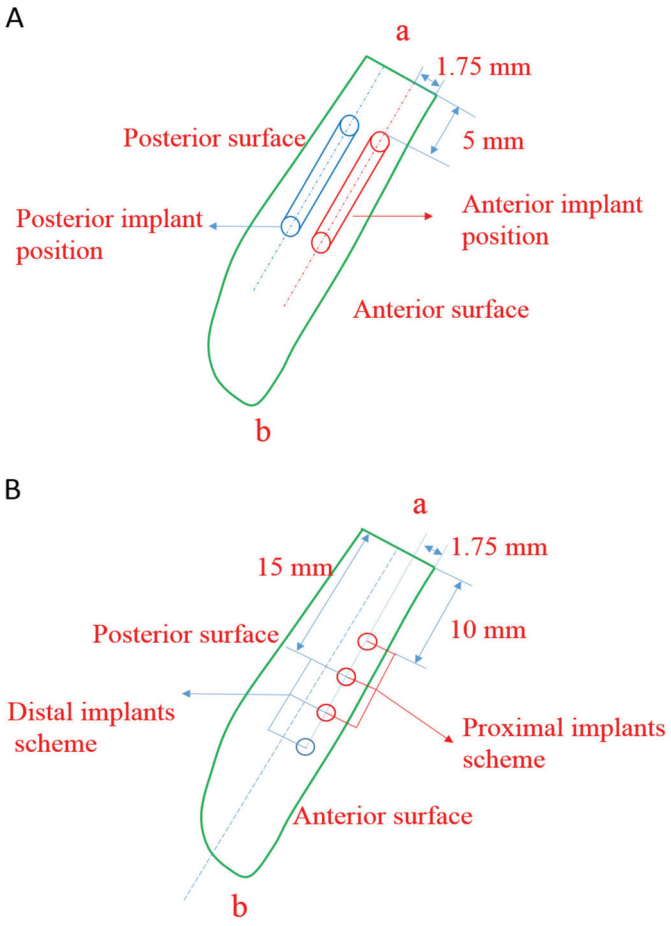

Fig. 2. Placement positions of the pillars. (A) Schematic of the longitudinal implant surgery with the midsagittal view of soft palate. The pillars had a 5 mm interval to boundary section between the soft palate and the hard palate (Friedman et al., 2006b). (For patient 2, due to the complex geometry, this interval was set to be 2 mm when the pillars' length is set to be 25 mm.) The distance between the centerline of the pillars and the anterior surface was set to be 1.75 mm for the anterior scheme and 6.75 mm for the posterior scheme. (B) Schematic for the proximal and distal place positions in the transverse-direction case with the midsagittal view of the soft palate. 10 mm interval and 15 mm interval to the section connected to the hard palate were used for the proximal and distal positions, respectively. Note that the uvula part was distinguished in the 3D models and transverse-placement positions of the pillars were deviated from the uvula part.

for a feasible insertion needle that does not cause unnecessary harm. The length of the pillars is typically set to 18 mm, which is approximately 50% of the mean length of the soft palate (37-45 mm) (Kurt et al., 2011; Lim et al., 2017). This ensures that the placement of the pillars with the cylindrical tube does not protrude into the distal end or interfere with the bony periosteal layer of the hard palate. In Table 1, in one case, the implants are

inserted along the entire length of the soft palate (Friedman et al., 2006b). This means the implants are inserted as deeply as possible until they approach the posterior surface of the soft palate.

As Fig. 2 shows, different placement positions were investigated. In addition, the influences of the number of pillars and the Young's modulus of the implants were evaluated with our numerical 3D model. In total, the summary of the tested schemes are listed in Table 2.

2.2. Numerical modeling

2.2.1. 3D patient-specific geometry

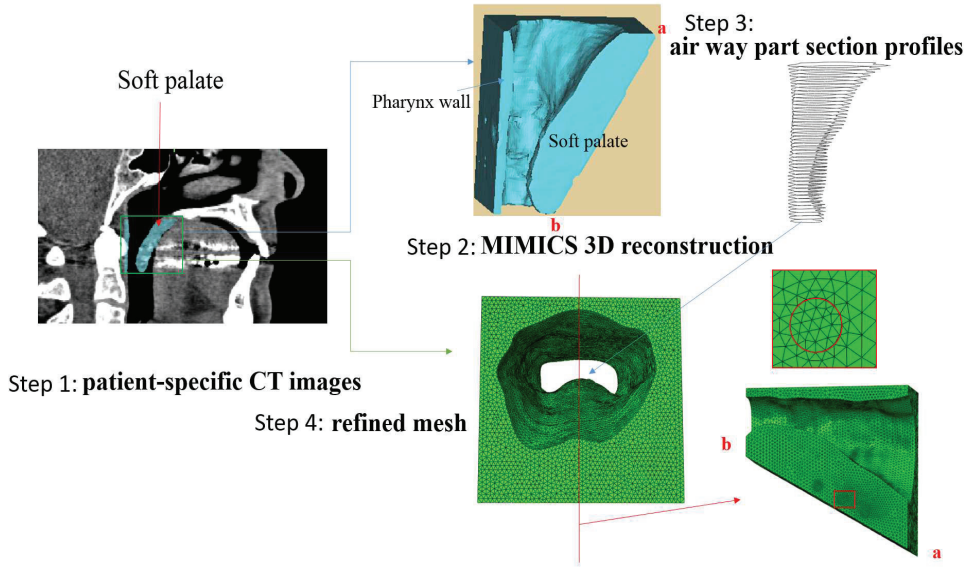

Fig. 3. 3D geometry reconstruction of the soft palate with respect to patient 1's CT images and Mimics. The markers 'a' and 'b' denote the side between the soft palate and the hard palate and the distal edge of the soft palate, respectively. In addition, a refined mesh was assigned to the pillars in the 3D FE model.

Table 3. Anatomy information of the soft palate for three patients. The thickness is the average of three sections along the length, and the length is the distance between 'a' and 'b' (Fig. 3). Note that, the width denotes the width of the airway in the section connected to the hard palate. Body mass index (BMI) and apnea hypopnoea index (AHI) are included.

No.	Gender	Age	Condition	Thickness (mm)	Length (mm)	Width (mm)	BMI	AHI
Patient1	Male	67	Mouth – close	9	34	23	28.4	22.8
Patient2	Male	44	Mouth – close	10	36	24	31.4	22.4
Patient3	Male	43	Mouth – open	8	37	30	24.3	18.0

In this study, based on the specific patients' CT images, we presented a way in which to model the soft palate. The academic use of these images was approved by the Norwegian Regional Committee for Medical

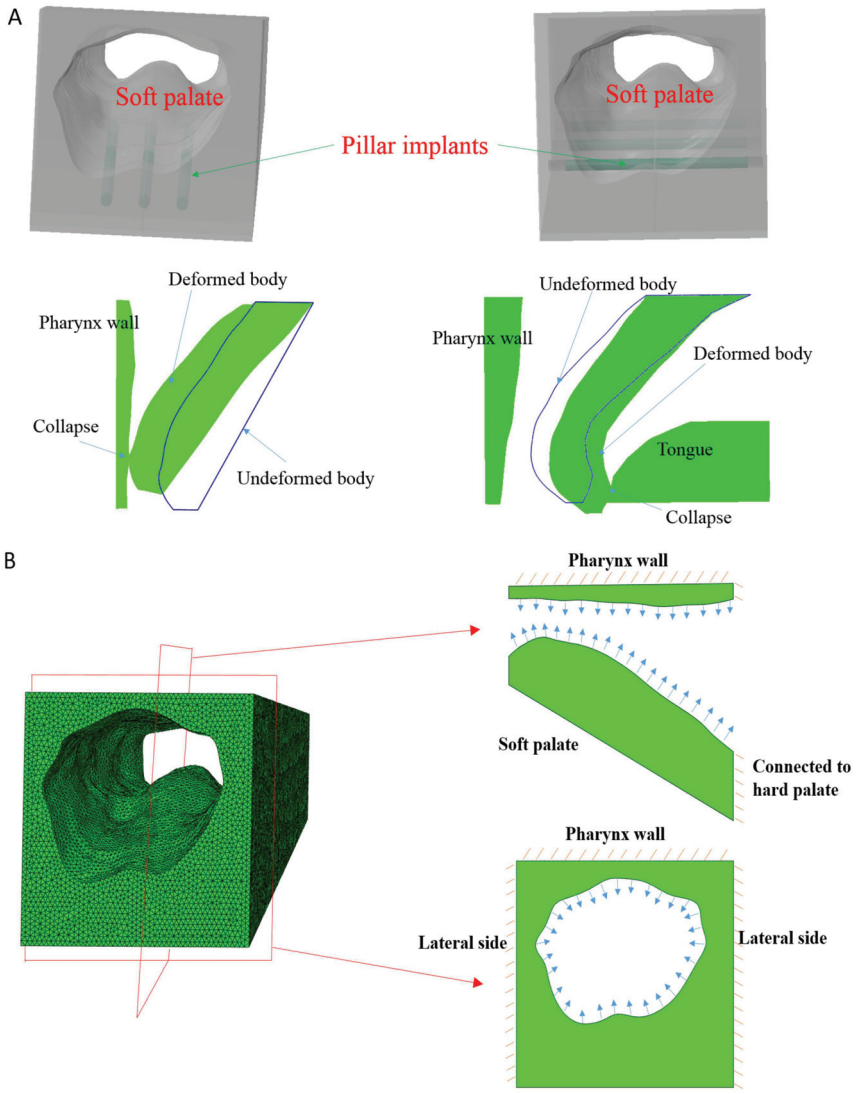

Fig. 4. 3D numerical modeling: (A) schematic of the implants region partition in the 3D model for the longitudinal case (up-left) and transverse case (up-right) and the collapse of the soft palate including the mouth-close condition (down-left) and mouth-open condition (down-right) with the midsagittal view of soft palate, (B) boundary conditions for the numerical model of the soft palate, the external surface of the pharynx wall, the lateral sides and the side connected to the hard palate were constrained in all directions, and the negative pressure was distributed on the inner airway surface.

Research Ethics (REK) and was registered at Clinicaltrials.gov. (NCT01282125). To have a feasible study, three patients' CT images were used. Many OSA patients have been found to breathe with mouth open during

sleep, and mouth-open breathing during sleep has been clarified to be a risk factor for causing OSA (Lee et al., 2007; Kim et al., 2011). Therefore, the mouth-open (patient 3) sleep condition was also investigated. The soft palate anatomy characteristics and demographic information of these three patients are listed in Table 3.

In detail, for 3D modeling, first, the DICOM file was imported into the commercial software MIMICS. Through some basic operations such as segmentation and mask editing, the soft palate was then isolated with some parts of the pharynx wall. To obtain a smoother geometry and refined mesh, we exported the planar polylines representing the airway and applied a smoothing edit on these polylines. Then, through importing them into ABAQUS, the final geometry was generated and meshed (Fig. 3). The modeling method for patient 2 and 3 is the same as that for patient 1 shown in Fig. 3.

The 3D model includes the airway in the soft palate region and a part of the pharynx wall to account for the airway's obstruction (Fig. 4 (A)). The geometrical boundary between the soft palate and tongue was determined manually according to the CT images, and the tongue's influence on the soft palate's biomechanical behavior was neglected in this study. For the mouth-open condition, the soft palate moved in the anterior direction toward the tongue. Then, part of the tongue was modeled for patient 3 (Fig. 4 (A)). The modeling of the pillar implants was achieved through some partition operations in ABAQUS. We assumed that the implants pillars were fully bonded to the soft tissue, i.e. the boundary surface of the pillars and soft tissue shared the same nodes in the FE models (Fig. 3).

2.2.2. Material property and boundary conditions

The soft palate was modeled as a neo-Hookean material defined by the following strain-energy function:

$$\Psi(\bar{I}_1, J) = \underbrace{c(\bar{I}_1 - 3)}_{\text{isochoric-isotropic}} + \underbrace{\frac{1}{D_1}(J-1)^2}_{\text{volumetric}}, \tag{1}$$

where, $\bar{I}_1$ is the first invariant of the modified right Cauchy-Green tensor $\overline{\mathbf{C}}$ and c, D_1 are material parameters derived from Young's modulus E and Poisson's ratio ν with the following relations (Berry et al., 1999):

$$c = \frac{E}{4(1+\nu)}, \quad D_1 = \frac{6(1-2\nu)}{E}. \tag{2}$$

We used the Young's modulus determined from the in vivo magnetic resonance elastography measurements provided by Cheng et al. (2011) for the human soft palate. Assuming a Poisson's ratio value of 0.49, the Young's modulus was calculated to be 7.539 kPa based on the measured shear modulus of 2.53 kPa. For patient 3, the Young's modulus of the tongue was determined using a shear modulus of 2.67 kPa provided by Cheng et al. (2011). For simplicity, the pharynx wall part was assigned the same property as the soft palate was. In addition, we performed uniaxial tension tests of the pillar implants, and the Young's modulus was measured to be 244 MPa. This agrees with the description for PET materials in Lam et al. (2003). The Poisson's ratio was assumed to be equal to 0.49, and the corresponding material property was assigned to the pillars in the 3D soft palate model (Fig. 4 (A)).

For the 3D soft palate model, the anatomical influence of the lateral-side tissue of the soft palate had to be considered in the numerical simulation. In addition, the pharynx wall also was constrained considering

it is attached to the cervical vertebra. Therefore, the boundary conditions for the soft palate FE model were as shown in Fig. 4 (B). In addition, the bottom surface of the tongue in patient 3's numerical model was constrained. Finally, for the negative pressure loading, we applied a uniform pressure field corresponding to the pressure difference between the anterior and posterior sides of the soft palate (Fig. 2) on the surface where the soft palate contacts the airway (Fig. 4 (B)). In this study, for the mouth-close condition, the negative pressure is defined as

$$P_{\text{negative}}^{\text{mouth-close}} = P_{\text{posterior}} - P_{\text{anterior}}. \tag{3}$$

Note that the definition of the negative pressure for the mouth-open condition is

$$P_{\text{negative}}^{\text{mouth-open}} = P_{\text{anterior}} - P_{\text{posterior}}. \tag{4}$$

When the negative pressure develops, the soft palate will have a posterior oblique deformation in the mouth-close condition and an anterior oblique deformation in the mouth-open condition. If the negative pressure is large enough, the soft palate will stick to the pharynx wall and the tongue for the above two conditions. Then, OSA occurs. We call this critical negative pressure the closing pressure, which is regarded as a critical parameter for evaluating the efficacy of palatal implant surgery because the more negative pressure value means it will be more difficult for the soft palate to collapse. A normal closing pressure for persons not having OSA problems has been found to be -13 cm H_2O (Schwartz et al., 1988). Typical closing pressures for OSA patients are -4-(-8) cm H_2O (Han et al., 2002). In addition, we use the following ratio to compare different procedures

$$R_{\text{strengthening-rate}} = \frac{P_{\text{closing-implant}} - P_{\text{closing-reference}}}{P_{\text{closing-reference}}}, \tag{5}$$

where $P_{\text{closing-implant}}$ denotes the closing pressure for the implants inserted model and $P_{\text{closing-reference}}$ denotes the closing pressure for the model without the implants.

2.2.3. Mesh convergence study

The 3D patient-specific FE models were meshed with four noded hybrid tetrahedral elements (C3D4H ABAQUS type). A mesh convergence study was performed on the patient 1 3D model, and the displacement of a point in the mid-section of the soft palate posterior surface was chosen as a critical parameter and compared for different mesh densities. A -5 cm H_2O negative pressure was applied, and the Neo-Hookean model with the aformentioned material properties data was assigned to the 3D patient-specific model. Four mesh densities were tested with 139 338, 397 716, 651 742, and 852 870 elements, corresponding to Mesh 1, Mesh 2, Mesh 3, and Mesh 4, respectively. The difference for the critical parameter between Mesh 3 and Mesh 4 was 0.7%. Therefore, considering the simulation accuracy and computational time efficiency, we use Mesh 3 in the remainder of this paper, and the models for patient 2 and patient 3 share the same mesh density as Mesh 3 does.

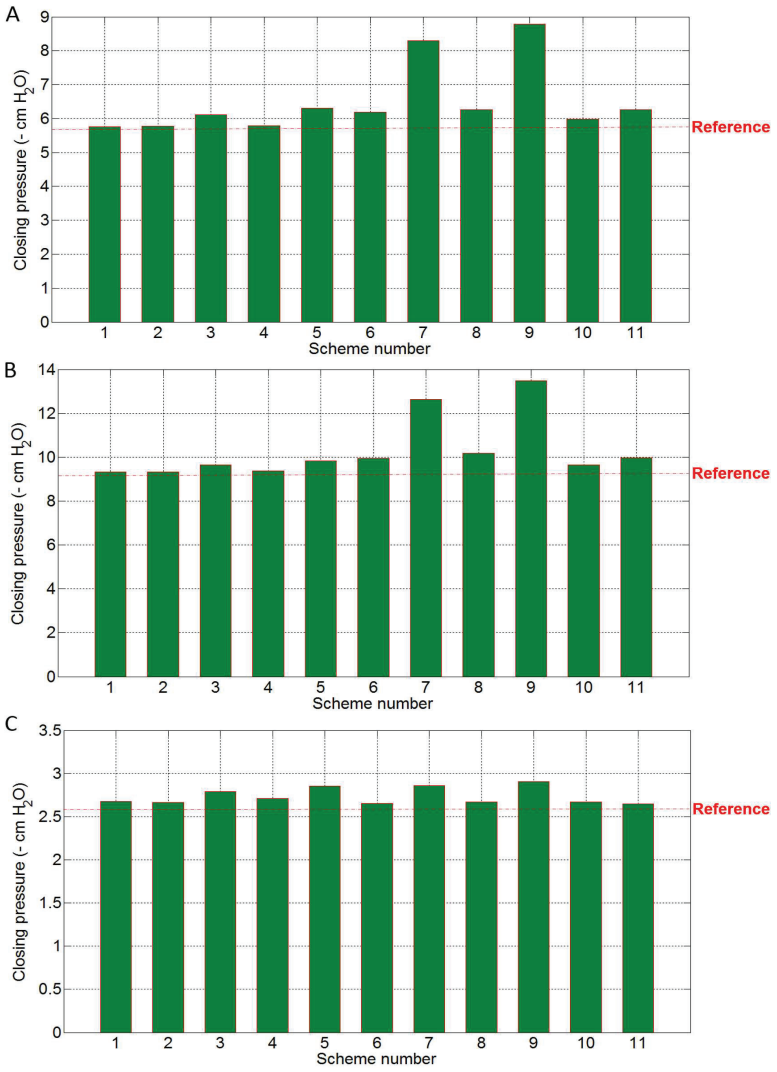

Fig. 5. Closing pressure for different surgical schemes in both the longitudinal and transverse orientation cases for three patients: (A) patient 1, (B) patient 2, (C) patient 3. The same variation trend of different schemes for these three patients was presented, and the scheme 7 and scheme 9 were found to be more efficient than other schemes.

3. Results

3.1. Longitudinal direction surgery with three pillars

For commonly used longitudinal-direction surgery, five different schemes (schemes 1-5) based on different array parameters of the implant pillars were designed. The detailed information is listed in Table 2. The

Table 4. Summary for the strengthening percentage of the designed schemes including the longitudinal schemes and transverse schemes based on the obtained closing pressures

No.	Patient1 (%)	Patient2 (%)	Patient3 (%)
Scheme 1	0.2	0.4	5.0
Scheme 2	0.5	0.5	4.4
Scheme 3	6.5	3.8	9.4
Scheme 4	0.8	0.9	6.2
Scheme 5	9.6	5.8	11.8
Scheme 6	7.7	7.2	4.1
Scheme 7	**44.4**	**36.1**	**12.2**
Scheme 8	9.0	9.5	4.7
Scheme 9	**52.8**	**45.3**	**14.0**
Scheme 10	4.2	4.0	4.6
Scheme 11	9.0	7.8	3.8

placement position is illustrated in Fig. 2 (A). Moreover, the reference closing pressures (without the implants inserted) for these three patients were calculated to be -5.75 cm H_2O, -9.29 cm H_2O, and -2.55 cm H_2O based on the patient-specific FE models, respectively.

According to the calculation results (Fig. 5), the implant surgery stiffened the soft palate because the closing pressure was calculated to be more negative than the reference value. However, the strengthening rate (see Table 4) calculated with Eq. (5) is moderate, and the most negative closing pressure (among schemes 1-5) is obtained from scheme 5, i.e. for the longest pillars with the largest radiuses. Therefore, based on the obtained simulation results evaluated with the closing pressure (Fig. 5), we know that the radii of the pillars and the interval space between the pillars have limited influences on stiffening the soft palate, but increasing the length of the pillars contributes to improving the strength of the soft palate (scheme 3 and 5). In addition, as Fig. 2 (A) shows, the influence of the anterior-posterior position of the implants pillars was investigated in scheme 12 using the same pillar parameters as in scheme 1 (see Table 2). The calculation results showed a small closing pressure variation between schemes 1 and 12. This indicates that the influence of the anterior and posterior positions for the pillars on the global response of the soft palate is very small.

3.2. Transverse direction surgery with three pillars

Here, we investigate a new surgical scheme: the transverse-direction implant scheme. Because there is still no transverse surgery being applied in the clinic, the investigation is interesting for further clinical research to improve the surgical efficacy. Similarly to the longitudinal case, different schemes were tested. Here, for simplicity, the length of the pillars for the transverse case was assigned with a length of 25 mm because it was shown earlier that increased pillar length will improve the surgery efficacy (Fig. 5). Moreover, as Fig. 2 (B)

shows, the difference between the proximal and distal positions can be tested. In total, four schemes (schemes 6-9) listed in Table 2 were addressed to investigate the efficacy of the transverse-direction surgery.

The simulation results are shown in Fig. 5 for schemes 6-9. According to Table 4, the strengthening percentage of scheme 9 is calculated to be the most efficient. Except for patient 3, patient 1 and patient 2 show a more-than-four-times improved efficacy compared with scheme 5, which is the most efficient scheme for the longitudinal surgery schemes. Due to a larger width of the airway (30 mm) for patient 3, the improvement was not so large but still increased significantly. In addition to scheme 9, the other schemes in the transverse case also showed a strengthening effect of the soft palate. This means that the transverse implant surgery has a higher efficacy compared with the longitudinal implant surgery based on our numerical simulation. Moreover, for the transverse implant surgery, according to the simulation results (Fig. 5), a distal placement (scheme 7 and scheme 9) of the implants might be preferable.

Additionally, the influence of the pillars in the soft tissue was investigated. Based on the simulation results, we obtained the main stress distribution characteristics. Due to the fully coupled pillar to soft tissue, there was a sharp transition in tissue stresses from the interface between the soft tissue and pillars into the surrounding soft tissue. The stress concentrations due to the pillars were observed, but the stress level in most of the tissue remained at the same level as for the tissue without implants. The detailed stress analysis is provided in the supplementary material.

3.3. Simulation for five pillars implant surgery and the influence of the pillar Young's modulus

Hypothetically, one can postulate that an increased number of implanted pillars might increase the strengthening efficacy. For simplicity, the array parameters of pillars for the five-pillar scheme (scheme 13 in Table 2) were set to be the same as those for scheme 1, also in the longitudinal direction. As the simulation results (Fig. 6) showed, increasing the number of the pillars may not be an efficient way of stiffening the soft palate.

In addition, as mentioned in the material section, the Young's modulus of the implants material was set to be 244 MPa based on our experimental test result for some implants material samples. The Young's modulus of the palatal implants reported in Gillis et al. (2016) and Huang et al. (2007) was set to be 2 MPa. Therefore, we compared the response for the different Young's moduli. We denoted 244 MPa as the strong stiffening case, while the 2 MPa was denoted the slight stiffening case. Scheme 3 for the longitudinal case and scheme 7 for the transverse case were addressed for comparison. The corresponding slight stiffening schemes were named scheme 10 and scheme 11 (see Table 2) respectively.

According to the simulation results (Fig. 5), the surgery with implants having a large Young's modulus showed a more negative closing pressure, especially in the transverse case. In detail, compared with scheme 10, scheme 3 had an average 2.3% lower closing pressure for these three patients. For the transverse case, compared with scheme 11, scheme 7 improved the soft palate stiffness dramatically and had an average 23.4% lower closing pressure. Therefore, the effect of increasing the Young's modulus of the implants to improve the soft palate stiffness in longitudinal direction was moderate. However, the larger Young's modulus implants

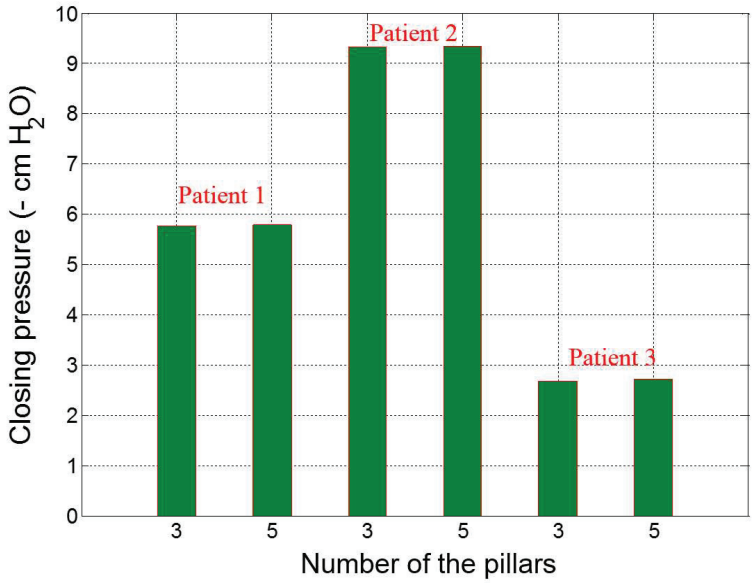

Fig. 6. Comparison between three and five pillars longitudinal implant surgery. A very limited strengthening efficacy was presented for the five implanted pillars surgical scheme compared with the three pillars scheme.

contributed to stiffening the soft palate efficiently for the transverse distal implant surgery. In addition, a comparison study of the stress distribution for these two different material properties cases was addressed. In short, the Young's moduli of 2 MPa (slight stiffening case) and 244 MPa (strong stiffening case) had a large influence on the stress levels in the pillars. The highest Young's modulus led to about a factor of 10 higher stresses in the pillars. However, except for the tissue near the interface to the pillars, the stress levels in the remaining tissue were similar for the two pillar stiffness cases. The detailed results are provided in the supplementary material.

4. Discussion

In this study, we presented a method for evaluating the efficacy of the palatal implant surgical schemes using 3D numerical simulations. A new scheme for transverse implant surgery was addressed. The simulation results showed an improved stiffness of the soft palate when palatal implant surgery was applied. However, the strengthening rate of the longitudinal direction implant surgery showed a moderate efficacy for OSA (see Fig. 5 and Table 4) that agrees with clinical study results (Steward et al., 2008; Maurer et al., 2012). In light of this, our 3D numerical simulation to some degree reflects the reality of clinical upper airway surgery. Moreover, the transverse-direction implant surgical scheme showed higher efficacy with more negative closing pressure compared with the longitudinal-direction implant surgery. A typical high efficacy close to a 50% strengthening rate was observed in the transverse distal implant scheme (see Table 4). Note that the five pillars for the transverse implant surgery were not addressed due to practical challenges with the surgery. In addition,

the deviation of the uvula part was also considered for the arrangement of placement positions (proximal and distal) in the transverse case. The transverse implant surgery schemes 7 and 9 was very efficient for patents 1 and 2. For patient 3 the improvement was moderate. Considering the palatal anatomy, it is noted that the width is larger for patient 3. This could indicate that a longer transverse implant would be more optimal for this patient. A further optimization study can reveal whether there is an optimal pillar length to width ratio.

Surgical treatment has favoured the longitudinal placement of pillars not only due to the easy handling of the delivery instrument in the anterior axis to the posterior axis, but also due to the tradition of applying the radiofrequency ablation of the soft palate in the same direction. In a clinical experiment, the placement of the pillars in the new, transverse, and distal position should not be more time consuming or more surgically challenging than placement in the longitudinal direction when patients are under general anaesthesia. However, there might be a need for new commercial hardware that is more suited to placing transverse pillars. In this regard, one should also consider the lengths of the pillars when performing the transverse placement in a future clinical trial. One could try a strict midline placement with uniform and rather long pillars, or one could try placing two shorter pillars laterally at each side of the midline. Our simulations did not show a definite strengthening efficacy when using five instead of three pillars. This reduces both the surgical timescale and the risk of adverse events, such as the chance of postoperative infection. Finally, one should remember that the stiffness of the pillar material will influence the movement of the palate, and a too-stiff or too-soft pillar could cause problems with successful ingrowth with the surrounding tissues, or even the extrusion of the pillars, which will lead to surgical removal of the implants. Supplementary material provides stress distributions in the pillars and soft tissue. It was observed that in the strong stiffening case (pillar Young's modulus 244 MPa), the stress concentration was large, and high stresses and strains occurred at the interface between the pillars and the soft tissue. Still, the levels are not as high as the measured failure strains (Peña, 2011; Martin and Sun, 2013). Further clinical studies using implants of different stiffness may reveal whether there is an optimal ratio between pillar and soft tissue stiffness.

We defined different schemes based on the existing surgery scheme in the literature shown as in Table 1. However, a more comprehensive optimization study of pillar designs is of interest and is proposed for further work. A topology optimization can be used for the pillar arrangement when the complex 3D patient-specific geometry is addressed. This current work shows a first step that provides general and comprehensive mechanical knowledge for Palatal implant surgery. This also provides input for a next-step topology optimization study.

In our numerical study, because the corresponding experimental data of the human soft palate were not available, the anisotropy from the muscle tissue and its neuromuscular activation effect were neglected. To refine our implants surgery numerical model, a more accurate material model is needed in the future work to obtain a more physiological simulation result for the global response of the soft palate. For simplicity, we applied the negative pressure as a uniformly distributed load. However, this is not the case in reality. Therefore, fluid-structure interaction analysis may be employed to predict a more realistic pressure distribution for the large deformation problems. This will be a task in further studies of the soft palate's response.

5. Conclusion

Based on the 3D FE models of the soft palate, we simulated different palatal implant surgical schemes with the numerical method. Our main findings can be summarized as follows:

1. The existing longitudinal palatal implant surgery can improve the stiffness of the soft palate, but the efficacy is moderate. This is coherent with clinical trials that showed moderate efficacy on OSA in adults (Steward et al., 2008).

2. The influence of the pillars' array parameters is small, but increasing the length of the pillars will increase the strengthening efficacy. In addition, increasing the number of pillars may not be efficient.

3. Based on the obtained closing pressures, placement of the implants in the transverse direction strengthens the soft palate more than placement in the longitudinal direction does.

4. Based on our numerical studies, we propose a possible clinical trial in which three palatal implants pillars are placed in the transverse direction and distal position with the following array parameters: a=5 mm, r=1 mm. The Young's modulus of the implants material should be large and have a good compliance with the soft tissues of the soft palate.

Conflict of interest statement

The authors declare that they have no conflict of interest.

Acknowledgements

The project has been funded in part from a grant from the Research Council of Norway and a grant from NTNU, Norway. The authors are also grateful for professor Ståle Nordgård (from the Department of Otolaryngology/Head and Neck Surgery, St. Olavs Hospital and NTNU) for providing the implants samples for the uniaxial test.

References

Berry, D., Moon, J., Kuehn, D., 1999. A finite element model of the soft palate. The Cleft Palate-Craniofacial Journal 36, 217–223.

Brooks, D., Horner, R., Kozar, L., Render-Teixeira, C., Phillipson, E., 1997. Obstructive sleep apnea as a cause of systemic hypertension. evidence from a canine model. Journal of Clinical Investigation 99, 106–109.

Cheng, S., Gandevia, S., Green, M., Sinkus, R., Bilston, L., 2011. Viscoelastic properties of the tongue and soft palate using mr elastography. Journal of Biomechanics 44, 450 – 454.

Cho, J., Kim, J., Lee, H., Yoon, J., 2013. Surgical anatomy of human soft palate. The Laryngoscope 123, 2900–2904.

Choi, J., Kim, S., Cho, J., 2013. Efficacy of the pillar implant in the treatment of snoring and mild-to-moderate obstructive sleep apnea: A meta-analysis. The Laryngoscope 123, 269–276.

Friedman, M., Schalch, P., Joseph, N., 2006a. Palatal stiffening after failed uvulopalatopharyngoplasty with the pillar implant system. The Laryngoscope 116, 1956–1961.

Friedman, M., Schalch, P., Lin, H., Kakodkar, K., Joseph, N., Mazloom, N., 2008. Palatal implants for the treatment of snoring and obstructive sleep apnea/hypopnea syndrome. Otolaryngology - Head and Neck Surgery 138, 209 – 216.

Friedman, M., Vidyasagar, R., Bliznikas, D., Joseph, N., 2006b. Patient selection and efficacy of pillar implant technique for treatment of snoring and obstructive sleep apnea/hypopnea syndrome. Otolaryngology-Head and Neck Surgery 134, 187–196.

Fujita, S., Conway, W., Zorick, F., Roth, T., 1981. Surgical correction of anatomic abnormalities in obstructive sleep apnea syndrome: Uvulopalatopharyngoplasty. Otolaryngology-Head and Neck Surgery 89, 923–934.

Gillis, E., Rampersaud, C., Pease, E., Buscemi, P., 2016. A novel implantable device for a minimally invasive surgical treatment of obstructive sleep apnea: design and preclinical safety assessment. Nature and Science of Sleep 8, 249–258.

Goessler, U., Hein, G., Verse, T., Stuck, B., Hormann, K., Maurer, J., 2007. Soft palate implants as a minimally invasive treatment for mild to moderate obstructive sleep apnea. Acta Oto-Laryngologica 127, 527–531.

Han, D., Ye, J., Wang, Q., Yang, J., Lin, Y., Wang, J., 2002. Determining the site of airway obstruction in obstructive sleep apnea with airway pressure measurements during sleep. The Laryngoscope 112, 2081–2085.

Holty, J., Guilleminault, C., 2010. Maxillomandibular advancement for the treatment of obstructive sleep apnea: A systematic review and meta-analysis. Sleep Medicine Reviews 14, 287 – 297.

Huang, Y., White, D., Malhotra, A., 2007. Use of computational modeling to predict responses to upper airway surgery in obstructive sleep apnea. The Laryngoscope 117, 648–653.

IP, M., Lam, B., NG, M., Lam, W., Tsang, K., Lam, K., 2002. Obstructive sleep apnea is independently associated with insulin resistance. American Journal of Respiratory and Critical Care Medicine 165, 670–676.

Kim, E.J.and Choi, J., Kim, K., Kim, T., Lee, S., Lee, H., Shin, C., Lee, K., Lee, S., 2011. The impacts of open-mouth breathing on upper airway space in obstructive sleep apnea: 3-d mdct analysis. European Archives of Oto-Rhino-Laryngology 268, 533–539.

Kribbs, N., Pack, A., Kline, L., Smith, P., Schwartz, A., Schubert, N., S.Redline, Henry, J., Getsy, J., Dinges, D., 1993. Objective measurement of patterns of nasal cpap use by patients with obstructive sleep apnea. American Review of Respiratory Disease 147, 887–895. PMID: 8466125.

Kurt, G., Sisman, C.and Akin, E., Akcam, T., 2011. Cephalometric comparison of pharyngeal airway in snoring and non-snoring patients. European Journal of Dentistry 5, 84.

Lam, S., Xue, P., Tao, X., Yu, T., 2003. Multi-scale study of tensile properties and large deformation mechanisms of polyethylene terephthalate/polypropylene knitted composites. Composites Science and Technology 63, 1337 – 1348.

Lee, S., Choi, J., Shin, C., Lee, H., Kwon, S.Y.and Lee, S., 2007. How does open-mouth breathing influence upper airway anatomy? The Laryngoscope 117, 1102–1106.

Lim, J., Lee, J., Han, C., Kwon, J., 2017. Correlation of soft palate length with velum obstruction and severity of obstructive sleep apnea syndrome. Auris Nasus Larynx .

Martin, C., Sun, W., 2013. Modeling of long-term fatigue damage of soft tissue with stress softening and permanent set effects. Biomechanics and Modeling in Mechanobiology , 1–11.

Maurer, J., Sommer, J., Hein, G., Hörmann, K., Heiser, C., Stuck, B., 2012. Palatal implants in the treatment of obstructive sleep apnea: a randomised, placebo-controlled single-centre trial. European Archives of Oto-Rhino-Laryngology 269, 1851–1856.

Mihaescu, M., Murugappan, S., Kalra, M., Khosla, S., Gutmark, E., 2008. Large eddy simulation and reynolds-averaged navier-stokes modeling of flow in a realistic pharyngeal airway model: An investigation of obstructive sleep apnea. Journal of Biomechanics 41, 2279 – 2288.

Mylavarapu, G., Murugappan, S., Mihaescu, M., Kalra, M., Khosla, S., Gutmark, E., 2009. Validation of computational fluid dynamics methodology used for human upper airway flow simulations. Journal of Biomechanics 42, 1553 – 1559.

Nordgard, S., Stene, B., Skjostad, K., 2006. Soft palate implants for the treatment of mild to moderate obstructive sleep apnea. Otolaryngology - Head and Neck Surgery 134, 565 – 570.

Nordgård, S., Wormdal, K., Bugten, V., Stene, B., Skjøstad, K., 2004. Palatal implants: a new method for the treatment of snoring. Acta Oto-Laryngologica 124, 970–975.

O'Connor-Reina, C., Garcia-Iriarte, M., Casado-Morente, J., Gomez-Angel, D., Rodriguez-Diaz, A., Plaza-Mayor, G., 2008. Snoring surgery with palatal implants after failed uvulopalatopharyngoplasty. European Archives of Oto-Rhino-Laryngology 265, 687–693.

Peña, E., 2011. Prediction of the softening and damage effects with permanent set in fibrous biological materials. Journal of the Mechanics and Physics of Solids 59, 1808–1822.

Redline, S., 2017. Screening for obstructive sleep apnea: Implications for the sleep health of the population. JAMA 317, 368–370.

Ryan, C., Bradley, T., 2005. Pathogenesis of obstructive sleep apnea. Journal of Applied Physiology 99, 2440–2450.

Schwartz, A., Smith, P., Wise, R., Gold, A., Permutt, S., 1988. Induction of upper airway occlusion in sleeping individuals with subatmospheric nasal pressure. Journal of Applied Physiology 64, 535–542.

Sera, T., Uesugi, K., Yagi, N., Yokota, H., 2015. Numerical simulation of airflow and microparticle deposition in a synchrotron micro-ct-based pulmonary acinus model. Computer Methods in Biomechanics and Biomedical Engineering 18, 1427–1435.

Sher, A., Schechtman, K., Piccirillo, J., 1996. The efficacy of surgical modifications of the upper airway in adults with obstructive sleep apnea syndrome. Sleep 19, 156–177.

Steward, D., Huntley, T., Woodson, B., Surdulescu, V., 2008. Palate implants for obstructive sleep apnea: Multi-institution, randomized, placebo-controlled study. Otolaryngology-Head and Neck Surgery 139, 506–510.

Tregear, S., Reston, J., Schoelles, K., Phillips, B., 2009. Obstructive sleep apnea and risk of motor vehicle crash: systematic review and meta-analysis. J Clin Sleep Med 5, 573–581.

Walker, R., Levine, H., Hopp, M., Greene, D., Pang, K., 2006. Palatal implants: A new approach for the treatment of obstructive sleep apnea. Otolaryngology-Head and Neck Surgery 135, 549–554.

Young, T., Peppard, P., Taheri, S., 2005. Excess weight and sleep-disordered breathing. Journal of Applied Physiology 99, 1592–1599.

Supplementary material

Stress analysis and influence of different material properties of implants

Patient 1's geometry model was addressed to show stress distribution in the soft tissue and pillar implants. Patients 2 and 3 show similar characteristics. In addition, in order to analyze the influence of different material properties of implants on the stress calculation, we displayed the stress results for the strong stiffening and slight stiffening cases, respectively. In detail, based on Table 2, schemes 3 and 7 using 244 MPa implants are strong stiffening cases for longitudinal and transverse directions, respectively. Their corresponding slight stiffening cases using 2 MPa implants are schemes 10 and 11. The load corresponds to the, the obtained closing pressures shown as in Fig. 5 for each cases. Hence, different cases have different closing pressures, but the deformation of soft palate is the same (collapsed shape). Note that, kPa was used for all the following stress contours. In addition, the contours were plotted on the undeformed body.

1, Longitudinal direction (comparison between schemes 3 and 10)

First, the longitudinal-direction simulation is presented with respect to implant scheme 3 and scheme 10. We chose the mid-sagittal section to show the stress distribution along the length of the implanted pillars and a transverse section 1 is chosen to show the stress in the cross-section of pillars (Fig. S1). The detailed stress contours are shown in Fig. S2 and Fig. S3. In addition, we defined a path shown in Fig. S1 to report a detailed stress distribution between the soft tissue and pillars. The stress distribution from the nodes, including the Mises stress and the corresponding stress components (σ_{xx}, σ_{yy}, σ_{zz}, and σ_{xy}) in section 1 on the defined path 1 is reported. The detailed results are shown in Fig. S4 and Fig. S5.

Based on Fig. S2 and Fig. S3, increasing the Young's modulus of pillars leads to a higher stress level for the implants pillars. In addition, since the anatomy is nonsymmetrical, the stress does not distribute strictly symmetrically to the mid-sagittal section. For more detailed stress report along path 1, according to Fig. S3, there is a sharp stress increase at the interface between the soft tissue and pillars corresponding to the large property difference between these two materials. Moreover, according to the comparison between the strong stiffening case and slight stiffening case, strengthening stiffness of the pillars causes a higher stress concentration for the pillars, but the overall stress in the soft tissue remains to be at the same level.

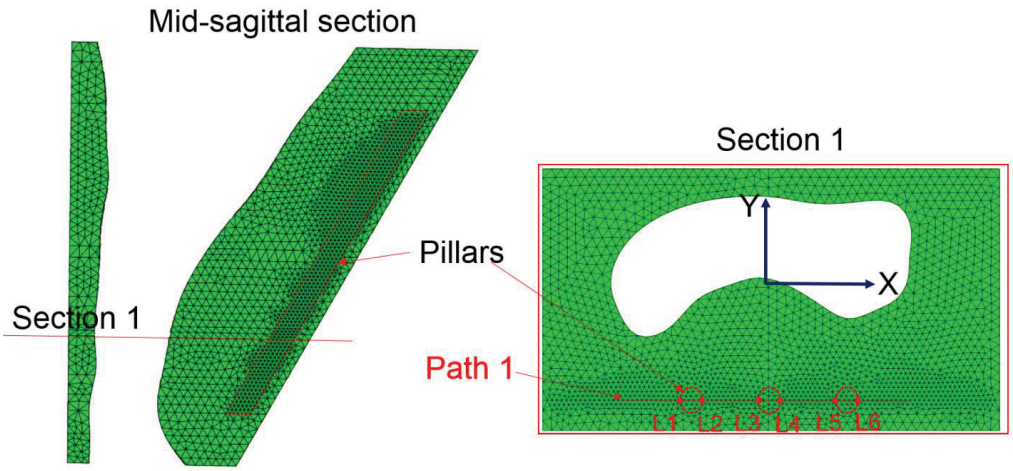

Fig. S1 Schematic for the path 1 and section 1 in the longitudinal case with respect to the undeformed body. Six joint nodes (path 1 and the pillars external circle boundary) L1, L2, L3, L4, L5, and L6 were chosen to report the stress distribution between the soft tissue and implants pillars. Moreover, the coordinate system in section 1 is defined.

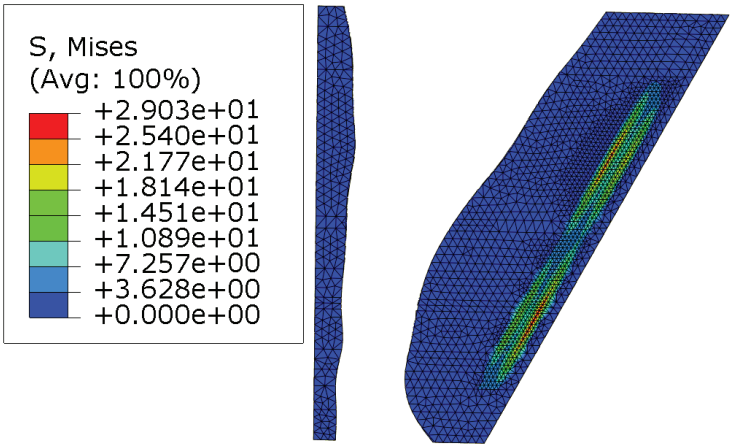

(a) Strong stiffening case (scheme 3)

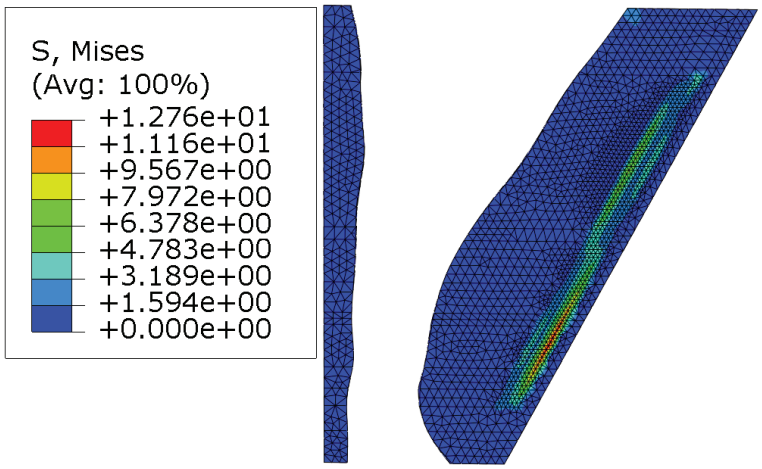

(b) Slight stiffening case (scheme 10)

Fig. S2 The stress contours in the mid-sagittal section for strong stiffening case (scheme 3) and slight stiffening case (scheme 10), respectively. The pillars show higher stress level than the soft tissue, and the pillar stress level for the strong stiffening case is higher than for the slight stiffening case.

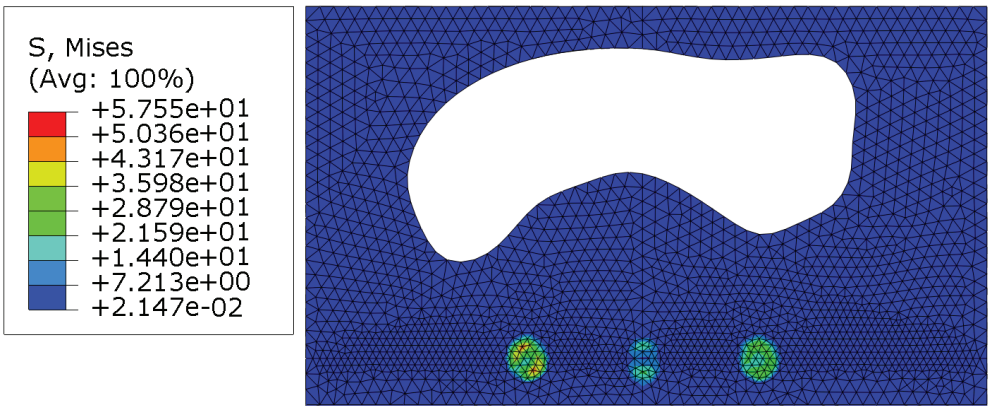

(a) Strong stiffening case (scheme 3)

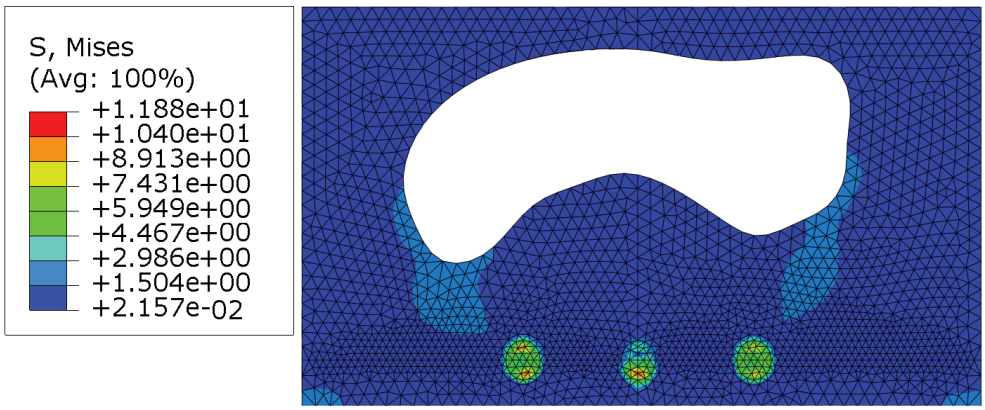

(b) Slight stiffening case (scheme 10)

Fig. S3 The stress contours in section 1 for strong stiffening case (scheme 3) and slight stiffening case (scheme 10), respectively. The stress concentration due to the pillars is illustrated.

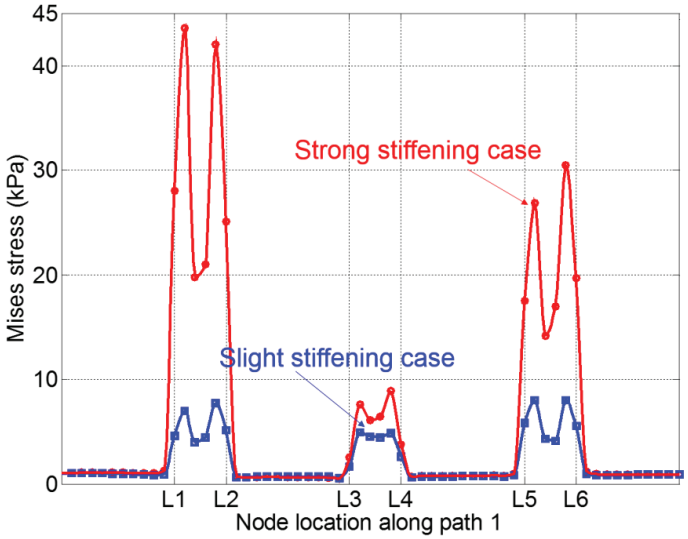

Fig. S4 The detailed stress distribution along path 1. A stress increasing at the joint nodes between the soft tissue and pillars is presented. The stresses of the joint nodes (L1, L2, L3, L4, L5, and L6) show the intermediate values between the lower soft tissue stress and higher pillar stress. Comparing the strong stiffening case with the slight stiffening case, the stresses for nodes in the soft tissue region have nearly the same stress level, but at the interfaces between soft tissue and pillars, different stress levels develops.

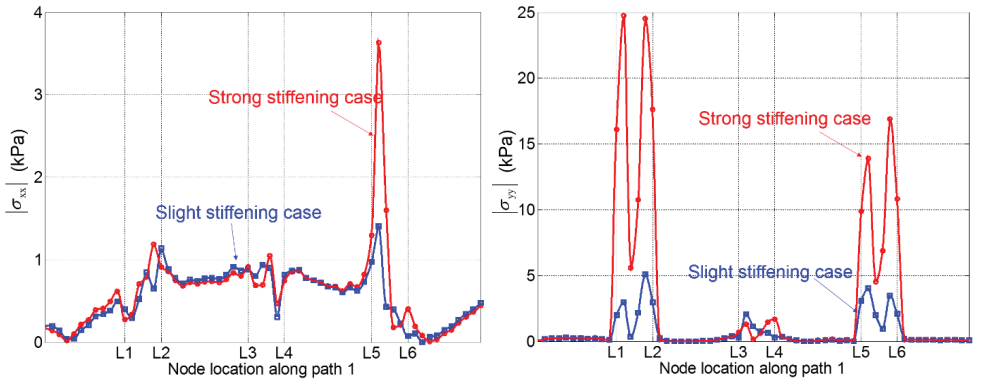

(a) Cauchy stress in x direction

(b) Cauchy stress in y direction

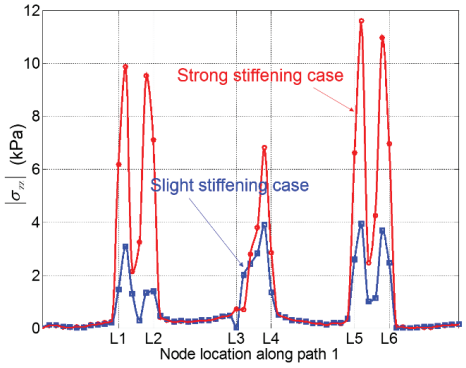

(d) Cauchy stress in z direction

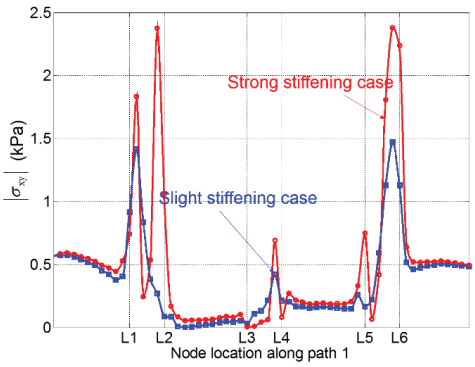

(d) Shear stress in the x-y plane

Fig. S5. Detailed stress distribution along path 1 in section 1 (cross-section of pillars). The stress component in y direction shows a higher level and the strong stiffening case shows a stronger stress concentration at the interface than the slight stiffening case. Apart from the interface regions, the soft issue share the same stress level in these two cases.

2, Transverse direction (comparison between schemes 7 and 11)

Second, the transverse-direction simulation is presented with respect to implant scheme 7 and scheme 11. We chose the mid-sagittal section to show the stress distribution in the cross-section of pillars and a transverse section 2 was chosen to show the stress distribution along the length of the implanted pillars (Fig. S6). A path in the mid-sagittal section was defined and six joint nodes between the soft tissue and pillars on path 2 were chosen to report a more detailed stress description between the soft tissue and pillars.

The stress contours in the mid-sagittal section and the section 2 are reported in Fig. S7 and Fig. S8. The same stress distribution characteristics as in the longitudinal case are presented, such as strong stiffening case giving a higher stress concentration and intermediate stress values for the joint nodes. In addition, the detailed stress distribution along path 2 is presented in Fig. S9 and Fig. S10. Moreover, for the transvers scheme, we found that the stress component (σ_{zz}) in the length direction of pillars for the nodes in the pillars has the highest stress level. This is reasonable due to significant bending of the pillars when the soft palate is collapsed.

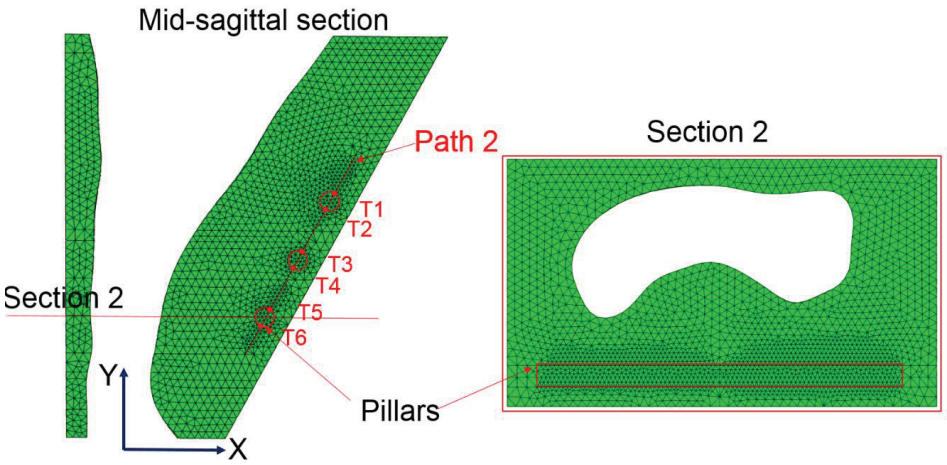

Fig. S6 Schematic for the path 2 and section 2 in the transverse case with respect to the undeformed body. Six joint nodes (path 2 and the pillars external circle boundary) T1, T2, T3, T4, T5, and T6 were chosen to report the stress distribution between the soft tissue and implants. Moreover, the coordinate system in the mid-sagittal section is defined.

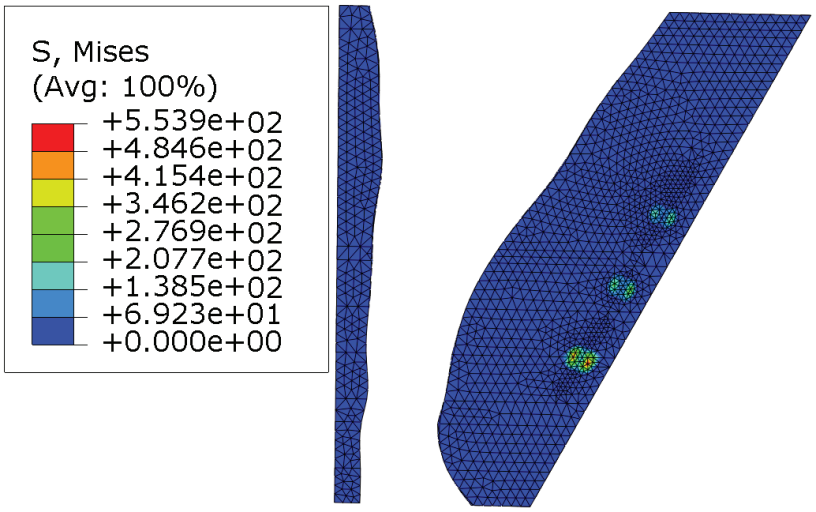

(a) Strong stiffening case (scheme 7)

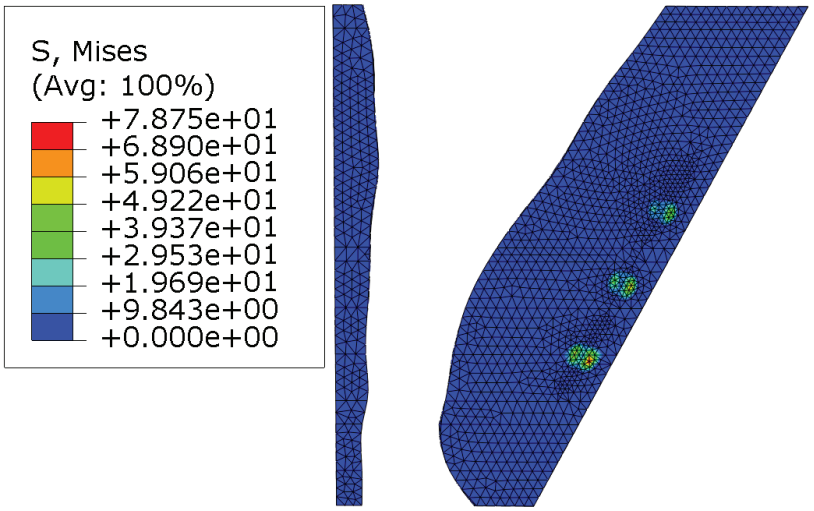

(b) Slight stiffening case (scheme 11)

Fig. S7. Stress contours for transverse placement schemes in the mid-sagittal section including the strong stiffening case (scheme 7) and slight stiffening case (scheme 11). The pillar in the distal part shows a higher stress concentration than the other two. This indicates that the distal pillars plays an important role in preventing the soft palate collapse. This also can explain why the distal placement schemes have a higher strengthening rate as shown in Table 4.

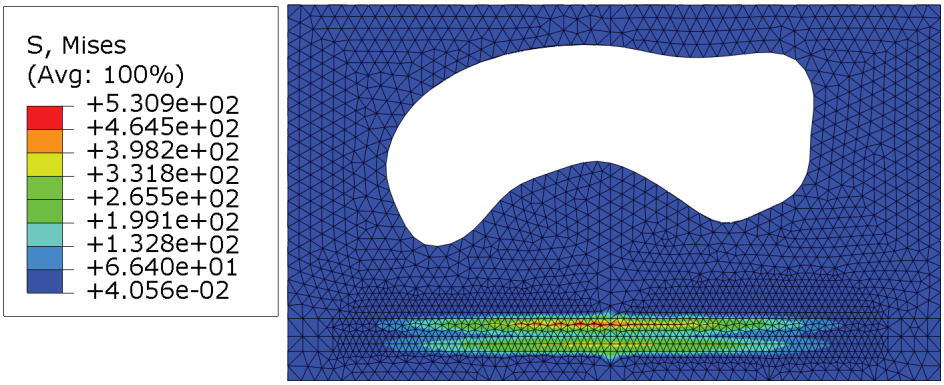

(a) Strong stiffening case (scheme 7)

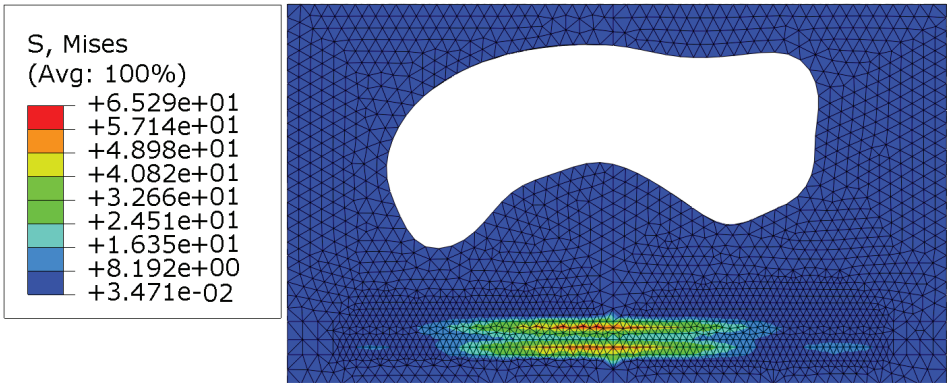

(b) Slight stiffening case (scheme 11)

Fig. S8 The stress contours in section 2 for transverse placement schemes including the strong stiffening case (scheme 7) and slight stiffening case (scheme 11).

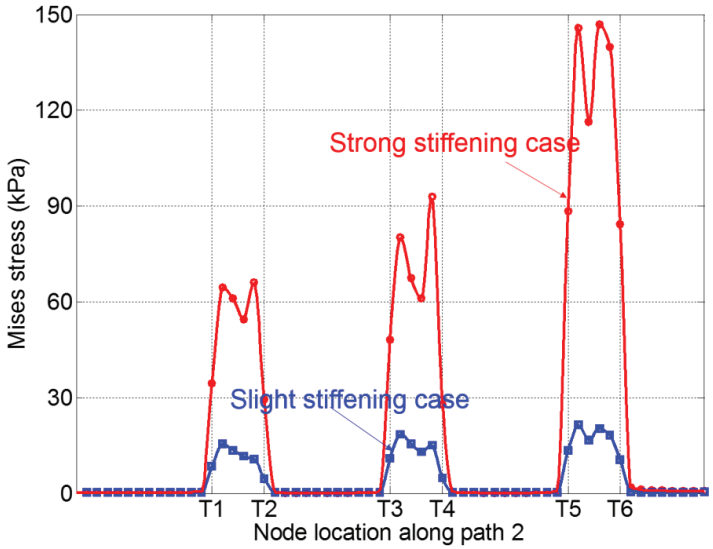

Fig. S9 Mises stress distribution.

Fig. S9 The detailed stress distribution along path 2. The same distribution characteristic as path 1 is presented. The stress increases gradually at the joint nodes between the soft tissue and pillars. Moreover, distal pillar has the highest stress level.

As shown in Fig. S9, for the strong stiffening case the highest stress value is close to 150 kPa. We investigated the corresponding strain distribution for the nodes on path 2 in the strong stiffening case. According to the results in Fig. S11, we find that the strain level for the soft tissue mainly remains in a small range close to 0.05. The peak strain 0.22 appears at the node located in the soft tissue close to the interface of the distal pillar, which has the highest stress concentration. This peak strain value 0.22 for soft tissue belongs to the large strain range. It is smaller than the failure strain for soft tissues, which is tested to be 0.45 in Martin and Sun (2013) and close to 0.6 in Peña (2011).

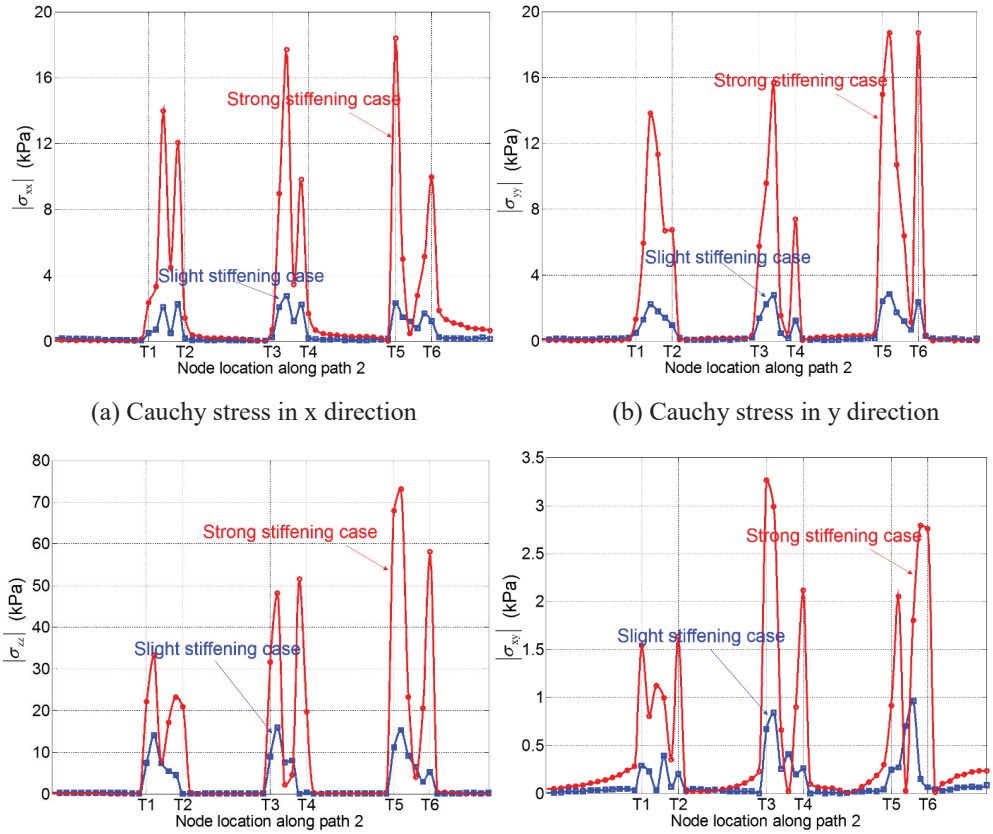

(a) Cauchy stress in x direction

(b) Cauchy stress in y direction

(d) Cauchy stress in z direction

(d) Shear stress in the x-y plane

Fig. S10. Stress distribution along path 2 in section 2 (cross-section of pillars). The stress components in x and y directions show the same stress level, but the highest component is in z direction along the length of pillars. Apart from the interface regions, the soft issue stress level for the strong stiffening is similar to slight stiffening case.

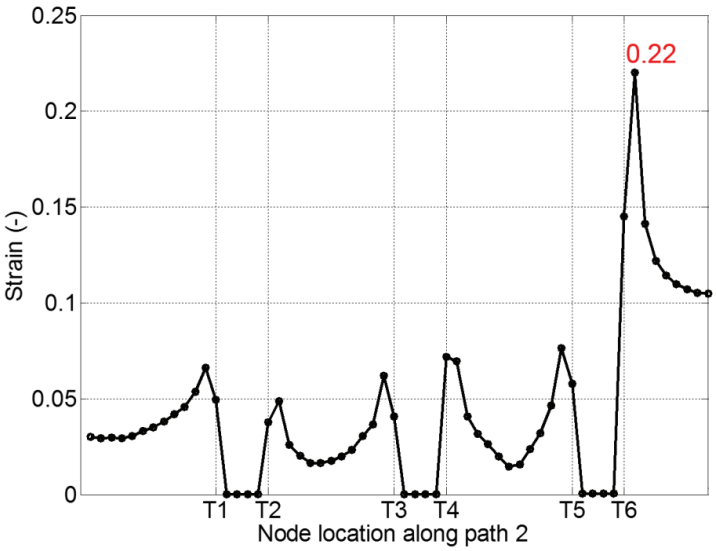

Fig. S11 The logarithmic strain distribution for the nodes along path 2 in the strong stiffening case (scheme 7). The strain level for the pillars is very low, and the strain is close to 0.05 for most of soft tissue. The peak strain presents at the node locating in the soft tissue close to the interface of the distal pillar.

References

Martin, C., Sun, W., 2013. Modeling of long-term fatigue damage of soft tissue with stress softening and permanent set effects. Biomechanics and Modeling in Mechanobiology, 1-11.

Peña, E., 2011. Prediction of the softening and damage effects with permanent set in fibrous biological materials. Journal of the Mechanics and Physics of Solids 59, 1808-1822.

A.3 Paper 3

Paper III

Soft palate muscle activation: a modeling approach for improved understanding of obstructive sleep apnea

Authors: Hongliang Liu, Victorien Emile Prot, Bjørn Helge Skallerud
Submitted to Biomechanics and Modeling in Mechanobiology

Is not included due to copyright

A.4 Paper 4

Paper IV

3D patient-specific numerical modeling of the soft palate considering adhesion from the tongue

Authors: Hongliang Liu, Victorien Emile Prot, Bjørn Helge Skallerud
Submitted to Journal of Biomechanics

Is not included due to copyright

A.5 Paper 5

Anisotropic finite strain viscoelasticity - constitutive modeling and finite element implementation

Authors: Hongliang Liu et al.
To be submitted

Paper V

Is not included due to copyright

Appendix B

Publication List-Department of Structural Engineering

Appendix B

DEPARTMENT OF STRUCTURAL ENGINEERING
NORWEGIAN UNIVERSITY OF SCIENCE AND TECHNOLOGY

N–7491 TRONDHEIM, NORWAY
Telephone: +47 73 59 47 00 Telefax: +47 73 59 47 01

"Reliability Analysis of Structural Systems using Nonlinear Finite Element Methods",
C. A. Holm, 1990:23, ISBN 82-7119-178-0.

"Uniform Stratified Flow Interaction with a Submerged Horizontal Cylinder",
Ø. Arntsen, 1990:32, ISBN 82-7119-188-8.

"Large Displacement Analysis of Flexible and Rigid Systems Considering
Displacement-Dependent Loads and Nonlinear Constraints",
K. M. Mathisen, 1990:33, ISBN 82-7119-189-6.

"Solid Mechanics and Material Models including Large Deformations",
E. Levold, 1990:56, ISBN 82-7119-214-0, ISSN 0802-3271.

"Inelastic Deformation Capacity of Flexurally-Loaded Aluminium Alloy Structures",
T. Welo, 1990:62, ISBN 82-7119-220-5, ISSN 0802-3271.

"Visualization of Results from Mechanical Engineering Analysis",
K. Aamnes, 1990:63, ISBN 82-7119-221-3, ISSN 0802-3271.

"Object-Oriented Product Modeling for Structural Design",
S. I. Dale, 1991:6, ISBN 82-7119-258-2, ISSN 0802-3271.

"Parallel Techniques for Solving Finite Element Problems on Transputer Networks",
T. H. Hansen, 1991:19, ISBN 82-7119-273-6, ISSN 0802-3271.

"Statistical Description and Estimation of Ocean Drift Ice Environments",
R. Korsnes, 1991:24, ISBN 82-7119-278-7, ISSN 0802-3271.

“Properties of concrete related to fatigue damage: with emphasis on high strength concrete”,
G. Petkovic, 1991:35, ISBN 82-7119-290-6, ISSN 0802-3271.

"Turbidity Current Modelling",
B. Brørs, 1991:38, ISBN 82-7119-293-0, ISSN 0802-3271.

"Zero-Slump Concrete: Rheology, Degree of Compaction and Strength. Effects of Fillers as Part Cement-Replacement",
C. Sørensen, 1992:8, ISBN 82-7119-357-0, ISSN 0802-3271.

"Nonlinear Analysis of Reinforced Concrete Structures Exposed to Transient Loading",
K. V. Høiseth, 1992:15, ISBN 82-7119-364-3, ISSN 0802-3271.

"Finite Element Formulations and Solution Algorithms for Buckling and Collapse Analysis of Thin Shells",
R. O. Bjærum, 1992:30, ISBN 82-7119-380-5, ISSN 0802-3271.

"Response Statistics of Nonlinear Dynamic Systems",
J. M. Johnsen, 1992:42, ISBN 82-7119-393-7, ISSN 0802-3271.

"Digital Models in Engineering. A Study on why and how engineers build and operate digital models for decisison support",
J. Høyte, 1992:75, ISBN 82-7119-429-1, ISSN 0802-3271.

"Sparse Solution of Finite Element Equations",
A. C. Damhaug, 1992:76, ISBN 82-7119-430-5, ISSN 0802-3271.

"Some Aspects of Floating Ice Related to Sea Surface Operations in the Barents Sea",
S. Løset, 1992:95, ISBN 82-7119-452-6, ISSN 0802-3271.

"Modelling of Cyclic Plasticity with Application to Steel and Aluminium Structures",
O. S. Hopperstad, 1993:7, ISBN 82-7119-461-5, ISSN 0802-3271.

"The Free Formulation: Linear Theory and Extensions with Applications to Tetrahedral Elements
with Rotational Freedoms",
G. Skeie, 1993:17, ISBN 82-7119-472-0, ISSN 0802-3271.

"Høyfast betongs motstand mot piggdekkslitasje. Analyse av resultater fra prøving i Veisliter'n",
T. Tveter, 1993:62, ISBN 82-7119-522-0, ISSN 0802-3271.

"A Nonlinear Finite Element Based on Free Formulation Theory for Analysis of Sandwich Structures",
O. Aamlid, 1993:72, ISBN 82-7119-534-4, ISSN 0802-3271.

"The Effect of Curing Temperature and Silica Fume on Chloride Migration and Pore Structure of High Strength Concrete",
C. J. Hauck, 1993:90, ISBN 82-7119-553-0, ISSN 0802-3271.

"Failure of Concrete under Compressive Strain Gradients",
G. Markeset, 1993:110, ISBN 82-7119-575-1, ISSN 0802-3271.

"An experimental study of internal tidal amphidromes in Vestfjorden",
J. H. Nilsen, 1994:39, ISBN 82-7119-640-5, ISSN 0802-3271.

"Structural analysis of oil wells with emphasis on conductor design",
H. Larsen, 1994:46, ISBN 82-7119-648-0, ISSN 0802-3271.

"Adaptive methods for non-linear finite element analysis of shell structures",
K. M. Okstad, 1994:66, ISBN 82-7119-670-7, ISSN 0802-3271.

"On constitutive modelling in nonlinear analysis of concrete structures",
O. Fyrileiv, 1994:115, ISBN 82-7119-725-8, ISSN 0802-3271.

"Fluctuating wind load and response of a line-like engineering structure with emphasis on motion-induced wind forces",
J. Bogunovic Jakobsen, 1995:62, ISBN 82-7119-809-2, ISSN 0802-3271.

"An experimental study of beam-columns subjected to combined torsion, bending and axial actions",
A. Aalberg, 1995:66, ISBN 82-7119-813-0, ISSN 0802-3271.

"Scaling and cracking in unsealed freeze/thaw testing of Portland cement and silica fume concretes",
S. Jacobsen, 1995:101, ISBN 82-7119-851-3, ISSN 0802-3271.

"Damping of water waves by submerged vegetation. A case study of laminaria hyperborea",
A. M. Dubi, 1995:108, ISBN 82-7119-859-9, ISSN 0802-3271.

"The dynamics of a slope current in the Barents Sea",
Sheng Li, 1995:109, ISBN 82-7119-860-2, ISSN 0802-3271.

"Modellering av delmaterialenes betydning for betongens konsistens",
Ernst Mørtsell, 1996:12, ISBN 82-7119-894-7, ISSN 0802-3271.

"Bending of thin-walled aluminium extrusions",
Birgit Søvik Opheim, 1996:60, ISBN 82-7119-947-1, ISSN 0802-3271.

"Material modelling of aluminium for crashworthiness analysis",
Torodd Berstad, 1996:89, ISBN 82-7119-980-3, ISSN 0802-3271.

"Estimation of structural parameters from response measurements on submerged floating tunnels",
Rolf Magne Larssen, 1996:119, ISBN 82-471-0014-2, ISSN 0802-3271.

“Numerical modelling of plain and reinforced concrete by damage mechanics”,
Mario A. Polanco-Loria, 1997:20, ISBN 82-471-0049-5, ISSN 0802-3271.

“Nonlinear random vibrations - numerical analysis by path integration methods”,
Vibeke Moe, 1997:26, ISBN 82-471-0056-8, ISSN 0802-3271.

“Numerical prediction of vortex-induced vibration by the finite element method”,
Joar Martin Dalheim, 1997:63, ISBN 82-471-0096-7, ISSN 0802-3271.

“Time domain calculations of buffeting response for wind sensitive structures”,
Ketil Aas-Jakobsen, 1997:148, ISBN 82-471-0189-0, ISSN 0802-3271.

"A numerical study of flow about fixed and flexibly mounted circular cylinders",
Trond Stokka Meling, 1998:48, ISBN 82-471-0244-7, ISSN 0802-3271.

“Estimation of chloride penetration into concrete bridges in coastal areas”,
Per Egil Steen, 1998:89, ISBN 82-471-0290-0, ISSN 0802-3271.

“Stress-resultant material models for reinforced concrete plates and shells”,
Jan Arve Øverli, 1998:95, ISBN 82-471-0297-8, ISSN 0802-3271.

“Chloride binding in concrete. Effect of surrounding environment and concrete composition”,
Claus Kenneth Larsen, 1998:101, ISBN 82-471-0337-0, ISSN 0802-3271.

“Rotational capacity of aluminium alloy beams”,
Lars A. Moen, 1999:1, ISBN 82-471-0365-6, ISSN 0802-3271.

“Stretch Bending of Aluminium Extrusions”,
Arild H. Clausen, 1999:29, ISBN 82-471-0396-6, ISSN 0802-3271.

“Aluminium and Steel Beams under Concentrated Loading”,
Tore Tryland, 1999:30, ISBN 82-471-0397-4, ISSN 0802-3271.

"Engineering Models of Elastoplasticity and Fracture for Aluminium Alloys",
Odd-Geir Lademo, 1999:39, ISBN 82-471-0406-7, ISSN 0802-3271.

"Kapasitet og duktilitet av dybelforbindelser i trekonstruksjoner",
Jan Siem, 1999:46, ISBN 82-471-0414-8, ISSN 0802-3271.

“Etablering av distribuert ingeniørarbeid; Teknologiske og organisatoriske erfaringer fra en norsk ingeniørbedrift”,
Lars Line, 1999:52, ISBN 82-471-0420-2, ISSN 0802-3271.

“Estimation of Earthquake-Induced Response”,
Símon Ólafsson, 1999:73, ISBN 82-471-0443-1, ISSN 0802-3271.

“Coastal Concrete Bridges: Moisture State, Chloride Permeability and Aging Effects”
Ragnhild Holen Relling, 1999:74, ISBN 82-471-0445-8, ISSN 0802-3271.

”Capacity Assessment of Titanium Pipes Subjected to Bending and External Pressure”,
Arve Bjørset, 1999:100, ISBN 82-471-0473-3, ISSN 0802-3271.

“Validation of Numerical Collapse Behaviour of Thin-Walled Corrugated Panels”,
Håvar Ilstad, 1999:101, ISBN 82-471-0474-1, ISSN 0802-3271.

“Strength and Ductility of Welded Structures in Aluminium Alloys”,
Miroslaw Matusiak, 1999:113, ISBN 82-471-0487-3, ISSN 0802-3271.

“Thermal Dilation and Autogenous Deformation as Driving Forces to Self-Induced Stresses in High Performance Concrete”,
Øyvind Bjøntegaard, 1999:121, ISBN 82-7984-002-8, ISSN 0802-3271.

“Some Aspects of Ski Base Sliding Friction and Ski Base Structure”,
Dag Anders Moldestad, 1999:137, ISBN 82-7984-019-2, ISSN 0802-3271.

"Electrode reactions and corrosion resistance for steel in mortar and concrete",
Roy Antonsen, 2000:10, ISBN 82-7984-030-3, ISSN 0802-3271.

"Hydro-Physical Conditions in Kelp Forests and the Effect on Wave Damping and Dune Erosion. A case study on Laminaria Hyperborea",
Stig Magnar Løvås, 2000:28, ISBN 82-7984-050-8, ISSN 0802-3271.

"Random Vibration and the Path Integral Method",
Christian Skaug, 2000:39, ISBN 82-7984-061-3, ISSN 0802-3271.

"Buckling and geometrical nonlinear beam-type analyses of timber structures",
Trond Even Eggen, 2000:56, ISBN 82-7984-081-8, ISSN 0802-3271.

”Structural Crashworthiness of Aluminium Foam-Based Components”,
Arve Grønsund Hanssen, 2000:76, ISBN 82-7984-102-4, ISSN 0809-103X.

“Measurements and simulations of the consolidation in first-year sea ice ridges, and some aspects of mechanical behaviour”,
Knut V. Høyland, 2000:94, ISBN 82-7984-121-0, ISSN 0809-103X.

”Kinematics in Regular and Irregular Waves based on a Lagrangian Formulation”,
Svein Helge Gjøsund, 2000-86, ISBN 82-7984-112-1, ISSN 0809-103X.

”Self-Induced Cracking Problems in Hardening Concrete Structures”,
Daniela Bosnjak, 2000-121, ISBN 82-7984-151-2, ISSN 0809-103X.

"Ballistic Penetration and Perforation of Steel Plates",
Tore Børvik, 2000:124, ISBN 82-7984-154-7, ISSN 0809-103X.

"Freeze-Thaw resistance of Concrete. Effect of: Curing Conditions, Moisture Exchange and Materials",
Terje Finnerup Rønning, 2001:14, ISBN 82-7984-165-2, ISSN 0809-103X

"Structural behaviour of post tensioned concrete structures. Flat slab. Slabs on ground",
Steinar Trygstad, 2001:52, ISBN 82-471-5314-9, ISSN 0809-103X.

"Slipforming of Vertical Concrete Structures. Friction between concrete and slipform panel",
Kjell Tore Fosså, 2001:61, ISBN 82-471-5325-4, ISSN 0809-103X.

"Some numerical methods for the simulation of laminar and turbulent incompressible flows",
Jens Holmen, 2002:6, ISBN 82-471-5396-3, ISSN 0809-103X.

“Improved Fatigue Performance of Threaded Drillstring Connections by Cold Rolling”,
Steinar Kristoffersen, 2002:11, ISBN: 82-421-5402-1, ISSN 0809-103X.

"Deformations in Concrete Cantilever Bridges: Observations and Theoretical Modelling",
Peter F. Takâcs, 2002:23, ISBN 82-471-5415-3, ISSN 0809-103X.

"Stiffened aluminium plates subjected to impact loading",
Hilde Giæver Hildrum, 2002:69, ISBN 82-471-5467-6, ISSN 0809-103X.

"Full- and model scale study of wind effects on a medium-rise building in a built up area",
Jónas Thór Snæbjørnsson, 2002:95, ISBN82-471-5495-1, ISSN 0809-103X.

“Evaluation of Concepts for Loading of Hydrocarbons in Ice-infested water”,
Arnor Jensen, 2002:114, ISBN 82-417-5506-0, ISSN 0809-103X.

”Numerical and Physical Modelling of Oil Spreading in Broken Ice”,
Janne K. Økland Gjøsteen, 2002:130, ISBN 82-471-5523-0, ISSN 0809-103X.

”Diagnosis and protection of corroding steel in concrete”,
Franz Pruckner, 20002:140, ISBN 82-471-5555-4, ISSN 0809-103X.

“Tensile and Compressive Creep of Young Concrete: Testing and Modelling”,
Dawood Atrushi, 2003:17, ISBN 82-471-5565-6, ISSN 0809-103X.

“Rheology of Particle Suspensions. Fresh Concrete, Mortar and Cement Paste with Various Types of Lignosulfonates”,
Jon Elvar Wallevik, 2003:18, ISBN 82-471-5566-4, ISSN 0809-103X.

“Oblique Loading of Aluminium Crash Components”,
Aase Reyes, 2003:15, ISBN 82-471-5562-1, ISSN 0809-103X.

“Utilization of Ethiopian Natural Pozzolans”,
Surafel Ketema Desta, 2003:26, ISSN 82-471-5574-5, ISSN:0809-103X.

“Behaviour and strength prediction of reinforced concrete structures with discontinuity regions”, Helge Brå, 2004:11, ISBN 82-471-6222-9, ISSN 1503-8181.

“High-strength steel plates subjected to projectile impact. An experimental and numerical study”, Sumita Dey, 2004:38, ISBN 82-471-6282-2 (printed version), ISBN 82-471-6281-4 (electronic version), ISSN 1503-8181.

“Alkali-reactive and inert fillers in concrete. Rheology of fresh mixtures and expansive reactions.”
Bård M. Pedersen, 2004:92, ISBN 82-471-6401-9 (printed version), ISBN 82-471-6400-0 (electronic version), ISSN 1503-8181.

“On the Shear Capacity of Steel Girders with Large Web Openings”.
Nils Christian Hagen, 2005:9 ISBN 82-471-6878-2 (printed version), ISBN 82-471-6877-4 (electronic version), ISSN 1503-8181.

”Behaviour of aluminium extrusions subjected to axial loading”.
Østen Jensen, 2005:7, ISBN 82-471-6873-1 (printed version), ISBN 82-471-6872-3 (electronic version), ISSN 1503-8181.

”Thermal Aspects of corrosion of Steel in Concrete”.
Jan-Magnus Østvik, 2005:5, ISBN 82-471-6869-3 (printed version), ISBN 82-471-6868 (electronic version), ISSN 1503-8181.

”Mechanical and adaptive behaviour of bone in relation to hip replacement.” A study of bone remodelling and bone grafting.
Sébastien Muller, 2005:34, ISBN 82-471-6933-9 (printed version), ISBN 82-471-6932-0 (electronic version), ISSN 1503-8181.

“Analysis of geometrical nonlinearities with applications to timber structures”.
Lars Wollebæk, 2005:74, ISBN 82-471-7050-5 (printed version), ISBN 82-471-7019-1 (electronic version), ISSN 1503-8181.

“Pedestrian induced lateral vibrations of slender footbridges”,
Anders Rönnquist, 2005:102, ISBN 82-471-7082-5 (printed version), ISBN 82-471-7081-7 (electronic version), ISSN 1503-8181.

“Initial Strength Development of Fly Ash and Limestone Blended Cements at Various Temperatures Predicted by Ultrasonic Pulse Velocity”,
Tom Ivar Fredvik, 2005:112, ISBN 82-471-7105-8 (printed version), ISBN 82-471-7103-1 (electronic version), ISSN 1503-8181.

“Behaviour and modelling of thin-walled cast components”,
Cato Dørum, 2005:128, ISBN 82-471-7140-6 (printed version), ISBN 82-471-7139-2 (electronic version), ISSN 1503-8181.

“Behaviour and modelling of selfpiercing riveted connections”,
Raffaele Porcaro, 2005:165, ISBN 82-471-7219-4 (printed version), ISBN 82-471-7218-6 (electronic version), ISSN 1503-8181.

”Behaviour and Modelling og Aluminium Plates subjected to Compressive Load”,
Lars Rønning, 2005:154, ISBN 82-471-7169-1 (printed version), ISBN 82-471-7195-3 (electronic version), ISSN 1503-8181.

”Bumper beam-longitudinal system subjected to offset impact loading”,
Satyanarayana Kokkula, 2005:193, ISBN 82-471-7280-1 (printed version), ISBN 82-471-7279-8 (electronic version), ISSN 1503-8181.

“Control of Chloride Penetration into Concrete Structures at Early Age”,
Guofei Liu, 2006:46, ISBN 82-471-7838-9 (printed version), ISBN 82-471-7837-0 (electronic version), ISSN 1503-8181.

“Modelling of Welded Thin-Walled Aluminium Structures”,
Ting Wang, 2006:78, ISBN 82-471-7907-5 (printed version), ISBN 82-471-7906-7 (electronic version), ISSN 1503-8181.

”Time-variant reliability of dynamic systems by importance sampling and probabilistic analysis of ice loads”,
Anna Ivanova Olsen, 2006:139, ISBN 82-471-8041-3 (printed version), ISBN 82-471-8040-5 (electronic version), ISSN 1503-8181.

“Fatigue life prediction of an aluminium alloy automotive component using finite element analysis of surface topography”.
Sigmund Kyrre Ås, 2006:25, ISBN 82-471-7791-9 (printed version), ISBN 82-471-7791-9 (electronic version), ISSN 1503-8181.

”Constitutive models of elastoplasticity and fracture for aluminium alloys under strain path change”,
Dasharatha Achani, 2006:76, ISBN 82-471-7903-2 (printed version), ISBN 82-471-7902-4 (electronic version), ISSN 1503-8181.

“Simulations of 2D dynamic brittle fracture by the Element-free Galerkin method and linear fracture mechanics”,
Tommy Karlsson, 2006:125, ISBN 82-471-8011-1 (printed version), ISBN 82-471-8010-3 (electronic version), ISSN 1503-8181.

“Penetration and Perforation of Granite Targets by Hard Projectiles”,
Chong Chiang Seah, 2006:188, ISBN 82-471-8150-9 (printed version), ISBN 82-471-8149-5 (electronic version), ISSN 1503-8181.

“Deformations, strain capacity and cracking of concrete in plastic and early hardening phases”,
Tor Arne Hammer, 2007:234, ISBN 978-82-471-5191-4 (printed version), ISBN 978-82-471-5207-2 (electronic version), ISSN 1503-8181.

“Crashworthiness of dual-phase high-strength steel: Material and Component behaviour”, Venkatapathi Tarigopula, 2007:230, ISBN 82-471-5076-4 (printed version), ISBN 82-471-5093-1 (electronic version), ISSN 1503-8181.

“Fibre reinforcement in load carrying concrete structures”,
Åse Lyslo Døssland, 2008:50, ISBN 978-82-471-6910-0 (printed version), ISBN 978-82-471-6924-7 (electronic version), ISSN 1503-8181.

“Low-velocity penetration of aluminium plates”,
Frode Grytten, 2008:46, ISBN 978-82-471-6826-4 (printed version), ISBN 978-82-471-6843-1 (electronic version), ISSN 1503-8181.

“Robustness studies of structures subjected to large deformations”,
Ørjan Fyllingen, 2008:24, ISBN 978-82-471-6339-9 (printed version), ISBN 978-82-471-6342-9 (electronic version), ISSN 1503-8181.

“Constitutive modelling of morsellised bone”,
Knut Birger Lunde, 2008:92, ISBN 978-82-471-7829-4 (printed version), ISBN 978-82-471-7832-4 (electronic version), ISSN 1503-8181.

“Experimental Investigations of Wind Loading on a Suspension Bridge Girder”,
Bjørn Isaksen, 2008:131, ISBN 978-82-471-8656-5 (printed version), ISBN 978-82-471-8673-2 (electronic version), ISSN 1503-8181.

“Cracking Risk of Concrete Structures in The Hardening Phase”,
Guomin Ji, 2008:198, ISBN 978-82-471-1079-9 (printed version), ISBN 978-82-471-1080-5 (electronic version), ISSN 1503-8181.

“Modelling and numerical analysis of the porcine and human mitral apparatus”,
Victorien Emile Prot, 2008:249, ISBN 978-82-471-1192-5 (printed version), ISBN 978-82-471-1193-2 (electronic version), ISSN 1503-8181.

“Strength analysis of net structures”,
Heidi Moe, 2009:48, ISBN 978-82-471-1468-1 (printed version), ISBN 978-82-471-1469-8 (electronic version), ISSN1503-8181.

“Numerical analysis of ductile fracture in surface cracked shells”,
Espen Berg, 2009:80, ISBN 978-82-471-1537-4 (printed version), ISBN 978-82-471-1538-1 (electronic version), ISSN 1503-8181.

"Subject specific finite element analysis of bone – for evaluation of the healing of a leg lengthening and evaluation of femoral stem design",
Sune Hansborg Pettersen, 2009:99, ISBN 978-82-471-1579-4 (printed version), ISBN 978-82-471-1580-0 (electronic version), ISSN 1503-8181.

"Evaluation of fracture parameters for notched multi-layered structures",
Lingyun Shang, 2009:137, ISBN 978-82-471-1662-3 (printed version), ISBN 978-82-471-1663-0 (electronic version), ISSN 1503-8181.

"Modelling of Dynamic Material Behaviour and Fracture of Aluminium Alloys for Structural Applications"
Yan Chen, 2009:69, ISBN 978-82-471-1515-2 (printed version), ISBN 978-82 471-1516-9 (electronic version), ISSN 1503-8181.

"Nanomechanics of polymer and composite particles"
Jianying He 2009:213, ISBN 978-82-471-1828-3 (printed version), ISBN 978-82-471-1829-0 (electronic version), ISSN 1503-8181.

"Mechanical properties of clear wood from Norway spruce"
Kristian Berbom Dahl 2009:250, ISBN 978-82-471-1911-2 (printed version) ISBN 978-82-471-1912-9 (electronic version), ISSN 1503-8181.

"Modeling of the degradation of TiB_2 mechanical properties by residual stresses and liquid Al penetration along grain boundaries"
Micol Pezzotta 2009:254, ISBN 978-82-471-1923-5 (printed version) ISBN 978-82-471-1924-2 (electronic version) ISSN 1503-8181.

"Effect of welding residual stress on fracture"
Xiabo Ren 2010:77, ISBN 978-82-471-2115-3 (printed version) ISBN 978-82-471-2116-0 (electronic version), ISSN 1503-8181.

"Pan-based carbon fiber as anode material in cathodic protection system for concrete structures"
Mahdi Chini 2010:122, ISBN 978-82-471-2210-5 (printed version) ISBN 978-82-471-2213-6 (electronic version), ISSN 1503-8181.

"Structural Behaviour of deteriorated and retrofitted concrete structures"
Irina Vasililjeva Sæther 2010:171, ISBN 978-82-471-2315-7 (printed version) ISBN 978-82-471-2316-4 (electronic version) ISSN 1503-8181.

"Prediction of local snow loads on roofs"
Vivian Meløysund 2010:247, ISBN 978-82-471-2490-1 (printed version) ISBN 978-82-471-2491-8 (electronic version) ISSN 1503-8181.

"Behaviour and modelling of polymers for crash applications"
Virgile Delhaye 2010:251, ISBN 978-82-471-2501-4 (printed version) ISBN 978-82-471-2502-1 (electronic version) ISSN 1503-8181.

“Blended cement with reducted CO_2 emission – Utilizing the Fly Ash-Limestone Synergy”,
Klaartje De Weerdt 2011:32, ISBN 978-82-471-2584-7 (printed version) ISBN 978-82-471-2584-4 (electronic version) ISSN 1503-8181.

“Chloride induced reinforcement corrosion in concrete” Concept of critical chloride content – methods and mechanisms.
Ueli Angst 2011:113, ISBN 978-82-471-2769-9 (printed version) ISBN 978-82-471-2763-6 (electronic version) ISSN 1503-8181.

“A thermo-electric-Mechanical study of the carbon anode and contact interface for Energy savings in the production of aluminium”.
Dag Herman Andersen 2011:157, ISBN 978-82-471-2859-6 (printed version) ISBN 978-82-471-2860-2 (electronic version) ISSN 1503-8181.

“Structural Capacity of Anchorage Ties in Masonry Veneer Walls Subjected to Earthquake”. The implications of Eurocode 8 and Eurocode 6 on a typical Norwegain veneer wall.
Ahmed Mohamed Yousry Hamed 2011:181, ISBN 978-82-471-2911-1 (printed version) ISBN 978-82-471-2912-8 (electronic ver.) ISSN 1503-8181.

“Work-hardening behaviour in age-hardenable Al-Zn-Mg(-Cu) alloys”.
Ida Westermann , 2011:247, ISBN 978-82-471-3056-8 (printed ver.) ISBN 978-82-471-3057-5 (electronic ver.) ISSN 1503-8181.

“Behaviour and modelling of selfpiercing riveted connections using aluminium rivets”.
Nguyen-Hieu Hoang, 2011:266, ISBN 978-82-471-3097-1 (printed ver.) ISBN 978-82-471-3099-5 (electronic ver.) ISSN 1503-8181.

“Fibre reinforced concrete”.
Sindre Sandbakk, 2011:297, ISBN 978-82-471-3167-1 (printed ver.) ISBN 978-82-471-3168-8 (electronic ver) ISSN 1503:8181.

“Dynamic behaviour of cablesupported bridges subjected to strong natural wind”.
Ole Andre Øiseth, 2011:315, ISBN 978-82-471-3209-8 (printed ver.) ISBN 978-82-471-3210-4 (electronic ver.) ISSN 1503-8181.

“Constitutive modeling of solargrade silicon materials”
Julien Cochard, 2011:307, ISBN 978-82-471-3189-3 (printed ver). ISBN 978-82-471-3190-9 (electronic ver.) ISSN 1503-8181.

“Constitutive behavior and fracture of shape memory alloys”
Jim Stian Olsen, 2012:57, ISBN 978-82-471-3382-8 (printed ver.) ISBN 978-82-471-3383-5 (electronic ver.) ISSN 1503-8181.

“Field measurements in mechanical testing using close-range photogrammetry and digital image analysis”
Egil Fagerholt, 2012:95, ISBN 978-82-471-3466-5 (printed ver.) ISBN 978-82-471-3467-2 (electronic ver.) ISSN 1503-8181.

“Towards a better under standing of the ultimate behaviour of lightweight aggregate concrete in compression and bending”,
Håvard Nedrelid, 2012:123, ISBN 978-82-471-3527-3 (printed ver.) ISBN 978-82-471-3528-0 (electronic ver.) ISSN 1503-8181.

“Numerical simulations of blood flow in the left side of the heart”
Sigrid Kaarstad Dahl, 2012:135, ISBN 978-82-471-3553-2 (printed ver.) ISBN 978-82-471-3555-6 (electronic ver.) ISSN 1503-8181.

“Moisture induced stresses in glulam”
Vanessa Angst-Nicollier, 2012:139, ISBN 978-82-471-3562-4 (printed ver.) ISBN 978-82-471-3563-1 (electronic ver.) ISSN 1503-8181.

“Biomechanical aspects of distraction osteogensis”
Valentina La Russa, 2012:250, ISBN 978-82-471-3807-6 (printed ver.) ISBN 978-82-471-3808-3 (electronic ver.) ISSN 1503-8181.

“Ductile fracture in dual-phase steel. Theoretical, experimental and numerical study”
Gaute Gruben, 2012:257, ISBN 978-82-471-3822-9 (printed ver.) ISBN 978-82-471-3823-6 (electronic ver.) ISSN 1503-8181.

“Damping in Timber Structures”
Nathalie Labonnote, 2012:263, ISBN 978-82-471-3836-6 (printed ver.) ISBN 978-82-471-3837-3 (electronic ver.) ISSN 1503-8181.

“Biomechanical modeling of fetal veins: The umbilical vein and ductus venosus bifurcation”
Paul Roger Leinan, 2012:299, ISBN 978-82-471-3915-8 (printed ver.) ISBN 978-82-471-3916-5 (electronic ver.) ISSN 1503-8181.

“Large-Deformation behaviour of thermoplastics at various stress states”
Anne Serine Ognedal, 2012:298, ISBN 978-82-471-3913-4 (printed ver.) ISBN 978-82-471-3914-1 (electronic ver.) ISSN 1503-8181.

“Hardening accelerator for fly ash blended cement”
Kien Dinh Hoang, 2012:366, ISBN 978-82-471-4063-5 (printed ver.) ISBN 978-82-471-4064-2 (electronic ver.) ISSN 1503-8181.

“From molecular structure to mechanical properties”
Jianyang Wu, 2013:186, ISBN 978-82-471-4485-5 (printed ver.) ISBN 978-82-471-4486-2 (electronic ver.) ISSN 1503-8181.

“Experimental and numerical study of hybrid concrete structures”
Linn Grepstad Nes, 2013:259, ISBN 978-82-471-4644-6 (printed ver.) ISBN 978-82-471-4645-3 (electronic ver.) ISSN 1503-8181.

“Mechanics of ultra-thin multi crystalline silicon wafers”
Saber Saffar, 2013:199, ISBN 978-82-471-4511-1 (printed ver.) ISBN 978-82-471-4513-5 (electronic ver). ISSN 1503-8181.

“Through process modelling of welded aluminium structures”
Anizahyati Alisibramulisi, 2013:325, ISBN 978-82-471-4788-7 (printed ver.) ISBN 978-82-471-4789-4 (electronic ver.) ISSN 1503-8181.

“Combined blast and fragment loading on steel plates”
Knut Gaarder Rakvåg, 2013:361, ISBN978-82-471-4872-3 (printed ver.) ISBN 978-82-4873-0 (electronic ver.). ISSN 1503-8181.

“Characterization and modelling of the anisotropic behaviour of high-strength aluminium alloy”
Marion Fourmeau, 2014:37, ISBN 978-82-326-0008-3 (printed ver.) ISBN 978-82-326-0009-0 (electronic ver.) ISSN 1503-8181.

“Behaviour of threated steel fasteners at elevated deformation rates”
Henning Fransplass, 2014:65, ISBN 978-82-326-0054-0 (printed ver.) ISBN 978-82-326-0055-7 (electronic ver.) ISSN 1503-8181.

“Sedimentation and Bleeding”
Ya Peng, 2014:89, ISBN 978-82-326-0102-8 (printed ver.) ISBN 978-82-326-0103-5 (electric ver.) ISSN 1503-8181.

“Impact against X65 offshore pipelines”
Martin Kristoffersen, 2014:362, ISBN 978-82-326-0636-8 (printed ver.) ISBN 978-82-326-0637-5 (electronic ver.) ISSN 1503-8181.

“Formability of aluminium alloy subjected to prestrain by rolling”
Dmitry Vysochinskiy, 2014:363,, ISBN 978-82-326-0638-2 (printed ver.) ISBN 978-82-326-0639-9 (electronic ver.) ISSN 1503-8181.

“Experimental and numerical study of Yielding, Work-Hardening and anisotropy in textured AA6xxx alloys using crystal plasticity models”
Mikhail Khadyko, 2015:28, ISBN 978-82-326-0724-2 (printed ver.) ISBN 978-82-326-0725-9 (electronic ver.) ISSN 1503-8181.

“Behaviour and Modelling of AA6xxx Aluminium Alloys Under a Wide Range of Temperatures and Strain Rates”
Vincent Vilamosa, 2015:63, ISBN 978-82-326-0786-0 (printed ver.) ISBN 978-82-326-0787-7 (electronic ver.) ISSN 1503-8181.

“A Probabilistic Approach in Failure Modelling of Aluminium High Pressure Die-Castings”
Octavian Knoll, 2015:137, ISBN 978-82-326-0930-7 (printed ver.) ISBN 978-82-326-0931-4 (electronic ver.) ISSN 1503-8181.

“Ice Abrasion on Marine Concrete Structures”
Egil Møen, 2015:189, ISBN 978-82-326-1034-1 (printed ver.) ISBN 978-82-326-1035-8 (electronic ver.) ISSN 1503-8181.

“Fibre Orientation in Steel-Fibre-Reinforced Concrete”
Giedrius Zirgulis, 2015:229, ISBN 978-82-326-1114-0 (printed ver.) ISBN 978-82-326-1115-7 (electronic ver.) ISSN 1503-8181.

“Effect of spatial variation and possible interference of localised corrosion on the residual capacity of a reinforced concrete beam”
Mohammad Mahdi Kioumarsi, 2015:282, ISBN 978-82-326-1220-8 (printed ver.) ISBN 978-82-1221-5 (electronic ver.) ISSN 1503-8181.

“The role of concrete resistivity in chloride-induced macro-cell corrosion”
Karla Horbostel, 2015:324, ISBN 978-82-326-1304-5 (printed ver.) ISBN 978-82-326-1305-2 (electonic ver.) ISSN 1503-8181.

“Flowable fibre-reinforced concrete for structural applications”
Elena Vidal Sarmiento, 2015-335, ISBN 978-82-326-1324-3 (printed ver.) ISBN 978-82-326-1325-0 (electronic ver.) ISSN 1503-8181.

“Development of chushed sand for concrete production with microproportioning”
Rolands Cepuritis, 2016:19, ISBN 978-82-326-1382-3 (printed ver.) ISBN 978-82-326-1383-0 (electronic ver.) ISSN 1503-8181.

“Withdrawal properties of threaded rods embedded in glued-laminated timer elements”
Haris Stamatopoulos, 2016:48, ISBN 978-82-326-1436-3 (printed ver.) ISBN 978-82-326-1437-0 (electronic ver.) ISSN 1503-8181.

“An Experimental and numerical study of thermoplastics at large deformation”
Marius Andersen, 2016:191, ISBN 978-82-326-1720-3 (printed ver.) ISBN 978-82-326-1721-0 (electronic ver.) ISSN 1503-8181.

“Modeling and Simulation of Ballistic Impact”
Jens Kristian Holmen, 2016:240, ISBN 978-82-326-1818-7 (printed ver). ISBN 978-82-326-1819-4 (electronic ver.) ISSN 1503-8181.

“Early age crack assessment of concrete structures”
Anja B. Estensen Klausen, 2016:256, ISBN 978-82-326-1850-7 (printed ver). ISBN 978-82-326-1851-4 (electronic ver.) ISSN 1503-8181.

“Uncertainty quantification and sensitivity analysis for cardiovascular models”
Vinzenz Gregor Eck, 2016:234, ISBN 978-82-326-1806-4 (printed ver.) ISBN 978-82-326-1807-1 (electronic ver.) ISSN 1503-8181.

“Dynamic behaviour of existing and new railway catenary systems under Norwegain conditions”
Petter Røe Nåvik, 2016:298, ISBN 978-82-326-1935-1 (printed ver.) ISBN 978-82-326-1934-4 (electronic ver.) ISSN 1503-8181.

“Mechanical behaviour of particle-filled elastomers at various temperatures”
Arne Ilseng, 2016-295, ISBN978-82-326-1928-3 (printed ver.) ISBN 978-82-326-1929-0 (electronic ver.) ISSN 1503-8181.

“Nanotechnology for Anti-Icing Application”
Zhiwei He, 2016:348, ISBN 978-82-326-2038-8 (printed ver.) ISBN 978-82-326-2019-5 (electronic ver.) ISSN 1503-8181.

“Conduction Mechanisms in Conductive Adhesives with Metal-Coated Polyer Spheres”
Sigurd Rolland Pettersen, 2016:349, ISBN 978-326-2040-1 (printed ver,) ISBN 978-82-326-2041-8 (electronic ver.) ISSN 1503-8181.

“The interaction between calcium lignosulfonate and cement”
Alessia Colombo, 2017:20, ISBN 978-82-326-2122-4 (printed ver.) ISBN 978-82-326-2123-1 (electronic ver.) ISSN 1503-8181.

“Behaviour and Modelling of Flexible Structures Subjected to Blast Loading”
Vegard Aune, 2017:101, ISBN 978-82-326-2274-0 (printed ver.) ISBN 978-82-326-2275-7 (electronic ver.) ISSN 1503-8181.

“Behaviour of steel connections under quasi-static and impact loading”
Erik Løhre Grimsmo, 2017:159, ISBN 978-82-326-2390-7 (printed ver.) ISBN 978-82-326-2391-4 (electronic ver.) ISSN 1503-8181.

“An experimental and numerical study of cortical bone at he macro and Nano-scale”
Masoud Ramenzanzadehkoldeh,, 2017:208, ISBN 978-82-326-2488-1 (printed ver.) ISBN 978-82-326-2489-8 (electronic ver.) ISSN 1503-8181.

“Optoelectrical Properties of a Novel Organic Semiconductor: 6,13-Dichloropentacene”
Mao Wang, 2017:130, ISBN 978-82-326-2332-7 (printed ver.) ISBN 978-82-326-2333-4) (electronic ver.) ISSN 1503-8181.

“Core-shell structured microgels and their behavior at oil and water interface”
Yi Gong, 2017:182, ISBN 978-82-326-2436-2 (printed. ver.) ISBN 978-82-326-2437-9 (electronic ver.) ISSN 1503-8181.

"Aspects of design of reinforced concrete structures using nonliear finite element analyses"
Morten Engen, 2017:149, ISBN 978-82-326-2370-9 (printed ver.) ISBN 978-82-326-2371-6 (electronic ver.) ISSN 1503-8181.

"Numerical studies on ductile failure of aluminium alloys"
Lars Edvard Dæhli, 2017:284, ISBN 978-82-326-2636-6 (printed ver.) ISBN 978-82-326-2637-3 (electronic ver.) ISSN 1503-8181.

"Modelling and Assessment of Hydrogen Embrittlement in Steels and Nickel Alloys"
Haiyang Yu, 2017:278, ISBN 978-82-326-2624-3 (printed. ver.) ISBN 978-82-326-2625-0 (electronic ver.) ISSN 1503-8181.

"Network arch timber bridges with light timber deck on transverse crossbeams"
Anna Weronika Ostrycharczyk, 2017:318, ISBN 978-82-326-2704-2 (printed ver.) ISBN 978-82-326-2705-9 (electronic ver.) ISSN 1503-8181.

"Splicing of Large Glued Laminated Timber Elements by Use of Long Threated Rods"
Martin Cepelka, 2017:320, ISBN 978-82-326-2708-0 (printed ver.) ISBN 978-82-326-2709-7 (electronic ver.) ISSN 1503-8181.

"Thermomechanical behaviour of semi-crystalline polymers: experiments, modelling and simulation"
Joakim Johnsen, 2017-317, ISBN 978-82-326-2702-8 (printed ver.) ISBN 978-82-326-2703-5 (electronic ver.) ISSN 1503-8181.

"Small-Scale Plasiticity under Hydrogen Environment"
Kai Zhao, 2017:356, ISBN 978-82-326-2782-0 (printed ver.) ISBN 978-82-326-2783-7 (electronic er.) ISSN 1503-8181.

"Risk and Reliability Based Calibration of Structural Design Codes"
Michele Baravalle, 2017:342, ISBN 978-82-326-2752-3 (printed ver,) ISBN 978-82-326-2753-0 (electronic ver.) ISSN 1503-8181.

"Dynamic behaviour of floating bridges exposed to wave excitation"
Knut Andreas Kvåle, 2017:365, ISBN 978-82-326-2800-1 (printed ver.) ISBN 978-82-326-2801-8 (electronic ver.) ISSN 1503-8181.

"Dolomite calcined clay composite cement – hydration and durability"
Alisa Lydia Machner, 2018:39, ISBN 978-82-326-2872-8 (printed ver.). ISBN 978-82-326-2873-5 (electronic ver.) ISSN 1503-8181.

"Modelling of the self-excited forces for bridge decks subjected to random motions: an experimental study"
Bartosz Siedziako, 2018:52, ISBN 978-82-326-2896-4 (printed ver.). ISBN 978-82-326-2897-1 (electronic ver.) ISSN 1503-8181.

“A probabilistic-based methodology for evaluation of timber facade constructions”
Klodian Gradeci, 2018:69, ISBN 978-82-326-2928-2 (printed ver.) ISBN 978-82-326-2929-9 (electronic ver.) ISSN 1503-8181.

“Behaviour and modelling of flow-drill screw connections”
Johan Kolstø Sønstabø, 2018:73, ISBN 978-82-326-2936-7 (printed ver.) ISBN 978-82-326-2937-4 (electronic ver.) ISSN 1503-8181.